AD 266 556

DISCLAIMER NOTICE

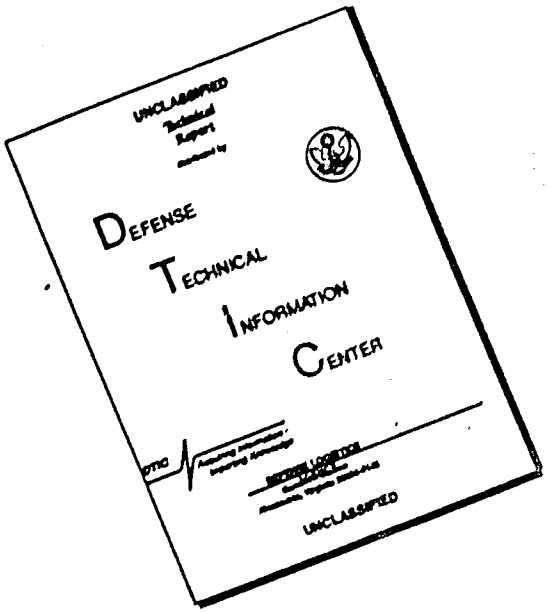

THIS DOCUMENT IS BEST QUALITY AVAILABLE. THE COPY FURNISHED TO DTIC CONTAINED A SIGNIFICANT NUMBER OF PAGES WHICH DO NOT REPRODUCE LEGIBLY.

ASD TECHNICAL REPORT 61-508

FACTOR OF SAFETY CONSIDERATIONS FOR AERODYNAMICALLY HEATED STRUCTURES SUBJECTED TO HIGH CYCLIC STRESSES

E. H. NICKELL
W. E. JACOBSEN

LOCKHEED MISSILES & SPACE COMPANY
GROUP DIVISION OF LOCKHEED AIRCRAFT CORPORATION
SUNNYVALE, CALIFORNIA

NOTICES

When Government drawings, specifications, or other data are used for any purpose other than in connection with a definitely related Government procurement operation, the United States Government thereby incurs no responsibility nor any obligation whatsoever; and the fact that the Government may have formulated, furnished, or in any way supplied the said drawings, specifications, or other data, is not to be regarded by implication or otherwise as in any manner licensing the holder or any other person or corporation, or conveying any rights or permission to manufacture, use, or sell any patented invention that may in any way be related thereto.

Qualified requesters may obtain copies of this report from the Armed Services Technical Information Agency, (ASTIA), Arlington Hall Station, Arlington 12, Virginia.

This report has been released to the Office of Technical Services, U. S. Department of Commerce, Washington 25, D. C., for sale to the general public.

Copies of ASD Technical Reports and Technical Notes should not be returned to the Aeronautical Systems Division unless return is required by security considerations, contractual obligations, or notice on a specific document.

ASD TECHNICAL REPORT 61-508

FACTOR OF SAFETY CONSIDERATIONS FOR AERODYNAMICALLY HEATED STRUCTURES SUBJECTED TO HIGH CYCLIC STRESSES

E. H. Nickell
W. E. Jacobsen

Lockheed Missiles & Space Company
A Group Division of Lockheed Aircraft Corporation
Sunnyvale, California

October 1961

Flight Dynamics Laboratory

Contract No. AF 33(616)-8000
Project No. 1367
Task No. 136703

AERONAUTICAL SYSTEMS DIVISION
AIR FORCE SYSTEMS COMMAND
UNITED STATES AIR FORCE
WRIGHT-PATTERSON AIR FORCE BASE, OHIO

FOREWORD

This report was prepared by Structural Mechanics, Lockheed Missiles & Space Company, under the direction of R. F. Crawford, Project Leader. The research was supported by the U.S. Air Force, under Contract AF 33(616)-8000 and monitored by the Design Criteria Section, Structures Branch, of the Flight Dynamics Laboratory, Aeronautical Systems Division, Wright-Patterson Air Force Base, with P. L. Hasty acting as Project Engineer.

This is the final report under the above contract and covers work done during the period 1 March 1961 to 31 August 1961.

ABSTRACT

A parametric study has been made from published low-cycle fatigue data showing the various effects on cycles-to-failure. Included are uniaxial and biaxial experimental results. True total strain range, ratio of minimum-to-maximum strain, and effects of geometry are the predominate parameters affecting fatigue life for mechanical cycling at room and elevated temperatures.

Structural life was investigated in terms of the parameters for mechanical cyclic loading as well as for cyclic thermal straining. In the former case, expressions relating the parameters to structural life were found. However, in the latter case, no reliable expression between these parameters and structural life was found. A specific expression for conservatively predicting structural life or endurance is developed and applies to all materials, ratios of minimum-to-maximum strains, temperatures, and states of stress. Also considered were single-cycle failures resulting from thermal shock.

PUBLICATION REVIEW

This report has been reviewed and is approved for the Commander:

WILLIAM C. NIELSEN
Colonel, USAF
Chief, Flight Dynamics Laboratory

TABLE OF CONTENTS

TABLE OF CONTENTS (CONTINUED)

ILLUSTRATIONS

Section 1
INTRODUCTION

1.1 GENERAL

The rapid development of high-performance manned flight vehicles subjected to extremely severe operational environments such as hypersonic flight and/or atmospheric re-entry emphasizes the need for re-examining structural factors of safety. These factors of safety applied to the operational environment define the boundaries for structural design. The effects of extremes in cyclic environment present a particularly crucial problem area, inasmuch as most of the existing theory of plastic stress analysis has, at best, questionable applicability to the cyclic case. To obtain realistic factors of safety for cyclic environment, detailed theoretical and experimental analyses of cyclic stresses beyond the limit load are required. These studies should include a re-evaluation and, perhaps, extension of existing methods of plastic stress analysis to the cyclic case, and they should determine the effects of high cyclic stresses on failure of materials. Although it is felt that successful investigations in both areas are necessary to determine realistically structural factors of safety, this report is limited to the latter, and the approach is confined to examining published data on effects of high cyclic stresses on failure of materials.

The serious consequences of cyclic loads applied to a structure in the high-stress range are well recognized, but the probability of structural failure, or, conversely, the ability of a given structure to resist a known pattern of high-magnitude loading, has not been thoroughly evaluated. This study has a threefold purpose: (1) to review past studies in low-cycle fatigue; (2) to determine extent of correlation between previous experimental results and proposed methods for predicting low-cycle fatigue; and (3) finally, to suggest possible approaches in which to direct further effort so that the influence of specific parameters can be better understood.

Manuscript released by the author September 1961 for publication as an ASD Technical Report.

A typical approach to fatigue investigation has been from the standpoint of stress. In the high-cycle fatigue regime, low stress is automatically implied; consequently, it has usually been possible to calculate stresses from an elastic analysis. In the range of low-cycle fatigue, a nonlinearity between stresses and strains usually exists, and further, stress becomes a relatively insensitive quantity as the ultimate stress and strain is approached. Design based upon stress is therefore not very meaningful. As a result, it appears that a rational approach in determining the low-cycle life of a structure should be based on the total strain range.

Many articles and reports have been written on fatigue. Since 1950, the American Society for Testing Materials has published annually an extensive abstract of references on fatigue (Ref. 1). Very few of these articles, however, have dealt with low-cycle fatigue. Actually, low-cycle fatigue has been considered extensively in only the last six years, and few investigations were made before then. In 1948, Sachs and co-workers (Ref. 2) began the initial investigation of low-cycle fatigue to find the effect of cyclic straining at room temperature on the fracture ductility and strain hardening of 24-ST. The next significant contributions to low-cycle fatigue were Coffin's (Ref. 3) and Manson's (Ref. 4) methods of predicting low-cycle fatigue. Coffin arrived at his method from thermal cycling of 347-stainless steel, while Manson derived his method from Sachs' previous investigation of 24-ST. In 1955, a five-year study of low-cycle fatigue was initiated at the Massachusetts Institute of Technology (Refs. 5–8). The MIT study is very complete and contributes significantly to the study of low-cycle fatigue by clearly determining that the total strain range is a very important parameter in low-cycle fatigue. They derived a method of predicting low-cycle fatigue similar to the method presented by Sachs, Gerberich, and Weiss (Ref. 9) in the same year, 1960. Other investigators studied the effects of various parameters on low-cycle fatigue.

The present study shows that while the total strain range is a very important parameter for predicting low-cycle fatigue failure under mechanically applied loading, neither total strain range nor plastic strain range is useful for predicting cyclic failure under thermally induced loading. For mechanical loading in general, increases in strain range

result in decreased fatigue life. This relationship is shown in Figs. 1-1 through 1-4 for mechanical cycling at room temperature and elevated temperature, thermal cycling, and biaxial mechanical cycling, respectively. In each case, total strain range is the ordinate and cycles-to-failure is the abscissa. Data for all the materials mechanically cycled at room and elevated temperatures lie within a somewhat narrow band. However, the thermal-cycling data lie in an almost horizontal band which is below that for mechanical cycling. The two bands merge at 10^4 cycles.

Only a few of the data for cycling under mechanically applied biaxial stresses lie outside the band for mechanical cycling, and it is expected that those few data are results of extraneous influences.

Two mathematical expressions are shown in Figs. 1-1 and 1-2 which form lower boundaries of the data. They are conservative and are recommended for predicting low-cycle fatigue failure for all but the thermal-cycling case.

The effects of less significant parameters affecting low-cycle fatigue life are not included in Figs. 1-1 through 1-4; however, they are discussed in the following sections. Cycle frequency and/or time at elevated temperature, as well as maximum temperature, which induces creep and metallurgical transition, are parameters that appear to be very important. But, because of insufficient data, they have not been evaluated so thoroughly as the strain parameter.

Sachs (Ref. 9) and D'Amato (Ref. 8) show that strain-ratio is a very important parameter in predicting low-cycle fatigue life. When R -1, which denotes cycling about a mean strain of zero, low-cycle fatigue life is essentially predicted by a straight line on log-log coordinates as shown in Fig. 1-5. However, for other strain ratios the work of Sachs and D'Amato, as shown in Fig. 1-5, shows appreciable deviation from the straight line for R -1 when N is less than 200.

Some of the scatter exhibited in the data used in this study may be attributed to variations in mean strain. Data presented for mechanical cycling at elevated temperatures include two stress ratios other than minus one. The thermal cycling data present a special case which may be possibly explained by further study directed toward determining the effective strain (or stress) ratio. It is expected that the bandwidths shown for mechanical cycling may be narrowed by normalizing total strain range with respect to the respective quarter-cycle fracture ductility. This was not attempted in this report due to insufficient ductility data, although it is recognized that ductility should be an important parameter of the problem.

Detailed discussions of each category of low-cycle fatigue follow immediately after a brief explanation of the terms used in this report.

1.2 LIMITATIONS AND DEFINITIONS

Low-cycle fatigue life is defined as the number of cycles to produce failure between 1/4 and 10,000. It would have been desirable to reduce the upper limit to 1,000 cycles, but in such a case, sufficient data for a satisfactory study would not have been available for either the elevated-temperature mechanical cycling, biaxial-stress mechanical cycling, or thermal cycling.

The strain parameters used in this study are defined below:

Strain cycling is performed between two constant strain values – the maximum strain $\left(\epsilon_{max}\right)$ and the minimum strain $\left(\epsilon_{min}\right)$ whose average value is the mean strain $\left(\epsilon_{m}\right)$, where

$$\epsilon_{m} = \frac{\epsilon_{max} + \epsilon_{min}}{2}$$

The total strain range is the difference between the maximum and minimum strains:

$$\Delta\epsilon_{TR} = \epsilon_{max} - \epsilon_{min}$$

The total strain range is also the sum of the elastic $\left(\Delta\epsilon_e\right)$ and plastic strain $\left(\Delta\epsilon_p\right)$ range,

$$\Delta\epsilon_{TR} = \Delta\epsilon_e + \Delta\epsilon_p$$

The plastic strain is quite often difficult to establish. All of the strains are the true or natural strains

$$\epsilon = \ln\left(1 + \frac{\Delta\ell}{\ell}\right)$$

The fracture strain $\left(\epsilon_f\right)$ is the strain at fracture due to a tensile static test:

$$\epsilon_f = \ln\left(\frac{A_o}{A_f}\right)$$

where A_o is the original cross section and A_f is the final cross section at failure.

Another strain parameter used in this work is the strain ratio (R) which is the minimum strain divided by the maximum strain:

$$R = \frac{\epsilon_{min}}{\epsilon_{max}} = \left(\frac{2\epsilon_m}{\epsilon_{max}} - 1\right)$$

The mean strain not only has a formal significance as a strain function, but also has a very distinct physical significance as a prestrain by which the metal had been first strained to some definite value and then cycled about that prestrain. Data for cycling about several strain ratios are shown in Fig. 1-6. Two general cycling schemes are

shown in Fig. 1-6(a) and (b). Two special cases, reversed and zero-to-maximum strain cycling, are shown in Fig. 1-6(c) and (d) where $\epsilon_{min} = \epsilon_{max}$, $\epsilon_m = 0$, and $R = -1$; and $\epsilon_m = \epsilon_{max}/2$ and $R = 0$, respectively.

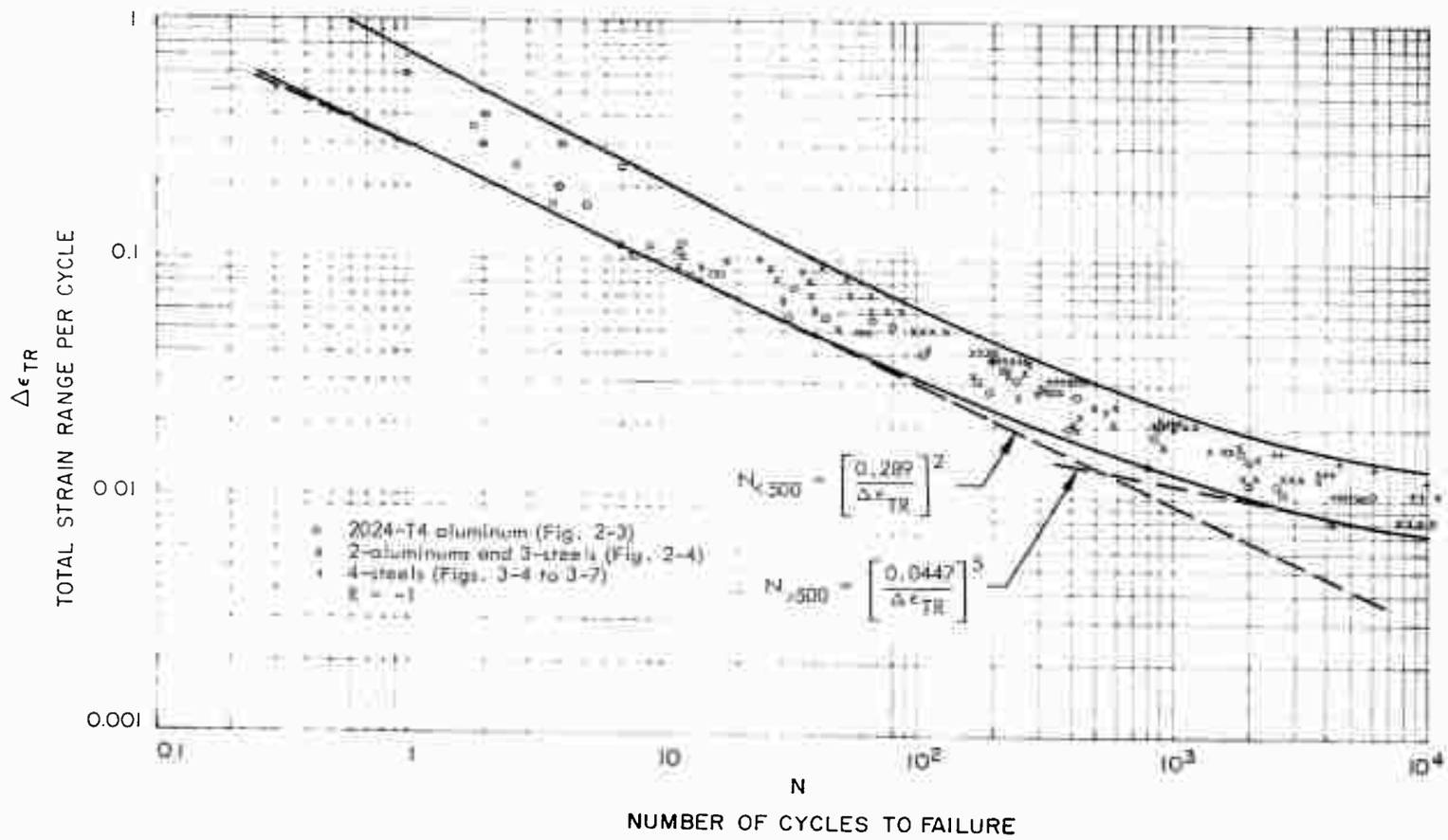

Fig. 1-1 Mechanical Cycling at Room Temperature

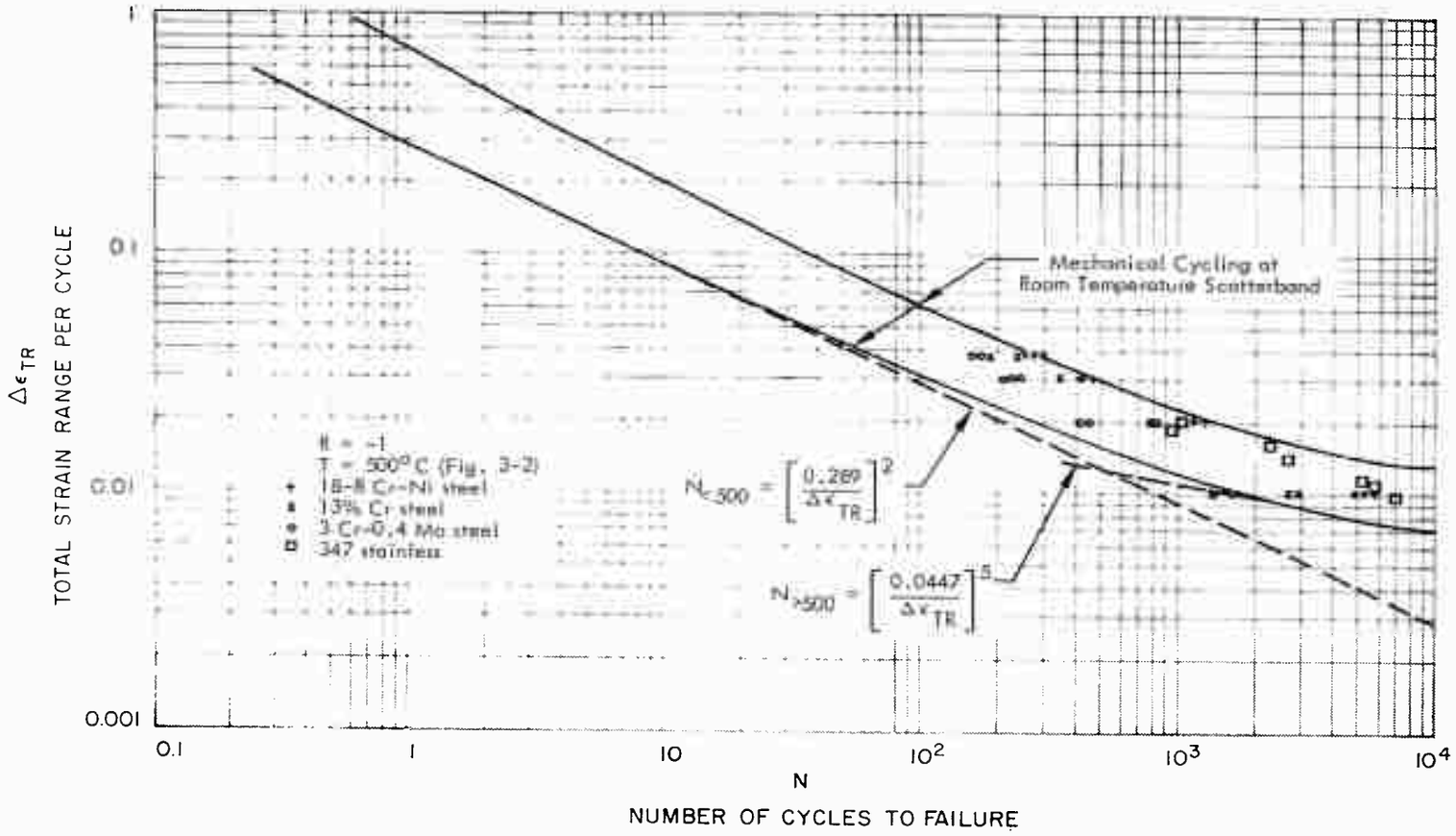

Fig. 1-2 Mechanical Cycling at Elevated Temperature

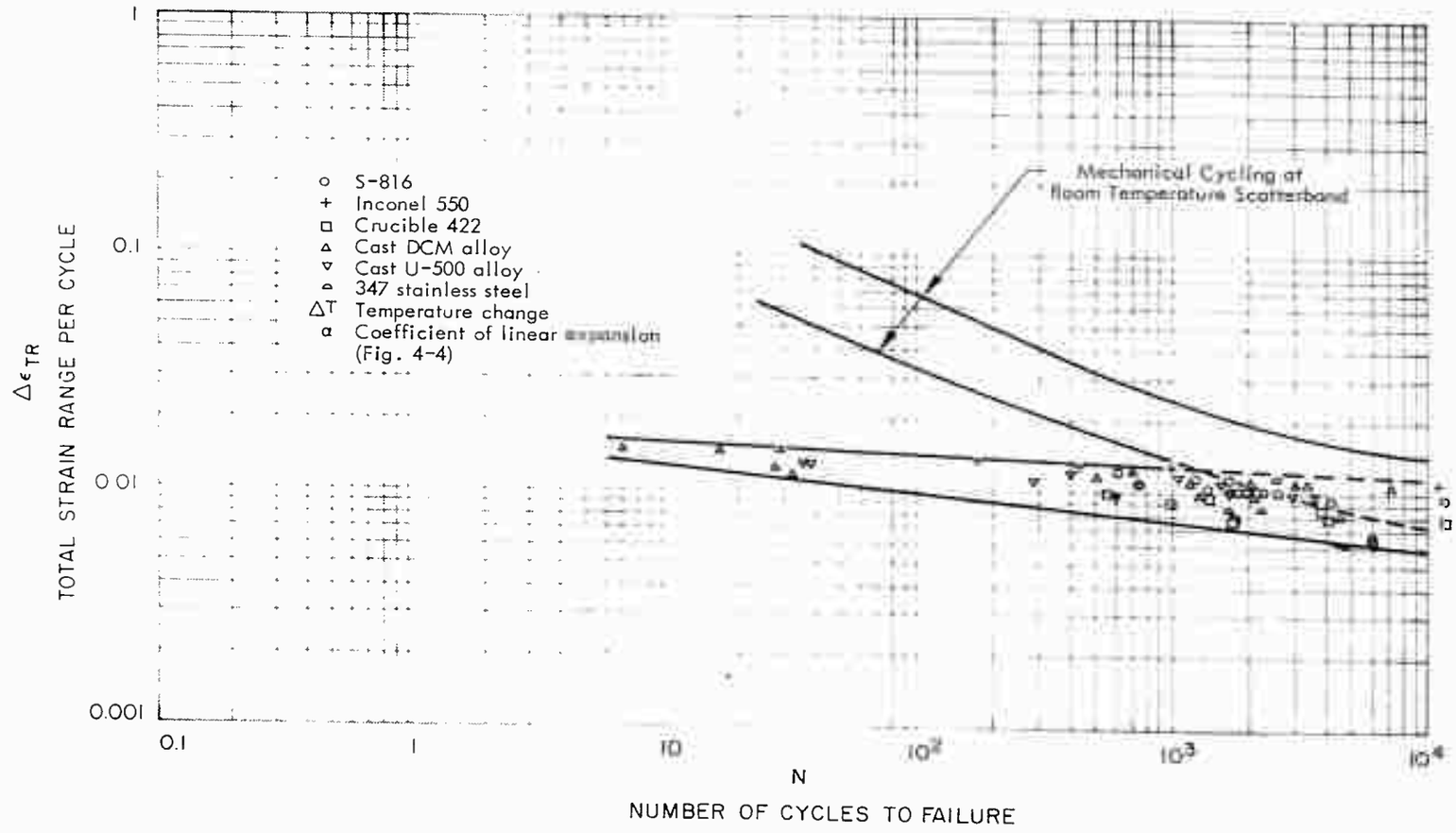

Fig. 1-3 Thermal Cycling of Various Materials

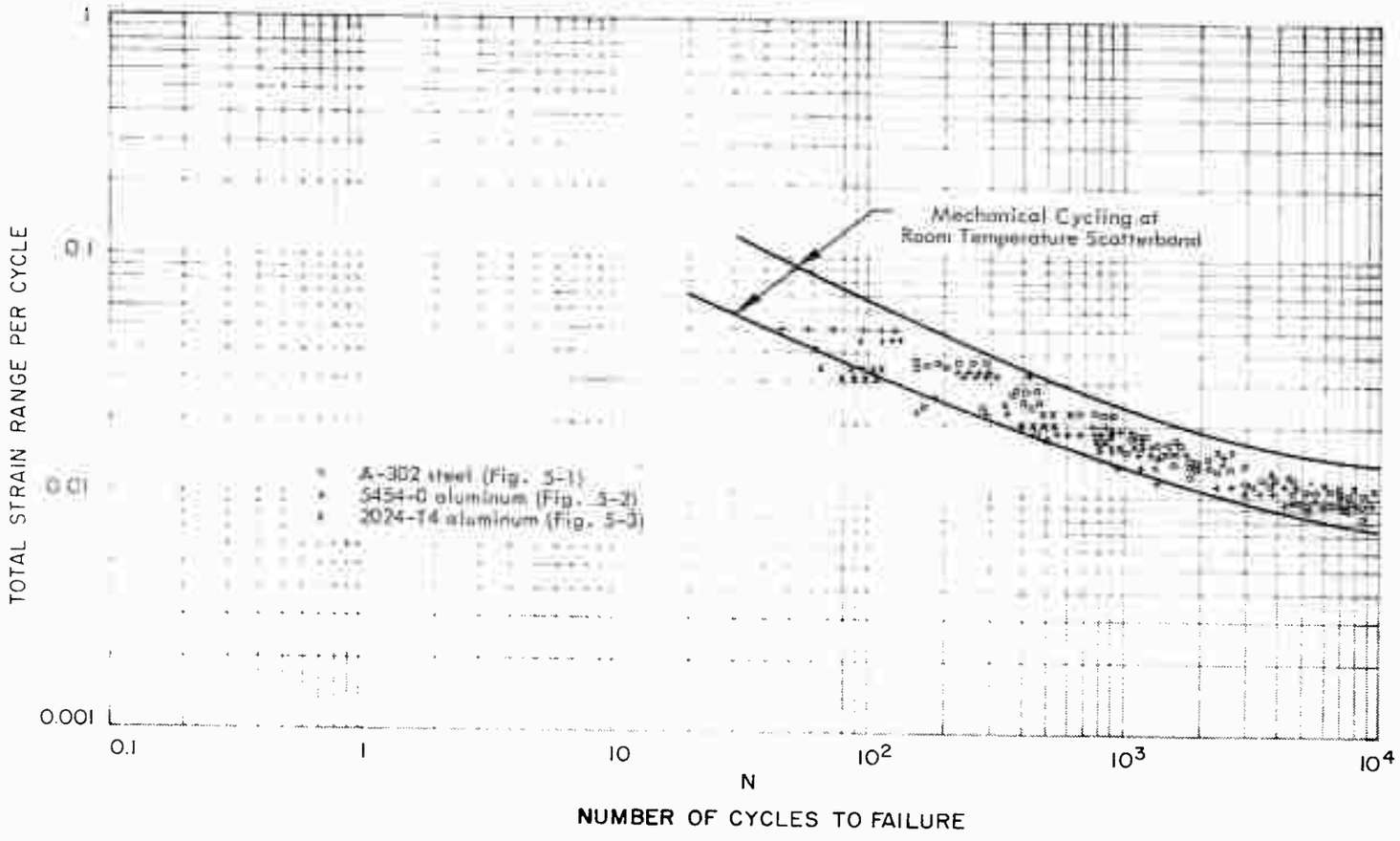

Fig. 1-4 Biaxial Stress Cycling of Three Materials at Various Strain Ratios

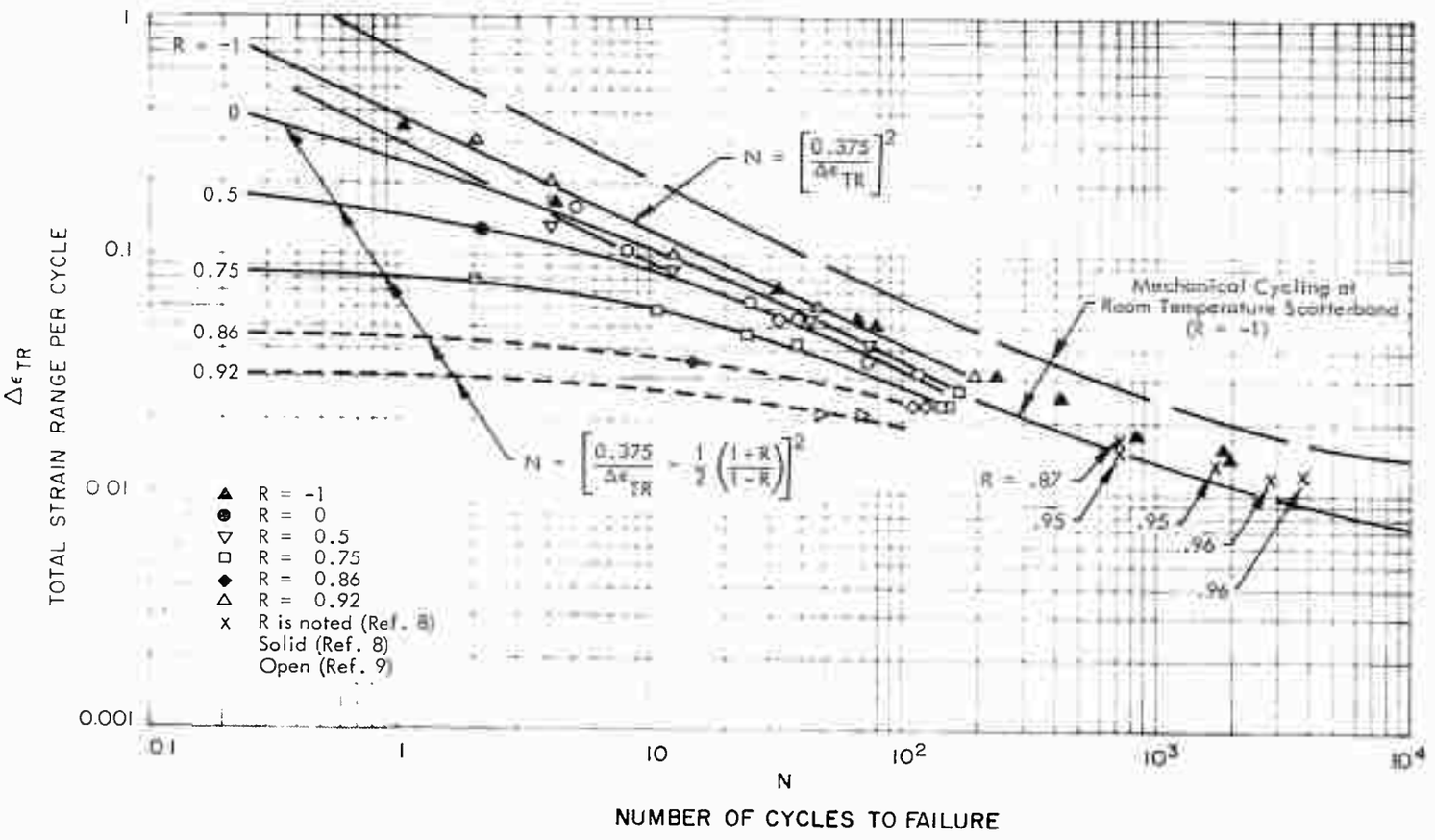

Fig. 1-5 Mechanical Cycling of 2024-T4 Aluminum Alloy at Various Strain Ratios

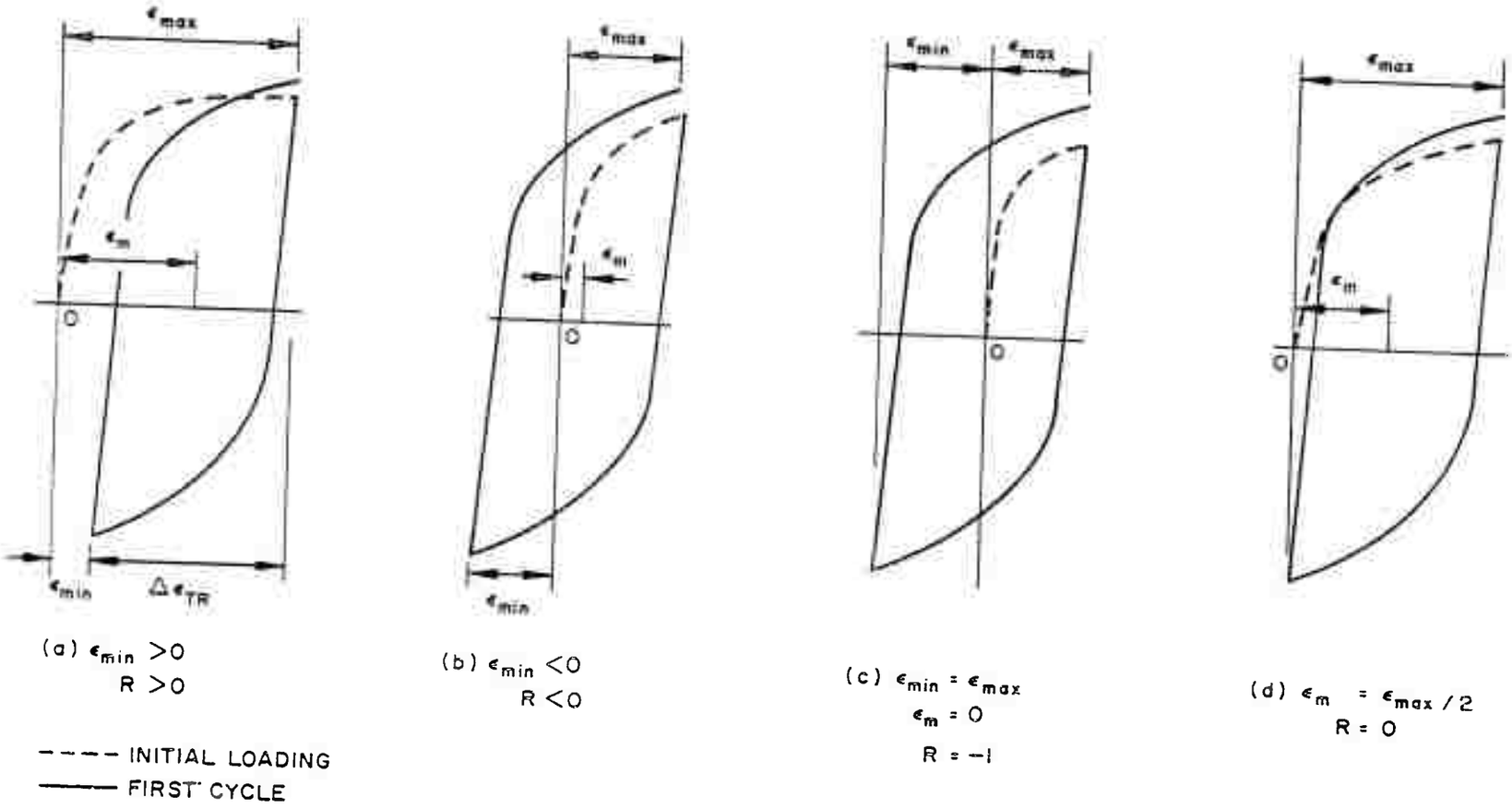

Fig. 1-6 General Types of Mechanical Cycling Possibilities

Section 2

MECHANICAL CYCLING AT ROOM TEMPERATURE

Since this portion of the study is concerned with low-cycle failure or high stressing of materials at room temperature, the time and temperature dependent influences of creep are justifiably assumed to be negligible. In addition to high-stress environment, certain material and geometric parameters are deemed important in their overall effect upon fatigue life. In this section, an attempt will be made to ascertain the significance of each of the following:

1. Amplitude of strain

   $\Delta\epsilon_{TR}$ = total strain range per cycle

   $\Delta\epsilon_{p}$ = plastic strain range per cycle
2. Strain ratio

$$R = \epsilon_{min}/\epsilon_{max}$$

Note: To consider strain ratios other than minus one denotes that a mean strain level exists:

$$\Delta\epsilon_{TR} = \epsilon_{max} - \epsilon_{min}$$

Eliminating ϵ_{min} from the above two equations,

$$\epsilon_{max} - \Delta\epsilon_{TR} = R\epsilon_{max}$$

$$\epsilon_{max} = \frac{\Delta\epsilon_{TR}}{1 - R}$$

$$\epsilon_m = \frac{\epsilon_{max} + \epsilon_{min}}{2} = \frac{\epsilon_{max}(1 + R)}{2}$$

$$= \frac{\frac{\Delta\epsilon_{TR}}{1 - R}\left[1 + R\right]}{2}$$

$$= \frac{\Delta\epsilon_{TR}}{2}\left(\frac{1 + R}{1 - R}\right) \qquad (2.1)$$

3. Cycle frequency
4. Specimen geometry
   a. Plates, bars
   b. Stress concentrations due to notches
5. Cumulative damage
   a. Programmed strain cycling
   b. Sequence of loading
6. Material properties
   a. Grain size
   b. Prestrain condition (strain-hardened or annealed)

2.1 AMPLITUDE OF STRAIN

From an extensive review of the literature pertaining to mechanical stress cycling at room temperature, a single expression for predicting low-cycle fatigue appears with regularity. The typical correlation expression is of the following basic form:

$$N \left[\frac{\epsilon_f}{\Delta\epsilon_p}\right]^2$$

where N = number of cycles to failure

ϵ_f = fracture ductility of the material

$\Delta\epsilon_p$ = plastic strain range per load cycle

A detailed discussion of the development of this equation is given in Section 6. Also, a comparison is made of the various equivalent forms of the expression which have been recommended by different investigators of low-cycle fatigue.

Graphical presentation of cyclic strain data have customarily been made in either of two ways (Ref. 10):

- Deformation approach – indicates the resistance of a material to strain cycling. Stress range is presented as a function of cycles of strain for various constant applied ranges of plastic strain. (See Fig. 2-1 for a schematic plot.) The representative curves are dependent upon the degree of prestrain and upon the amplitude of the diametral strain range through which the material is cycled.

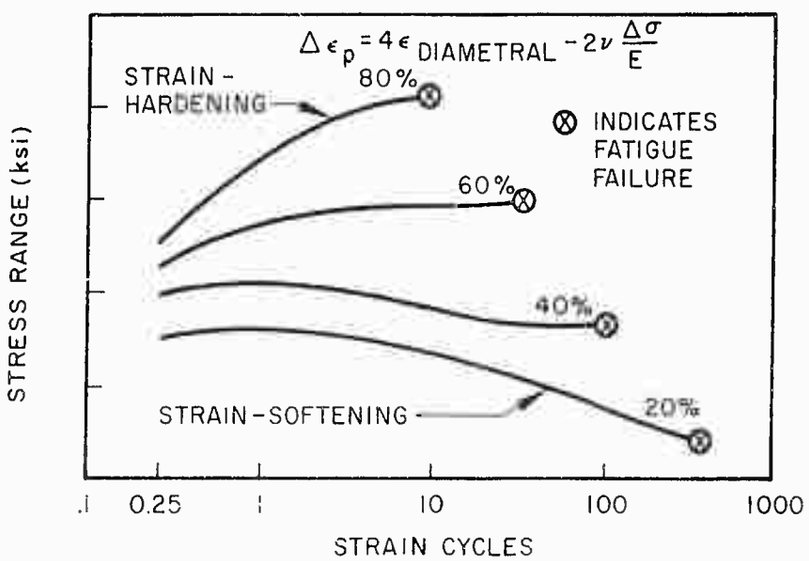

Fig. 2-1 Deformation Approach to Low-Cycle Fatigue

- Fracture approach – the relationship between cyclical range of plastic strain and cycles to failure is plotted (see Fig. 2-2). Since the curve in Fig. 2-2 adequately correlates the end result (i.e., the values of N), the fracture approach will be adopted to describe fatigue data.

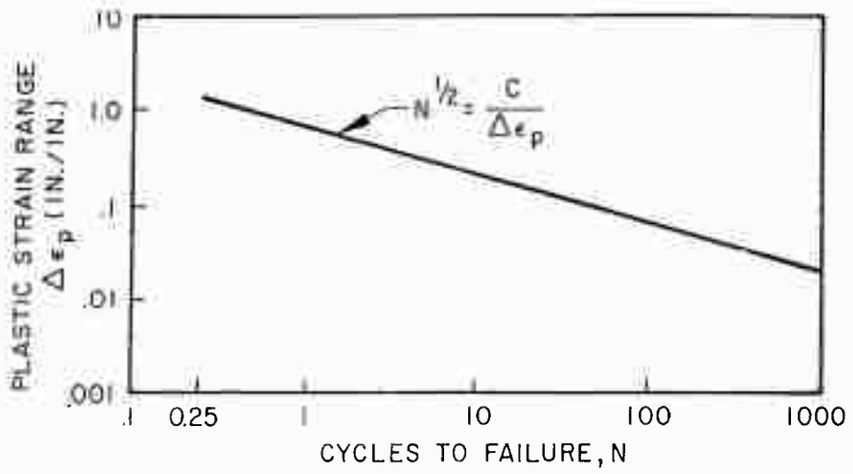

Fig. 2-2 Fracture Approach to Low-Cycle Fatigue

Excellent correlation of endurance N for mechanical cycling has been obtained on log-log plots by selecting ranges of total strain per cycle ($\Delta\epsilon_{TR}$) as the ordinate. True total strain is much easier to define and more directly obtained from test measurement than plastic strain. Also, for low-cycle failure, the plastic strain is so large compared to the elastic component that $\Delta\epsilon_p \approx \Delta\epsilon_{TR}$. Figure 2-3 indicates the narrow scatter-band of test data measured on 2024-T4 aluminum specimens. These data are for a mean strain level, ϵ_m, of zero and comprise results of tests performed upon round, tapered (hourglass-shaped) specimens under axial loading. Note how closely the dashed line drawn at a slope of -1/2 fits the low-cycle region.

A similar grouping of points is seen in Fig. 2-4, which shows Low's short-endurance fatigue values pertaining to various steel and aluminum alloys (Ref. 11). This test, again at a mean strain of zero, was conducted with flat, rectangular pieces having good ductility and loaded in reversed bending.

Figure 1-1 presents a composite of room temperature mechanical cycling data. The log-log straight-line relationship and associated slope of -1/2 still is quite apparent. Superimposed on the plot is a correlative equation which will conservatively predict

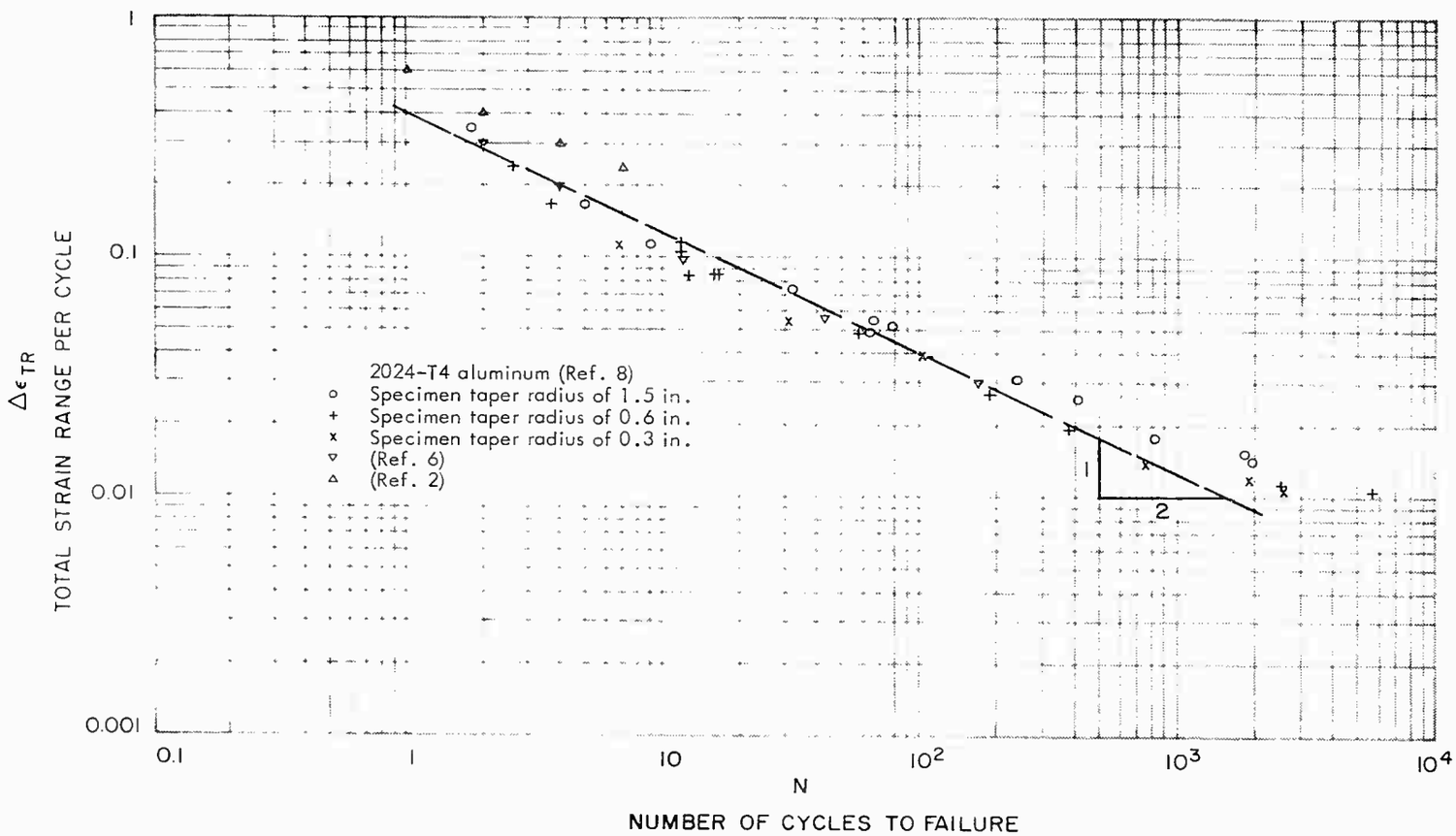

Fig. 2-3 Mechanical Cycling of 2024-T4 Aluminum at Room Temperature

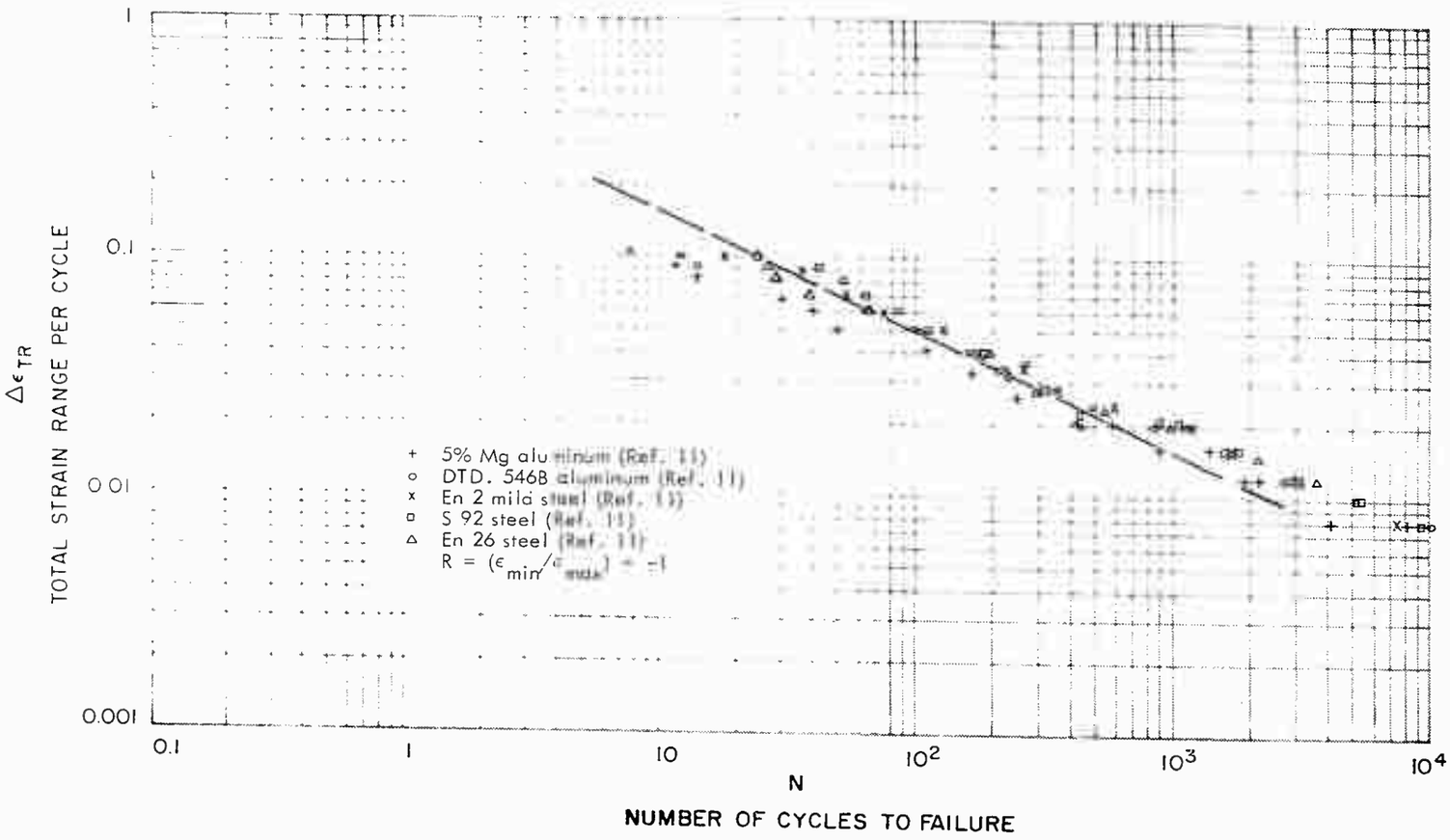

Fig. 2-4 Mechanical Cycling of **Various Materials** at Room Temperature

cycles-to-failure. Considering the limits of the band of data, it appears possible to predict confidently fatigue life well within an order of magnitude.

2.2 STRAIN RATIO

The effects of the strain ratio parameter R have been pointed out by several of the investigators, chiefly Pian and D'Amato (Ref. 6), and Sachs, Gerberich, and Weiss (Ref. 9). As stated in Eq. (2.1) the existence of a strain ratio, R , other than minus one is indicative of fatigue cycling about a mean strain level. At high levels of mean strain (especially in combination with high levels of cyclical strain range) fatigue life is definitely affected, as Fig. 1-5 clearly shows. To account for strain ratio, the equation given by Sachs, Gerberich, and Weiss (Ref. 9) is recommended. This is of the form:

$$N = \left[\frac{\epsilon_f - \epsilon_m}{\Delta\epsilon_{TR}}\right]^a \tag{2.2}$$

or, expressed in terms of strain ratio with the exponent (a) evaluated as two, the cycles-to-failure becomes:

$$N = \left[\frac{\epsilon_f}{\Delta\epsilon_{TR}} - \frac{1}{2}\left(\frac{1 + R}{1 - R}\right)\right]^2 \tag{2.3}$$

The latter expression appears later as Eq. (6.6c) and is described in more detail.

2.3 CYCLE FREQUENCY

The effects of loading frequency upon room-temperature fatigue life seem to be negligible as indicated by Lin and Kirsch (Ref. 5). These authors cited studies which had been conducted by others on unnotched sheet specimens of 2024-T3 with complete stress reversal at frequencies of 12 to 1000 cpm. The fatigue strength was very slightly lower at 12 cpm, but scatter made quantitative estimates impossible. The consensus among those who have investigated frequency is that no noticeable effect results from frequency changes in applied loading.

2.4 SPECIMEN GEOMETRY

Specimen geometry is the next parameter to be considered. As indicated previously and as can be seen by comparing best-fit curves of Figs. 2-3 and 2-4 (specimens of circular and rectangular cross-section, respectively), no appreciable effect can be ascertained in strain-cycled specimens of various sections, whether axially-loaded or cycled in reverse bending. Some specific results of tests comparing notched and unnotched specimens of 2024-aluminum alloy have been published by D'Amato and De Boer (Ref. 7) who tested flat-bar, edge-notched configurations having stress concentration factors (K_T) of 2.0 and 4.0 as well as round unnotched specimens. A linear relationship on a log-log plot was again established but a slight offset of the parallel curves (shorter fatigue life for lower K_T at a given range of strain) was measured. These results, for a strain ratio of zero, are shown in Fig. 2-5. When these strain cycling data are normalized to the quarter cycle fracture strain (by dividing all ordinate $\Delta\epsilon_{TR}$ by ϵ_f) they remarkably become nearly coincident. This indicates that starting from a given correlation equation (C_2 defined) for a known stress concentration factor,*

$$N = \left[\frac{C_2}{\Delta\epsilon_{TR}}\right]^2 \tag{2.4}$$

Then the applicable new value of C_2' can be obtained for any other stress concentration, provided the failure ductilities are known – that is,

$$C_2' = C_2 \frac{\epsilon_f'}{\epsilon_f} \tag{2.5}$$

The primes denote values associated with the second value of stress concentration. This tends to indicate that regardless of the material's ductility, life is equal to the square of the ratio of the quarter-cycle fracture strain to the total strain range applied.

---

* See also Eq. (6.10).

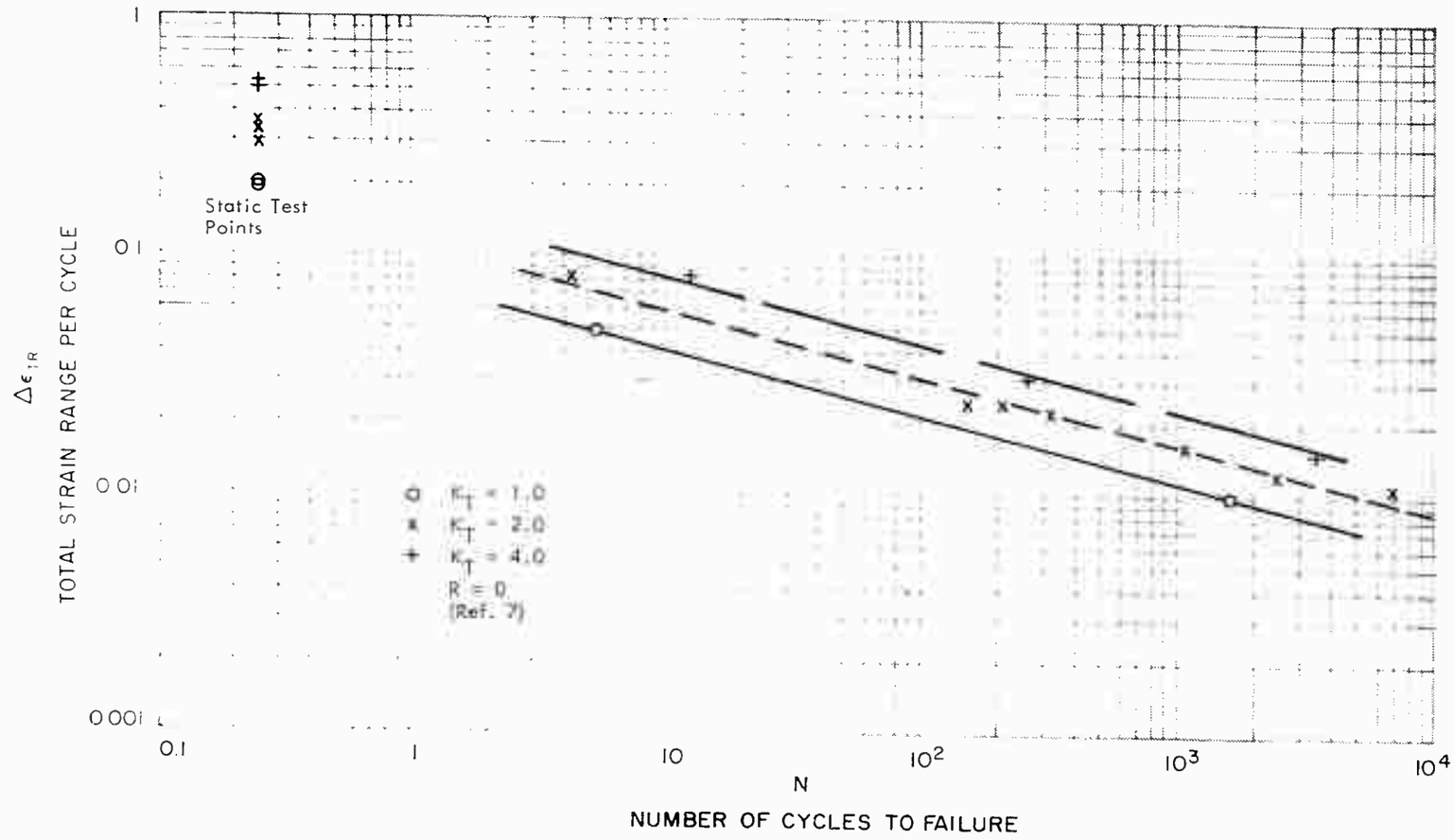

Fig. 2-5 Range of Strain vs. Cycles-to-Failure – Notched and Unnotched Specimens of 2024 Aluminum

Moreover, since biaxial stresses were present in the notched specimens, it appears that the same type of correlation equation exists for biaxial stressing in general. The topic is treated more thoroughly in Section 5.

D'Amato (Ref. 8), in his low-cycle fatigue studies involving axially loaded round specimens, investigated three different taper radii – 0.3, 0.6, and 1.5 inches. These specimens, tested between fixed limits of local strain, represented various notch factors. Tests were conducted at a mean strain of zero. Figure 2-6 shows a very slight improvement in fatigue life for the slightly larger radius specimen. A 1.5-in. taper radius may be considered as essentially unnotched. When these data in the low-cycle fatigue range are normalized (see Ref. 8) to quarter-cycle fracture strain, a single curve with very little scatter results.

2.5 CUMULATIVE DAMAGE

Another important effect in low-cycle fatigue is that of cumulative damage. This includes both a consideration of impressed block patterns and a consideration of the order of the applied straining – that is, whether the higher or lower magnitude strain range, for example, of a two block pattern is applied first. The low-cycle, cumulative-damage aspects of fatigue are particularly important because in actual service applications, a structure is rarely exposed to a single level of cyclic straining. Again, the tests conducted by D'Amato (Ref. 8) appear most significant. He applied two-level strain sequences of eight basic types, in which the combinations consisted of such patterns as a series of cycles at a high mean strain followed by a block at zero mean strain; a block at a high strain range followed by a block to failure at low strain range, both at constant ϵ_{max} ; a series of low-amplitude cycles at $\epsilon_m = 0$ then one high pulse, followed by a continuation of the original, low-amplitude cycles-to-failure.

The Miner's linear cumulative damage relation

$$\sum \left(\frac{n}{N}\right)_i = 1.0 \qquad (2.6)$$

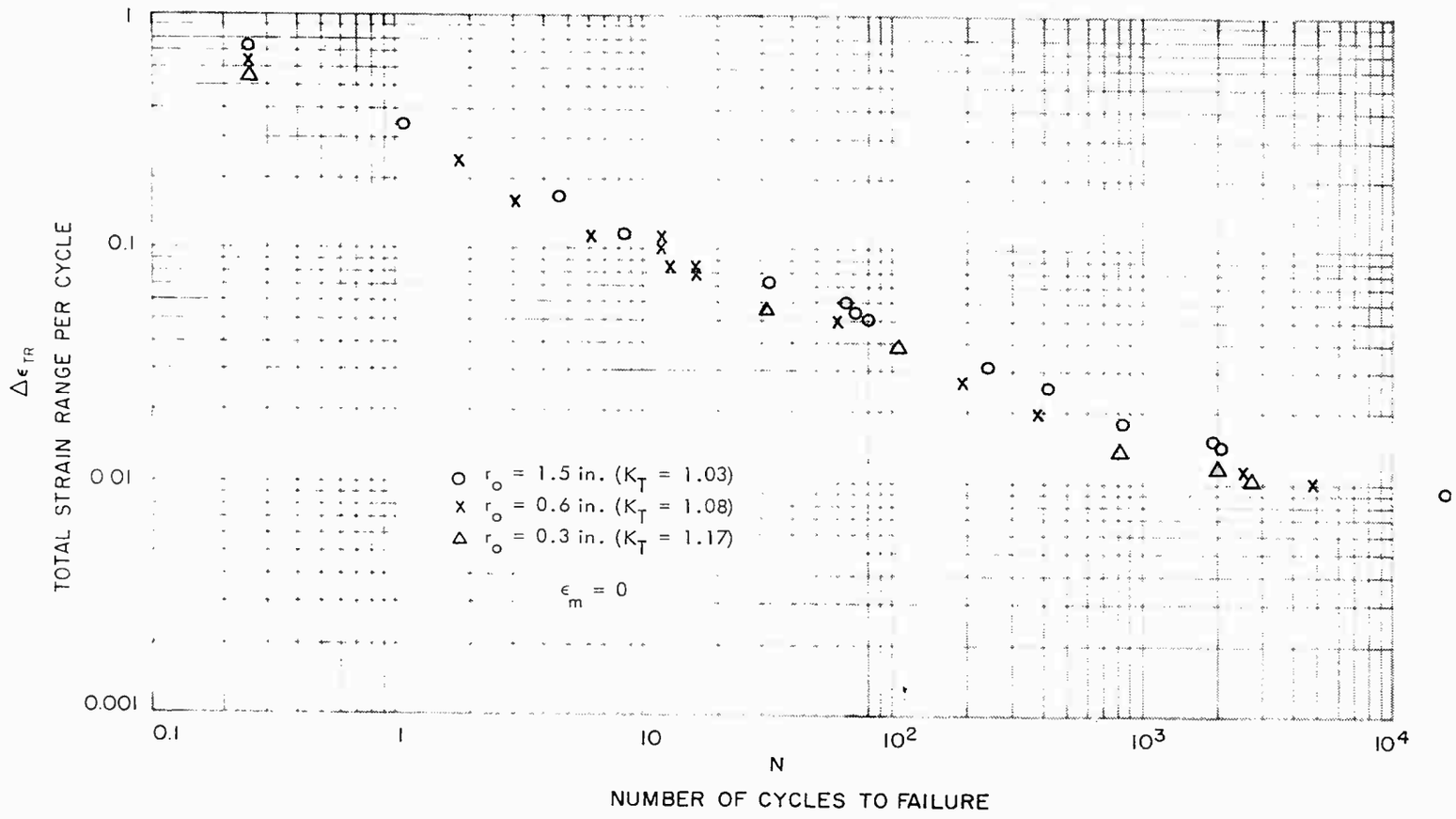

Fig. 2-6 Cycles-to-Failure for Three Configurations of 2024 Aluminum Alloy at Room Temperature

was used in the correlation of data. The number of cycles applied at the i^{th} level of strain is n_i, while N_i is the number of cycles which produce failures at the i^{th} level of strain. The two-level cumulative tests are represented schematically in Fig. 2-7.

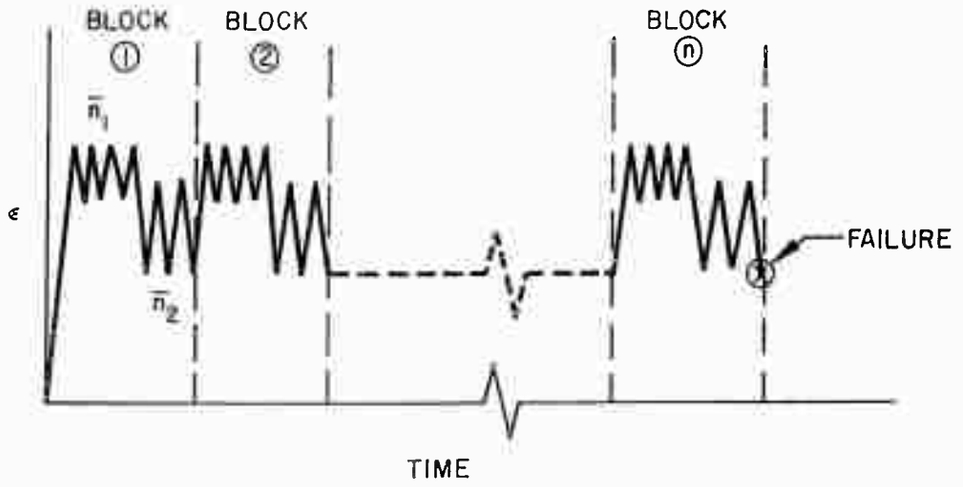

Fig. 2-7 Two-Level Straining Sequence

In Fig. 2-7, let n = total number of repetitive blocks

$\bar{n}_i$ = number of cycles of strain (per block) at the i^{th} level

n_i = total number of applied strain cycles at the i^{th} level ($= n\,\bar{n}_i$)

N_i = number of cycles to produce failure at the i^{th} strain level (determined experimentally)

$\bar{N}_p$ = predicted total cycles to failure

For each of the cases considered, the index $i = 1, 2$.

Re-writing Eq. (2.6) in expanded form, one obtains

$$\frac{n_1}{N_1} + \frac{n_2}{N_2} = 1$$

or

$$n\left(\frac{\bar{n}_1}{N_1} + \frac{\bar{n}_2}{N_2}\right) = 1 \tag{2.7}$$

But the total predicted cycles-to-failure is

$$\bar{N}_p = n(\bar{n}_1 + \bar{n}_2)$$

which gives

$$n = \frac{\bar{N}_p}{\bar{n}_1 + \bar{n}_2} \tag{2.8}$$

Substituting n from Eq. (2.7) into Eq. (2.8) gives, finally,

$$\bar{N}_p = \frac{\bar{n}_1 + \bar{n}_2}{\frac{\bar{n}_1}{N_1} + \frac{\bar{n}_2}{N_2}} \tag{2.9}$$

Using a plot of $\Delta\epsilon_{TR}$ vs. N, a predicted equivalent strain range can be found for the $\bar{N}_p$ derived for Eq. (2.9). Similarly, from a life ascertained from actual tests, an equivalent strain range is determined. D'Amato found the agreement for observed cumulative life and predicted cumulative life to be excellent for all programmed strains. Although Miner's method of prediction was excellent for these tests on 24ST, the method should be verified for other materials cycled at room temperature as well as elevated temperature.

2.6 MATERIAL PROPERTIES

Certain material properties are of interest because of their influence upon fatigue life. The effect of grain size at room temperature, although measurable, appears slight. Coarse-grained materials may be expected to have shorter lives; larger grain size implies larger crack-propagation rates according to an equation given by Valluri (Ref. 12).

Another property to consider is the material's prestrain condition. Coffin and Tavernelli (Ref. 10) have made analyses of materials at room temperature which were either in the fully annealed state or which had various amounts of prior strain hardening. The materials tested include 2S aluminum and OFHC copper. A most interesting conclusion was that cyclic strain tends to remove the effects of prior plastic deformation and restores the metal to that state which it would have achieved for the equivalent amount of strain in the absence of prior deformation. To bear out their findings, they presented deformation-based curves typified by Fig. 2-1. Regardless of the initial strain hardening, the curves, in approaching the cyclic life, appeared similar to those curves which applied to the annealed material and displayed nearly identical cycles-to-failure. Moreover, the stress ranges at failure were in agreement at a given strain-amplitude range. Fatigue failure often limited the process from achieving the equilibrium state. Figure 2-8 shows the results of 2S aluminum tests ($\Delta\epsilon_p$ vs. N). The observed scatter is considered minimal.

The room-temperature cyclic-strain behavior of various structural materials has been considered primarily from a phenomenological standpoint. For better insight into the actual physical processes which precipitate low-cycle failure, further testing is both warranted and recommended.

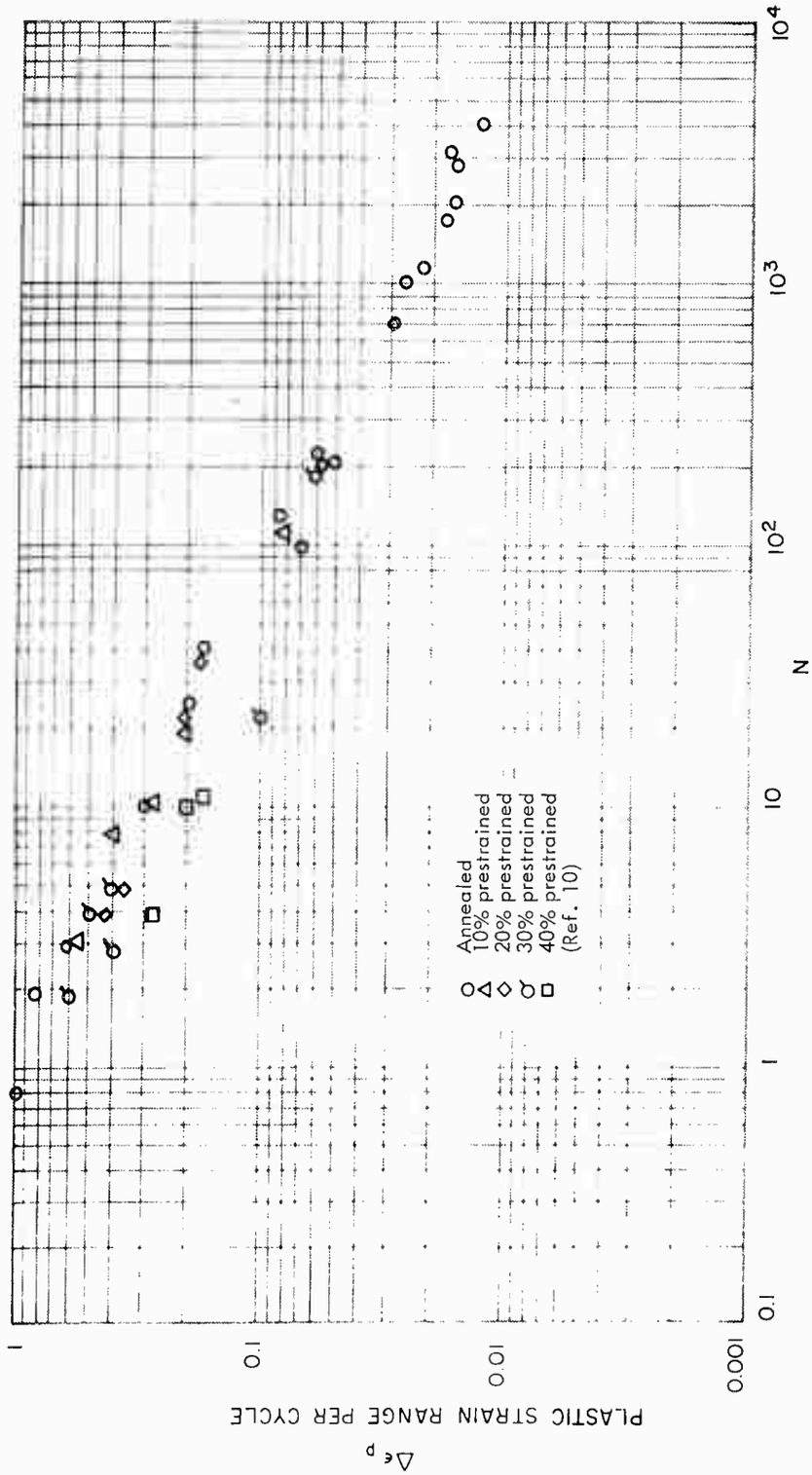

Fig. 2-8 Effect of Prior Strain on Cycles-to-Failure – 2S Aluminum

Section 3

MECHANICAL STRAIN CYCLING AT ELEVATED TEMPERATURES

Strain cycling at elevated temperatures or isothermal cycling have all of the variables present in strain cycling at room temperature plus the variables of temperature and time. As in cycling at room temperature, the total strain range $\left(\Delta\epsilon_{TR}\right)$ is the most important parameter, and cycles-to-failure decrease with an increase in total strain range. Only a slight decrease in life is obtained for a corresponding increase in cycling temperature until a critical temperature is reached when there is an abrupt decrease in life. Cycling at elevated temperatures makes cycle frequency an increasingly important parameter; a decrease in cycle frequency results in a considerable decrease in life. Frequency effects appeared to be insignificant for cycling at room temperature. Although these observations are the result of a limited amount of strain cycling data available from 1/4 to 10,000 cycles, they do show the importance of temperature and time. Additional investigations are necessary to evaluate more fully the effect of temperature and time on strain cycling.

Investigations of fatigue life of unnotched specimens (R = -1) were conducted by Johansson (Ref. 13); Baldwin, Sokol, et al. (Ref. 14); Douglas Aircraft Company (Ref. 15) Swindeman and Douglas (Ref. 16); Majors (Ref. 17); Kennedy and Douglas (Ref. 18); Coffin (Ref. 19); and Kennedy (Ref. 20). The following nine parameters were found to be significant:

1. Strain amplitude
2. Temperature
3. Cycle frequency
4. Load rate
5. Geometry

6. Grain size
7. Fracture ductility
8. Loading sequence
9. Material

3.1 STRAIN AMPLITUDE

The strain amplitude is the most important parameter investigated, since an increase in amplitude results in a decrease in cycles-to-failure. Some investigators recorded total strain range, while others recorded only the plastic strain range. Unfortunately, all investigators did not record both strains for a better comparison of its effect on each material. Figures 3-1 and 3-2 show the effects of total strain range per cycle and Fig. 3-3 shows the effects of plastic strain range per cycle. The total strain is consistent with that obtained from room temperature cycling, but the plastic strain plot varies with each material with scatter considerably greater than that at room temperature. It is possible that all of the materials except the high-strain cycling of the Inconel in Fig. 3-3 would fall within the room-temperature scatter band if the total strains had been recorded or, if in both cases, total strain ranges could have been normalized with respect to their respective and individual quarter-cycle fracture strains.

3.2 TEMPERATURE

The effect of temperature on cycles-to-failure is shown in Figs. 3-4 through 3-10 for five different steels. An increase in temperature has only a slight effect in reducing the cycles-to-failure until a critical temperature is reached; then there is a drastic reduction in life as shown in Fig. 3-10 for P.H. 15-7 Mo-R.H. 950 steel. The critical temperature is very close to the heat-treat temperature for the material.

Johansson's (Ref. 13) investigation of 18-8, 13% Cr, and 3Cr-4Mo steels recorded in Figs. 3-4, 3-5 and 3-6, respectively, show a slight decrease in life with increasing temperatures to 500° C with little scatter. The same observation can be made

for 347 and P.H. 15-7 steels as shown in Figs. 3-7 through 3-9. Only P.H. 15-7 cycled at 900° F showed a drastic reduction of life when an increase in temperature from 800° F to 900° F decreased the life from 2,000 cycles to 7 cycles. In other testing at the same temperature range for the same material, but at a more critical stress ratio (Fig. 3-8 and 3-9), a drastic reduction of life was not observed; therefore, at this critical temperature, there possibly would have been an extreme scatter in the results had there been sufficient data available. It is likely that the critical temperature where the metal becomes unstable is the heat-treat temperature. For structural soundness, this temperature should be avoided.

3.3 CYCLE FREQUENCY

The effects of cycle frequency are recorded in Figs. 3-8 through 3-11. The cycle frequency of 10 cpm and 700 cpm investigated by Douglas Aircraft Co. (Ref. 15), for P.H. 15-7 through a temperature range of 70° F to 900° F, had no effect on cycles-to-failure. Swindeman and Douglas' (Ref. 16) investigation of Inconel at 1500° F (Fig. 3-11) at frequencies of 1/2 and 1/30 cpm showed that a slight reduction of life was obtained at 1/30 cpm at lives up to 100 cycles. Above 100 cycles, an appreciable reduction is observed which indicates that time is an important parameter. Possibly, only the influence of time at temperature introduced creep effects into the results. Additional testing will be required to evaluate thoroughly the cycle-frequency effect.

3.4 LOAD RATE

Swindeman and Douglas studied the effect of cycle loading at a particular frequency on the number of cycles-to-failure. They tested Inconel at periods of 2 minutes per cycle using two different loading methods to determine the resultant effect. The first method, which they called creep cycling, was done by using a constant load and by creeping the test specimen to the desired strain. The second method, termed relaxation, was done by loading the specimen rapidly to the desired strain, then holding at that strain for the cyclical period. These two methods of loading resulted in no change in life as shown in Fig. 3-12 for Inconel at 1500° F.

3.5 GEOMETRY

The specimen geometry was investigated by Swindeman and Douglas. Most of the thermal cycling was done on hollow specimens, while the isothermal tests were on solid specimens. The effect of geometry should perhaps be questioned in comparing their test results. Figure 3-13 shows that at 1600° F, the Inconel tube and rods fail within the same scatterband, indicating no appreciable difference in results due to geometry. The rod data are on the high side and could be attributed to the grain size since the Inconel rod has finer grain than Inconel tubes.

3.6 GRAIN SIZE

The effect of grain size on cycle-to-failure on Inconel is shown in Fig. 3-14 for fine grain and Fig. 3-15 for coarse grain. At all temperatures – 1300, 1500, and 1600° F – the fine grain results in more fatigue life for the same plastic strain range $(\Delta\epsilon_p)$.

3.7 FRACTURE DUCTILITY

Fracture ductility (ϵ_f), which is the amount of true strain at failure for a static tensile test at $N = 1/4$ cycle, is an important parameter used in the equation for predicting cycles-to-failure. Baldwin, Sokol and Coffin (Ref. 14) compare the fracture ductility for type-347 stainless steel at various temperatures, with the constant "C" in equation $N^k \Delta\epsilon_p = C$. Their assumption was that $k = 1/2$; then $C = \epsilon_f/2$ when $N = 1/4$ and $\Delta\epsilon_p = \epsilon_f$. As the cycles decrease with an increase in temperature for a constant $\Delta\epsilon_p$, the fracture ductility (ϵ_f) does not decrease as the equation requires. A comparison of $2C$ with ϵ_f is shown in Table 3-1. The constant $2C$ varies from 0.86 to 1.90, while ϵ_f varies from 0.59 to 1.32 with the largest discrepancy at the higher temperatures; therefore, the correlation is not very good. The discrepancy may lie in the determination of C, since there is not sufficient data between $N = 1/4$ and 1000 cycles for isothermal testing to evaluate accurately the fracture ductility parameter, C, with the relationship $N^k \Delta\epsilon_p = C$.

Table 3-1

COMPARISON OF CONSTANT C WITH ACTUAL FRACTURE DUCTILITY (ϵ_f), WHERE $\epsilon_f = \ln A_o/A$, FOR TYPE 347 STAINLESS STEEL

($K = 1/2$, $N = 1/4$, $\Delta\epsilon_p = \epsilon_f$, and $2C = \epsilon_f$)

Shape	Grain Direction	ASTM Grain Size	Temp. (°C)	2C	ϵ_f
Rod	Long	7	R.T.	1.90	1.32
Rod	Long	7	200	1.56	1.30
Rod	Long	7	350	1.40	1.03
Rod	Long	7	500	1.18	1.09
Rod	Long	7	600	0.86	1.13
Plate 14993	Long	4 to 6	350	1.46	1.20
Plate 14993	Trans	4 to 6	350	1.16	0.59
Plate 15277	Long	4 to 6	350	1.46	1.06
Plate 15277	Trans	4 to 6	350	1.16	0.59
Pipe	Long	7	R.T.	1.50	1.20
Pipe	Trans	7	R.T.	1.20	1.11
Plate	Long	4 to 6	R.T.	1.40	1.19
Plate	Long	1 to 5	R.T.	1.18	1.26
Rod	Long	7	350	1.84	1.11
Rod	Long	2	350	1.70	1.18

3.8 LOADING SEQUENCE

Sequence of loading effect on cycles-to-failure was investigated by Baldwin, Sokol and Coffin for type-347 stainless steel at 350° C at very low plastic strain ranges. Only a slight effect in total cycles-to-failure was obtained for the eight sequences of testing. The use of Miner's linear rule indicated that initial low-amplitude strain cycling accumulated more damage (percent of life was higher) than for the tests where the high strains were cycled first. Table 3-2 lists the cycle plastic strains for each test, the total number of cycles-to-failure, and percent of life. The "A" tests were first cycled at a definite number of high strains, then cycled at a lower strain until failure. Tests "B" and "D" were cycled opposite to the "A". The two "C" tests were cycled at three strain levels. This testing was done at very low plastic strain ranges, and testing at higher total strain ranges could possibly improve the results. D'Amato (Ref. 8) did cycle 24ST at room temperature at higher magnitude total strain ranges and obtained excellent results using Miner's linear rule.

3.9 MATERIALS

The eight materials that were cycled at elevated temperatures are shown in Figs. 3-1, 3-2, and 3-3. Four of the steels were within the room temperature scatterband of total strain vs. cycles-to-failure. The other four materials tested had recorded the plastic strain only, and these are plotted in Fig. 3-3 along with the scatterband for room-temperature cycling. This plot of plastic strain does not result in a single band but is scattered throughout the chart giving a single straight line whose slope varies with each material. It is possible that if the total strains were known for these last four materials, then only the high-strain cycles for Inconel would not lie within the room-temperature band.

The following summarizes the effects of the three important parameters on cycles to failure for isothermal cycling:

- Total strain range is predominant
- Temperature has little effect until a metallurgically critical temperature is reached
- Very low cycle frequency is more detrimental to fatigue life.

Table 3-2

RESULTS OF SEQUENTIAL STRAIN-CYCLING TESTS
AT 350° C ON 347 STAINLESS STEEL

Test	p (%)	N	% of Life
A-1	1.05 .60	1,000 30,544 31,544	99
A-2	1.02 .64	3,000 17,117 20,117	97
A-3	1.00 .64	6,000 15,486 21,486	122
B-1	.61 1.03	3,000 11,300 14,300	154
B-2	.60 1.04	10,000 9,056 19,056	144
B-3	.60 1.06	20,000 4,322 24,322	112
C-1	1.19 .77 .60	1,509 2,536 21,350 25,395	88
C-2	1.21 .81 .61	1,449 2,888 23,934 27,731	112
D-1	.61 1.00	13,000 12,900 25,900	199

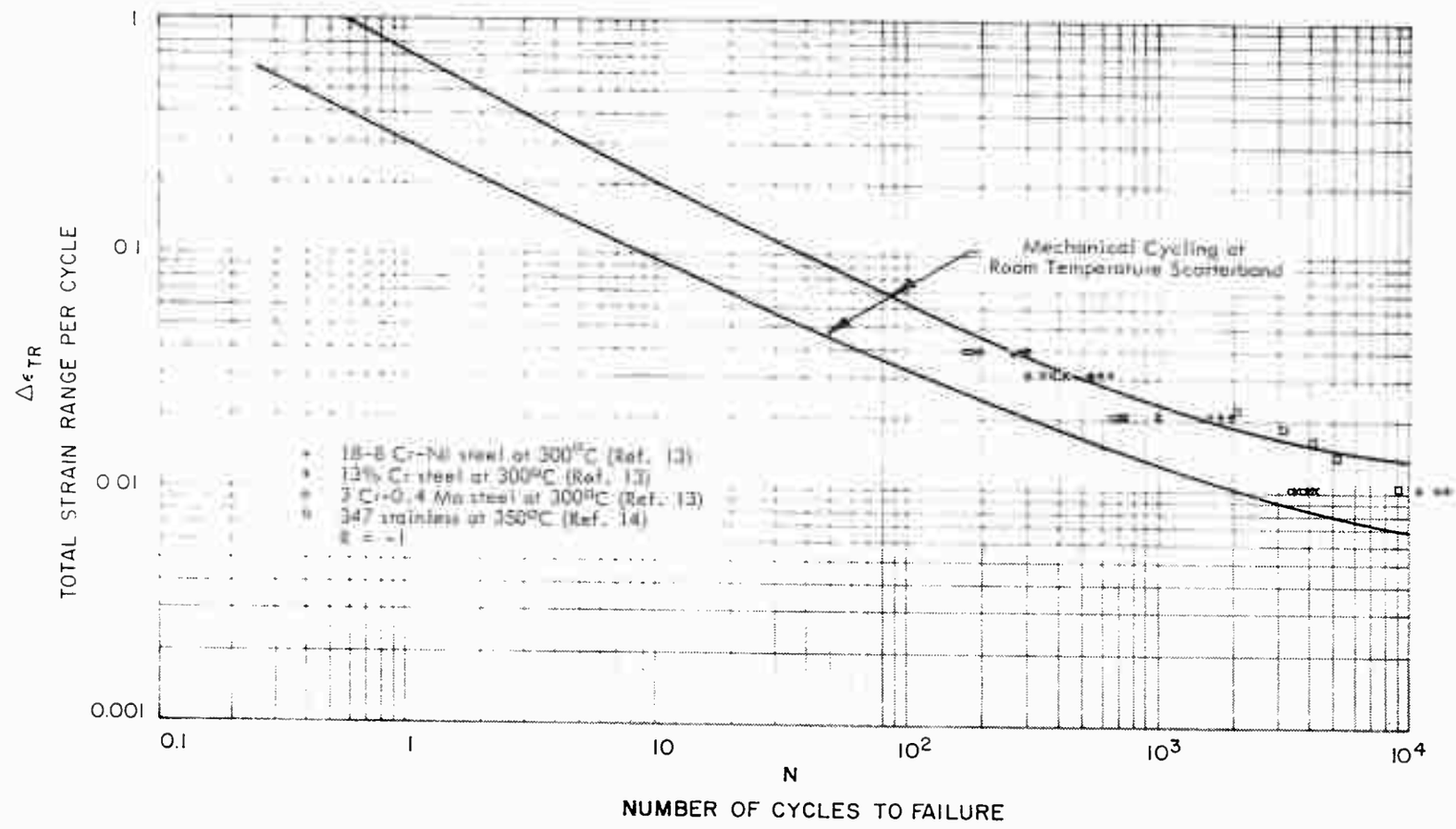

Fig. 3-1 Mechanical Cycling of Various Steels at 300° C

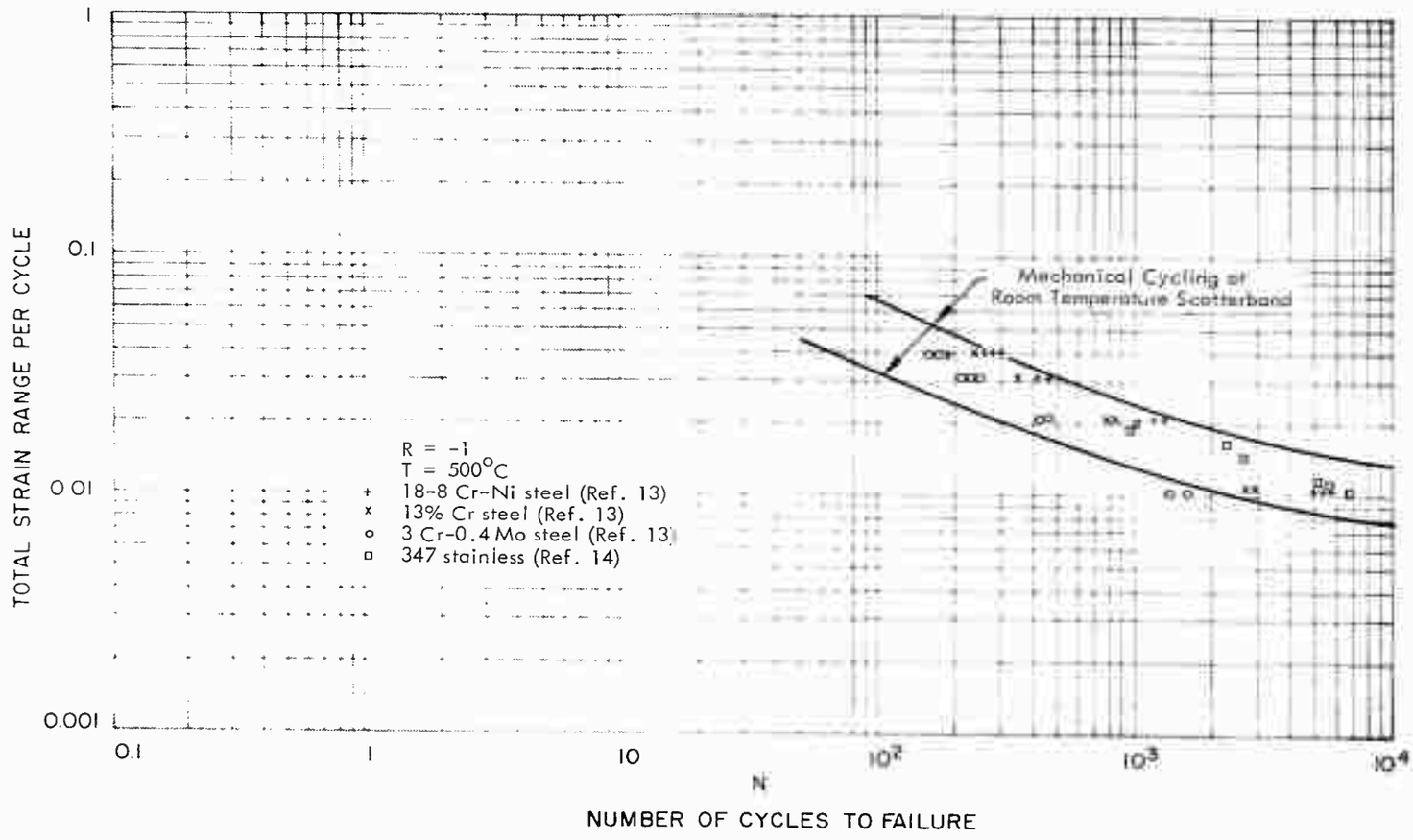

Fig. 3-2 Mechanical Cycling of Various Steels at 500°C

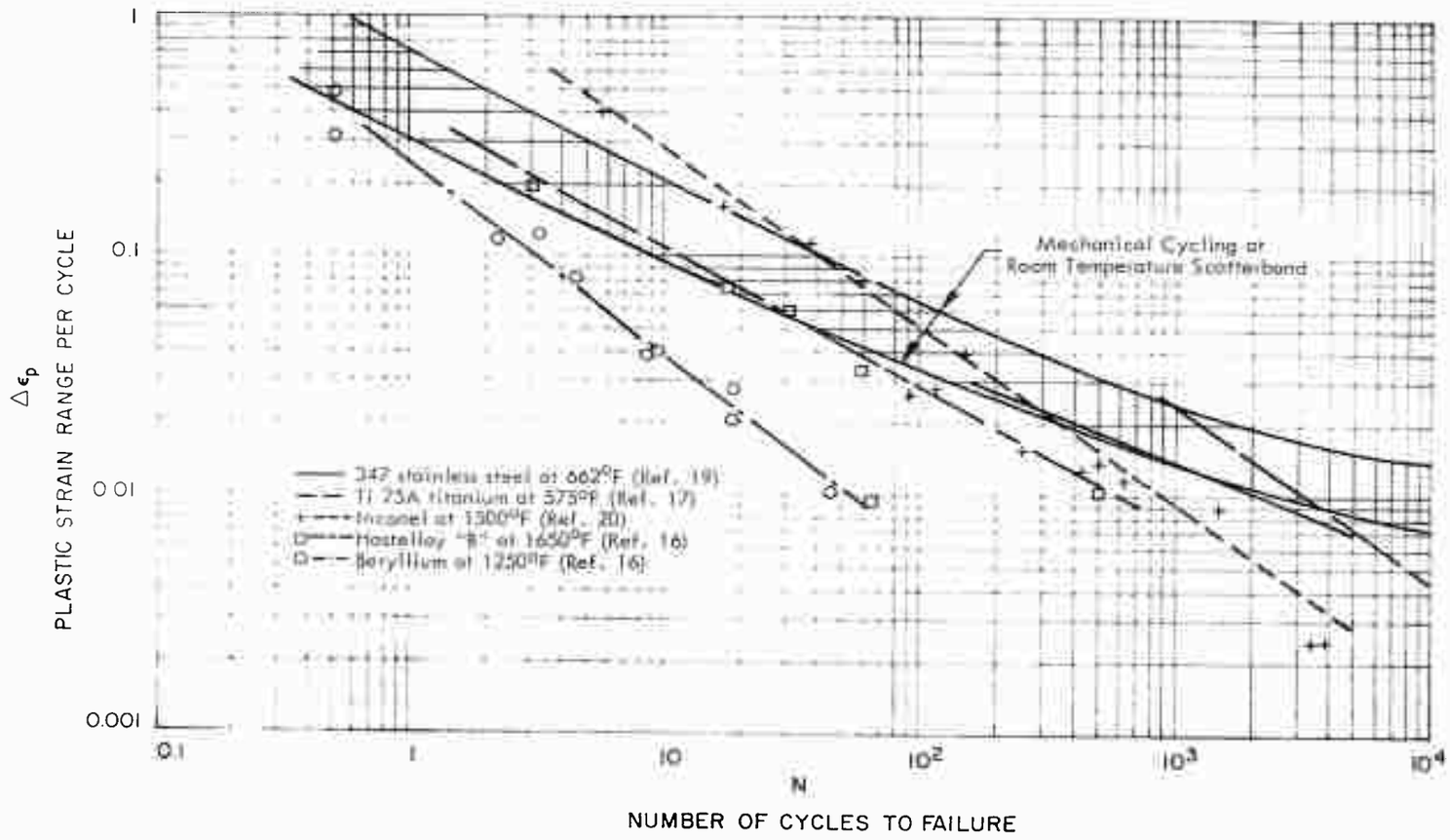

Fig. 3-3 Mechanical Cycling of Various Materials at Elevated Temperatures

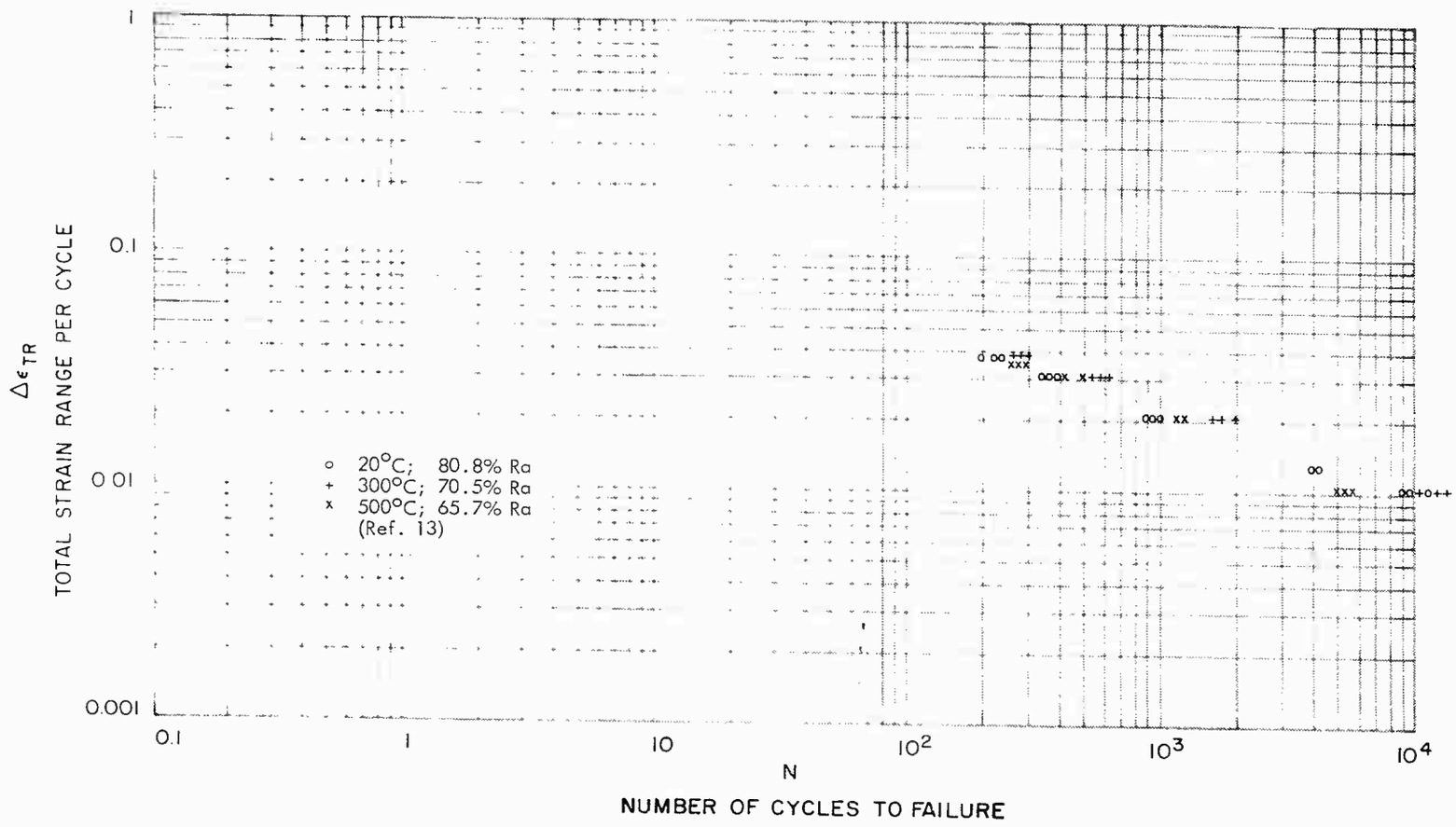

Fig. 3-4 Mechanical Cycling of 18-8 Steel at Elevated Temperatures

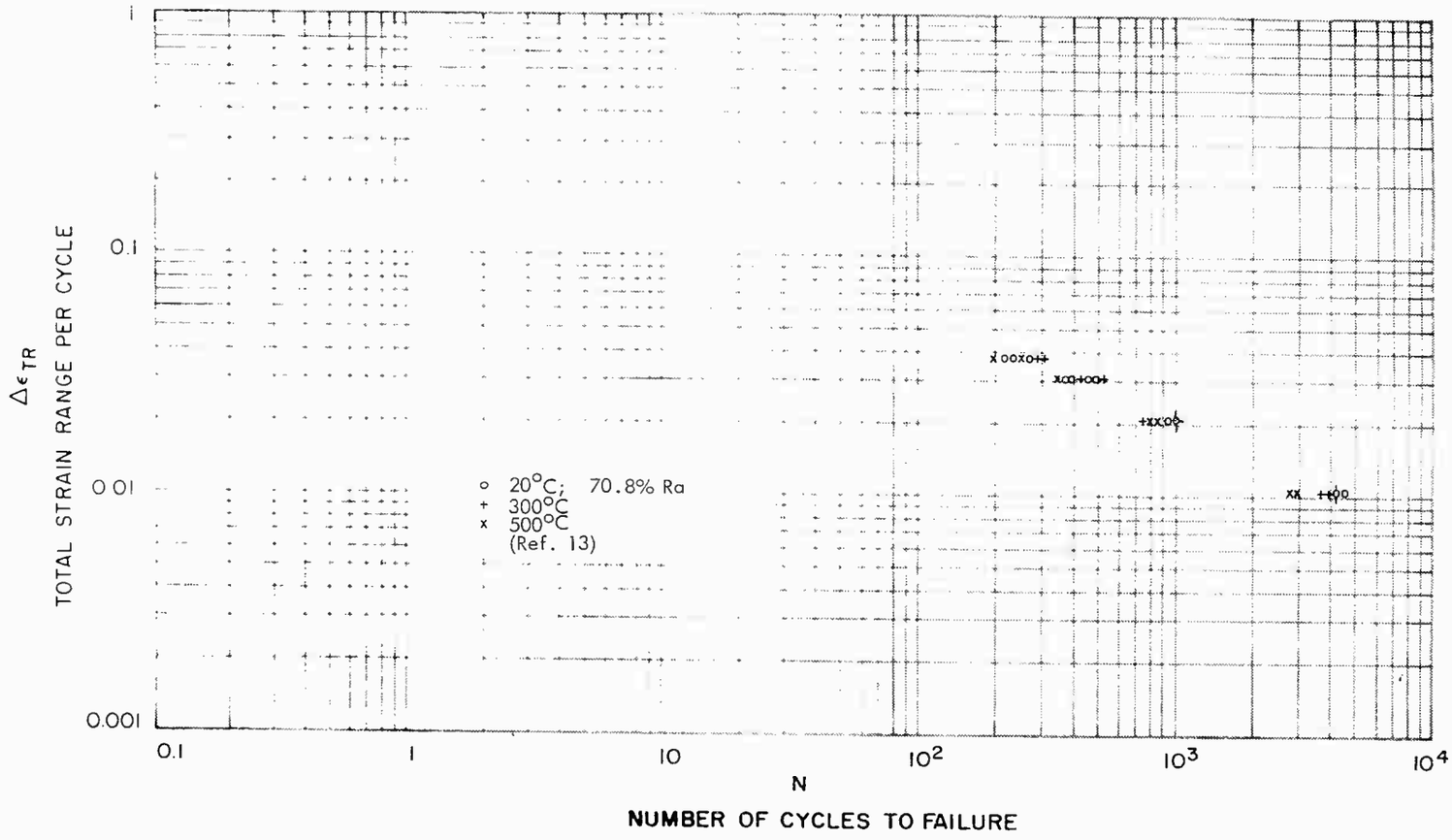

Fig. 3-5 Mechanical Cycling of 13% Cr-Steel at Elevated Temperatures

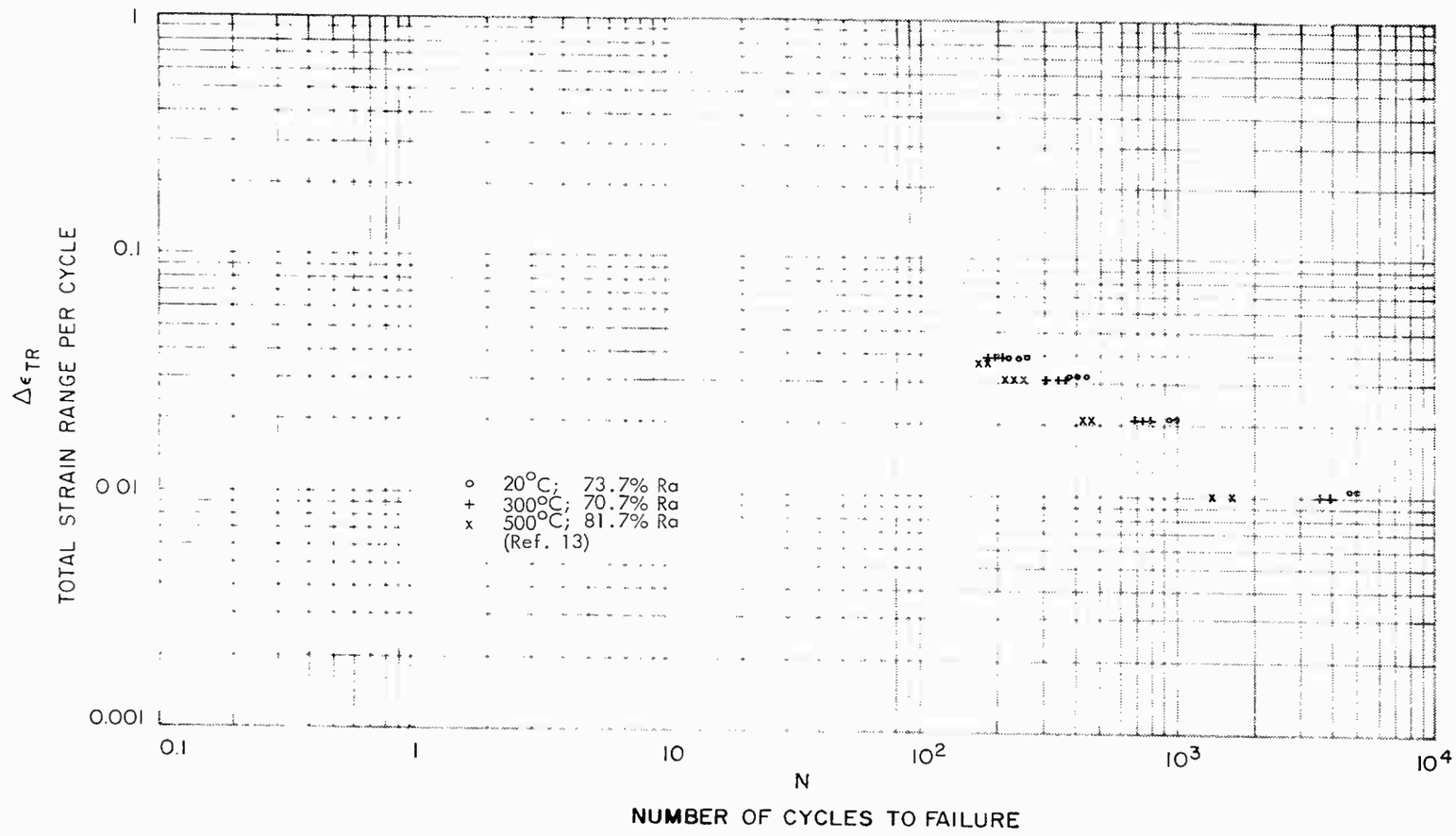

Fig. 3-6 Mechanical Cycling of 3Cr-0.4Mo Steel at Elevated Temperatures

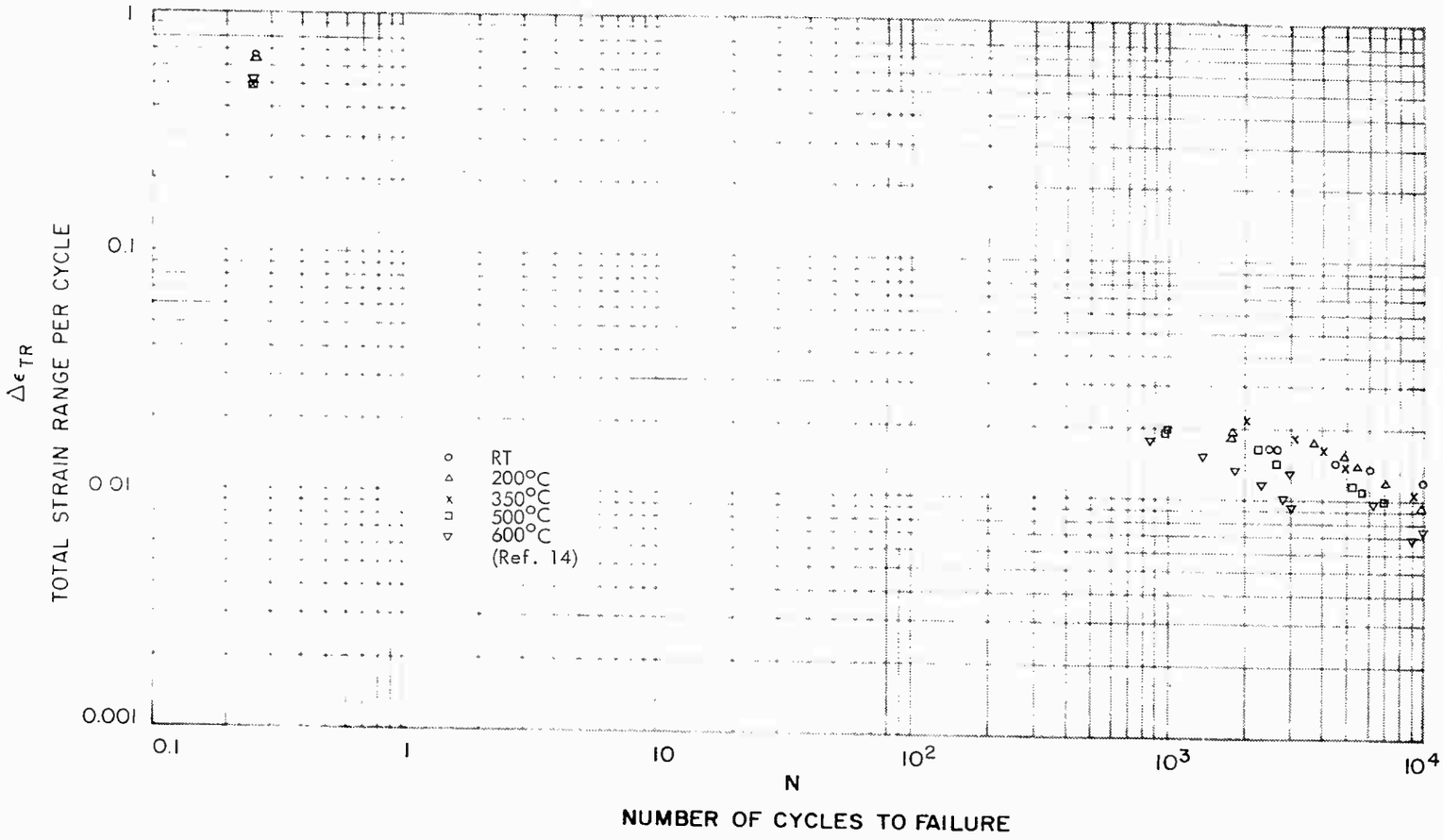

Fig. 3-7 Mechanical Cycling of Type-347 Stainless Steel at Elevated Temperatures

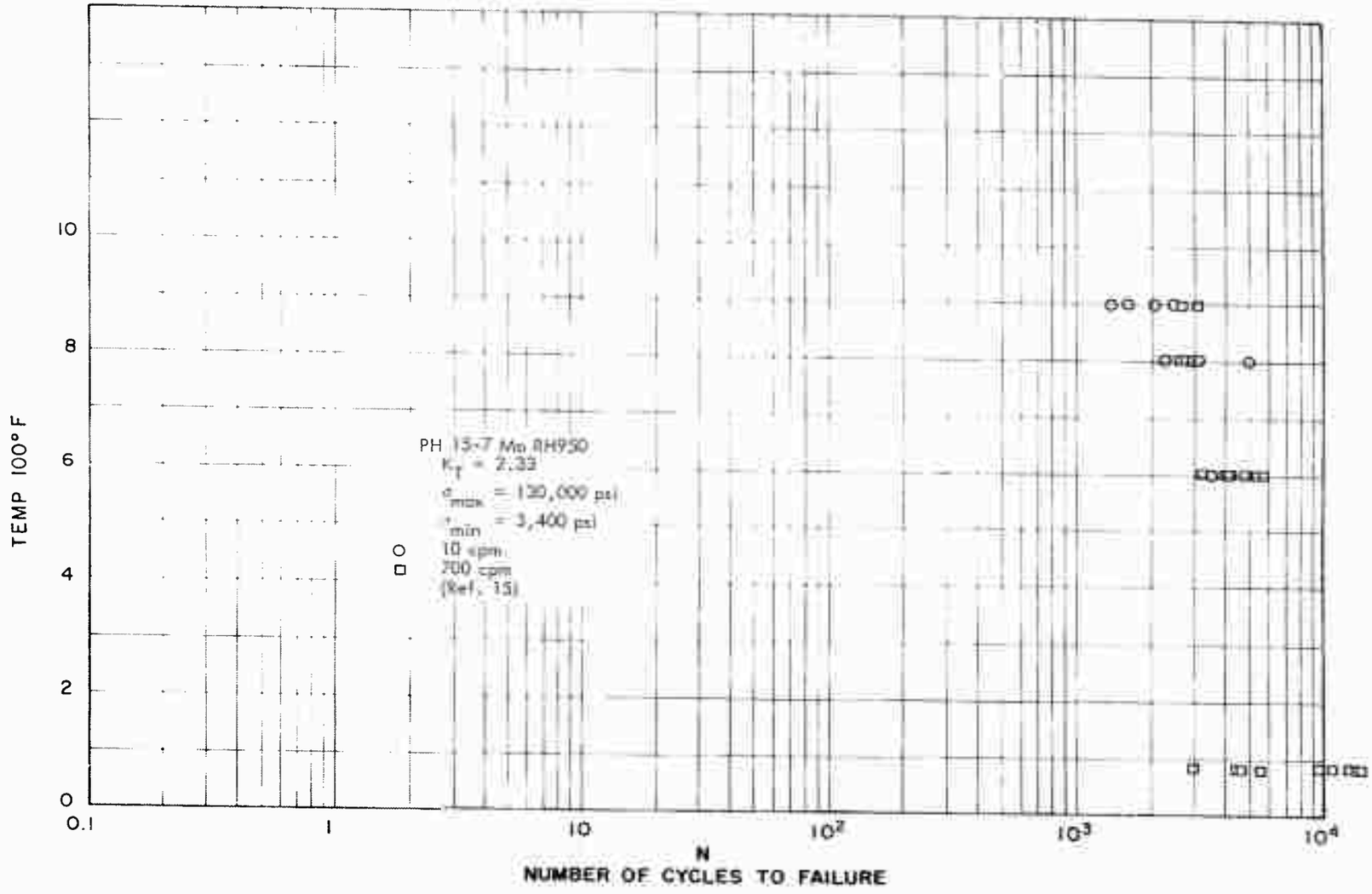

Fig. 3-8 Effect of Temperature on Mechanical Cycles-to-Failure for P.H. 15-7 Steel (σ_{max} = 130,000 psi)

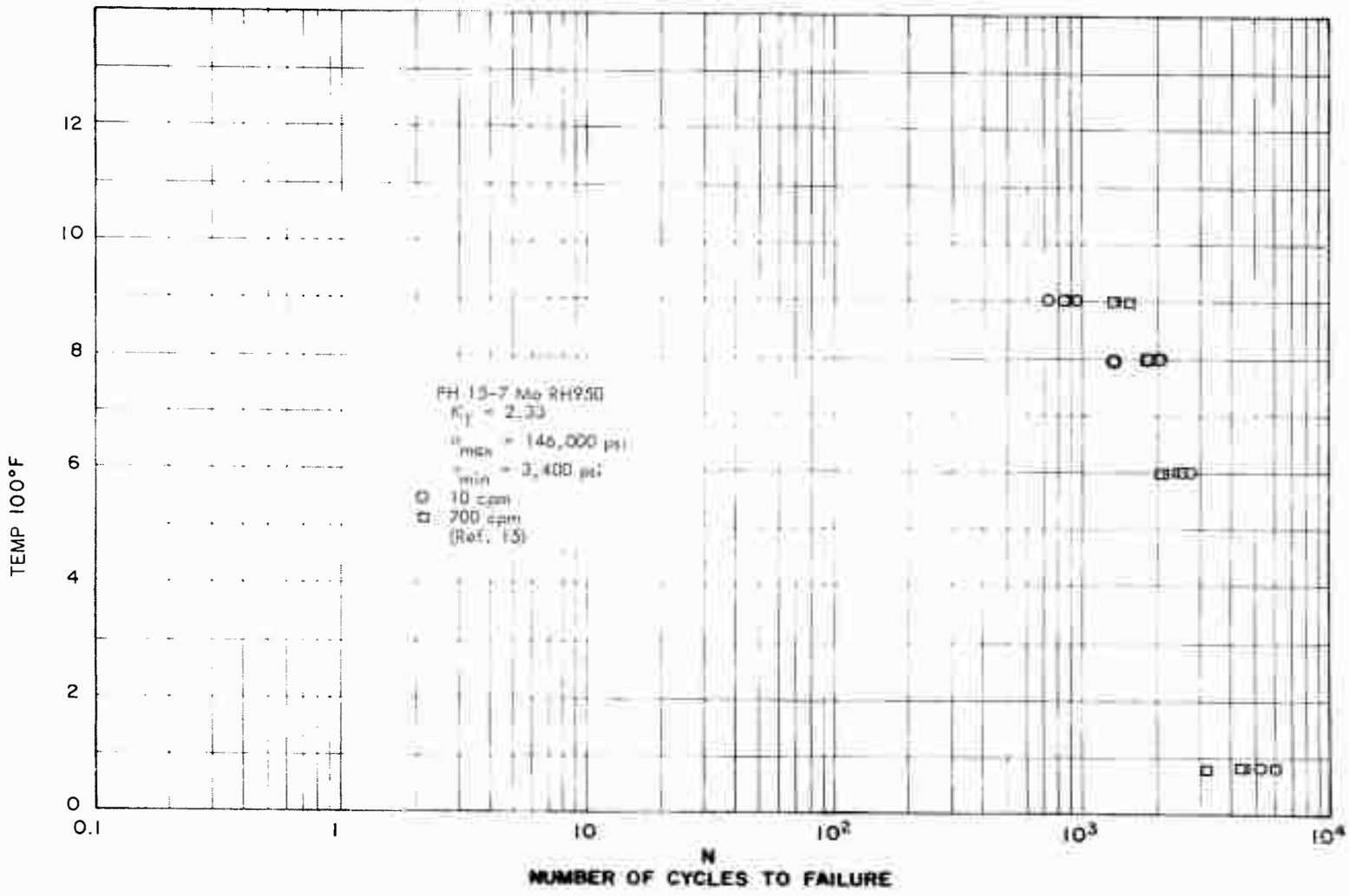

Fig. 3-9 Effect of Temperature on Mechanical Cycles-to-Failure for P.H. 15-7 Steel (σ_{max} = 146,000 psi)

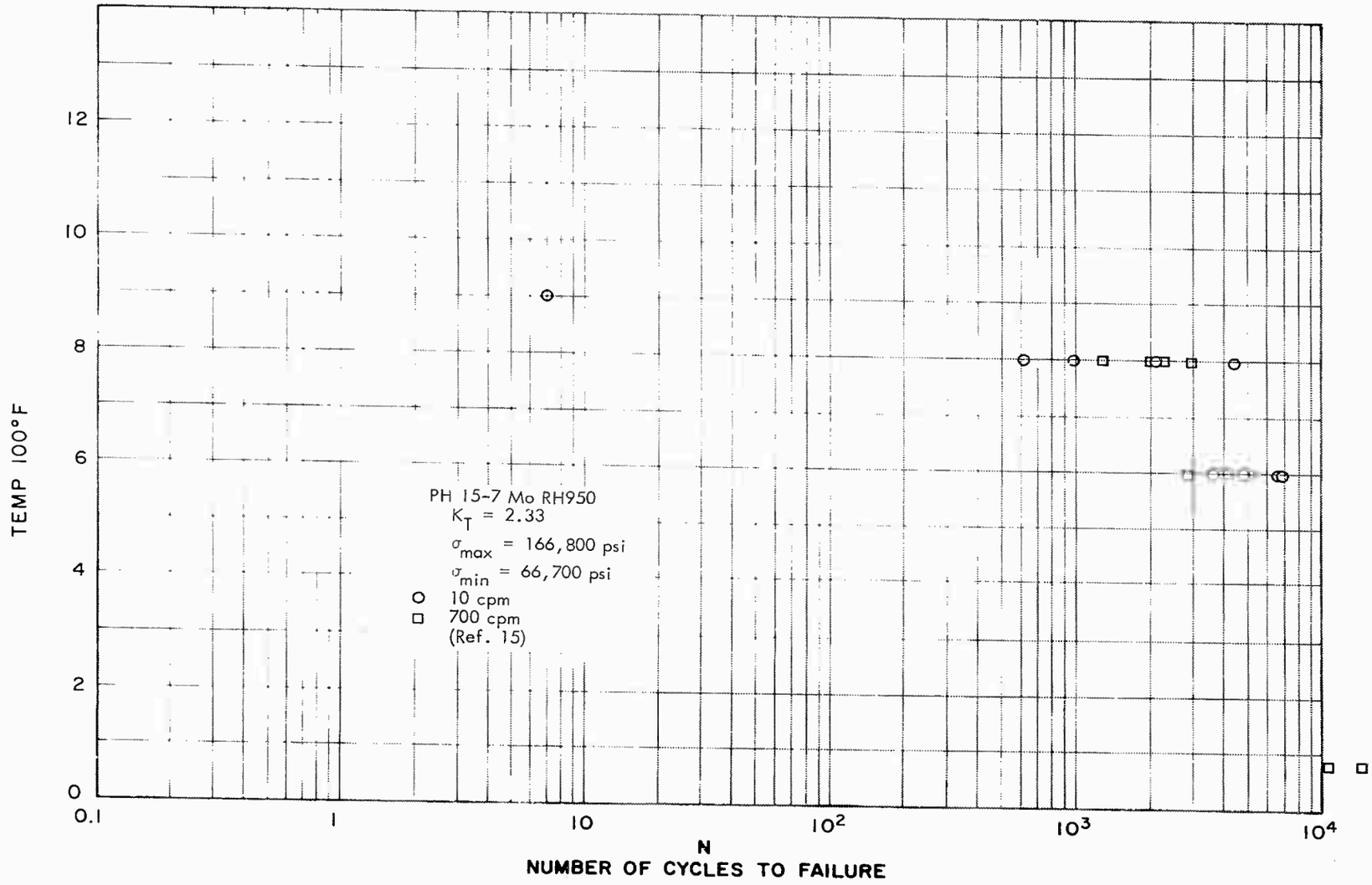

Fig. 3-10 Effect of Temperature on Mechanical Cycles-to-Failure for P.H. 15-7 Steel (σ_{max} = 166,800 psi)

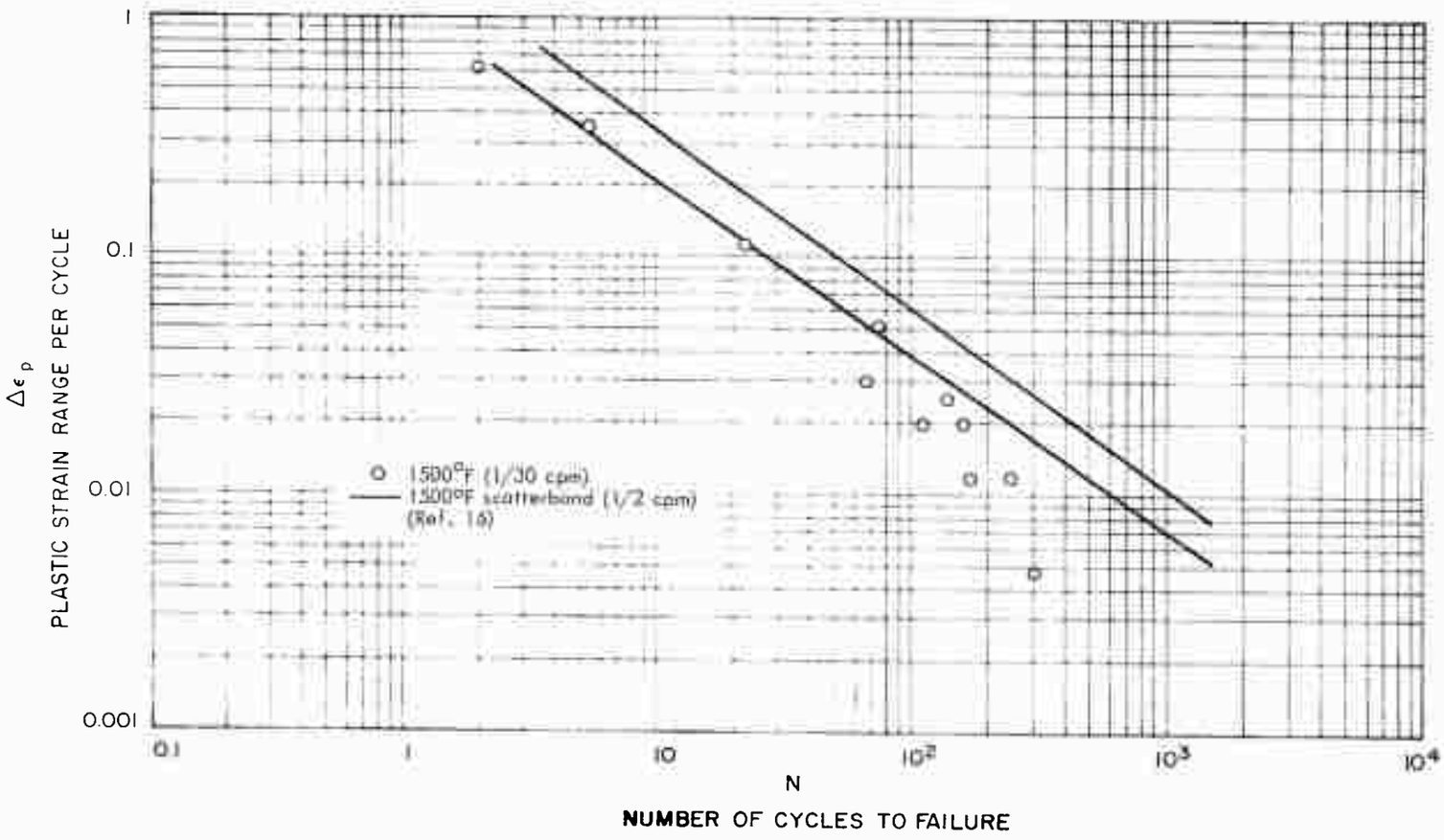

Fig. 3-11 Mechanical Cycling of Inconel at 1500° F

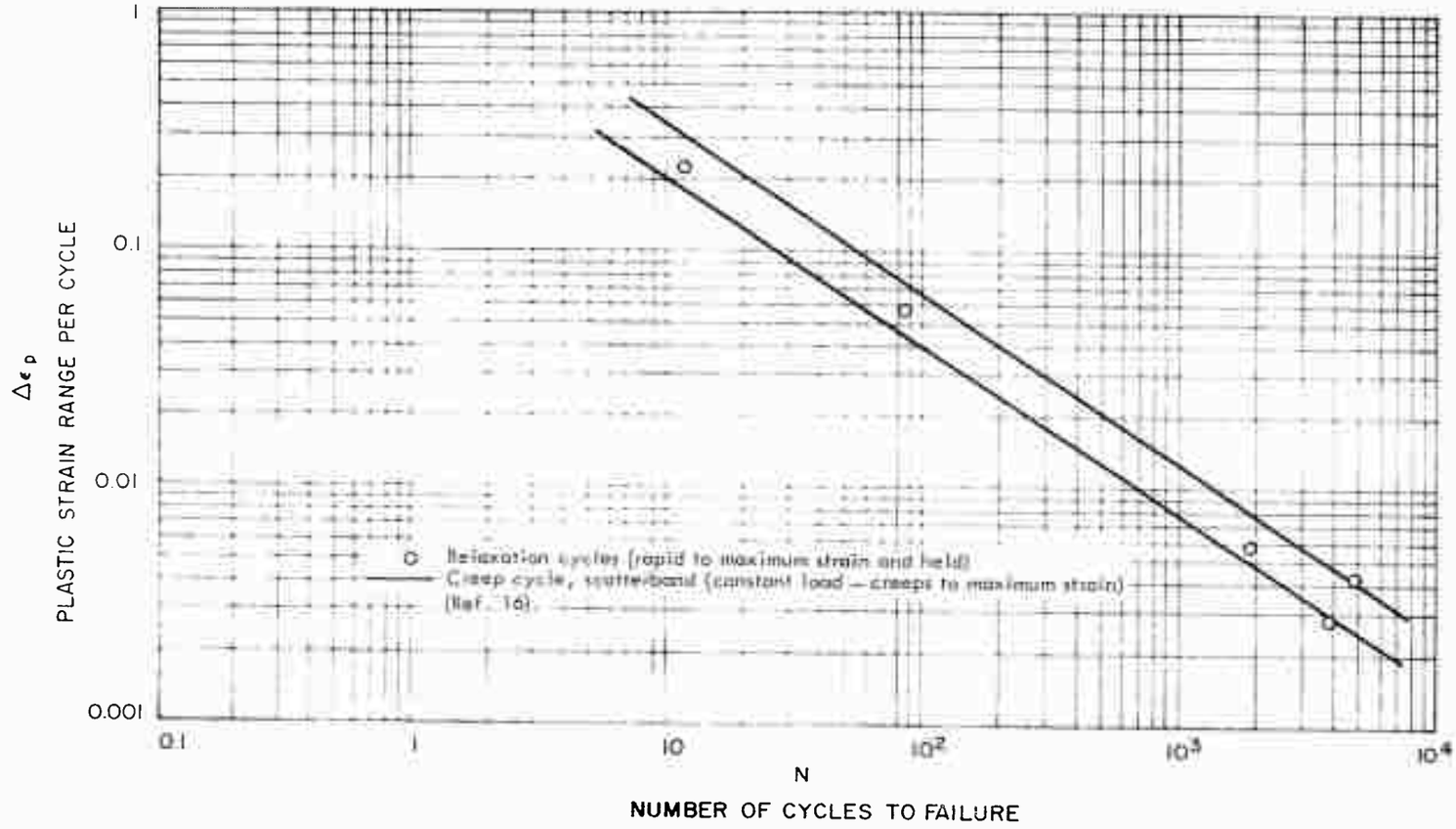

Fig. 3-12 Relaxation and Creep Cycling of Inconel at 1500°F

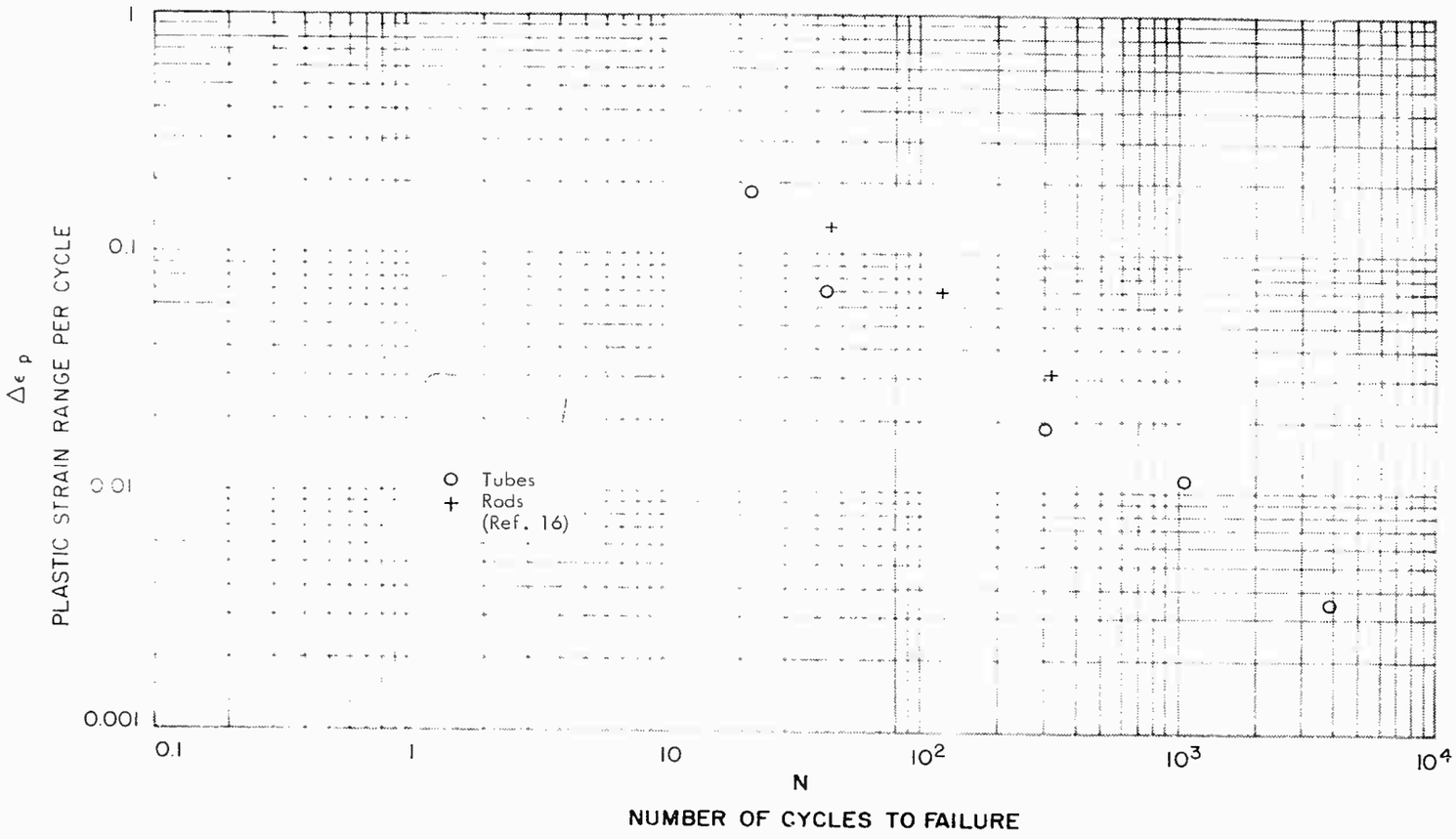

Fig. 3-13 Mechanical Cycling of Inconel Tubes and Rods at 1600° F

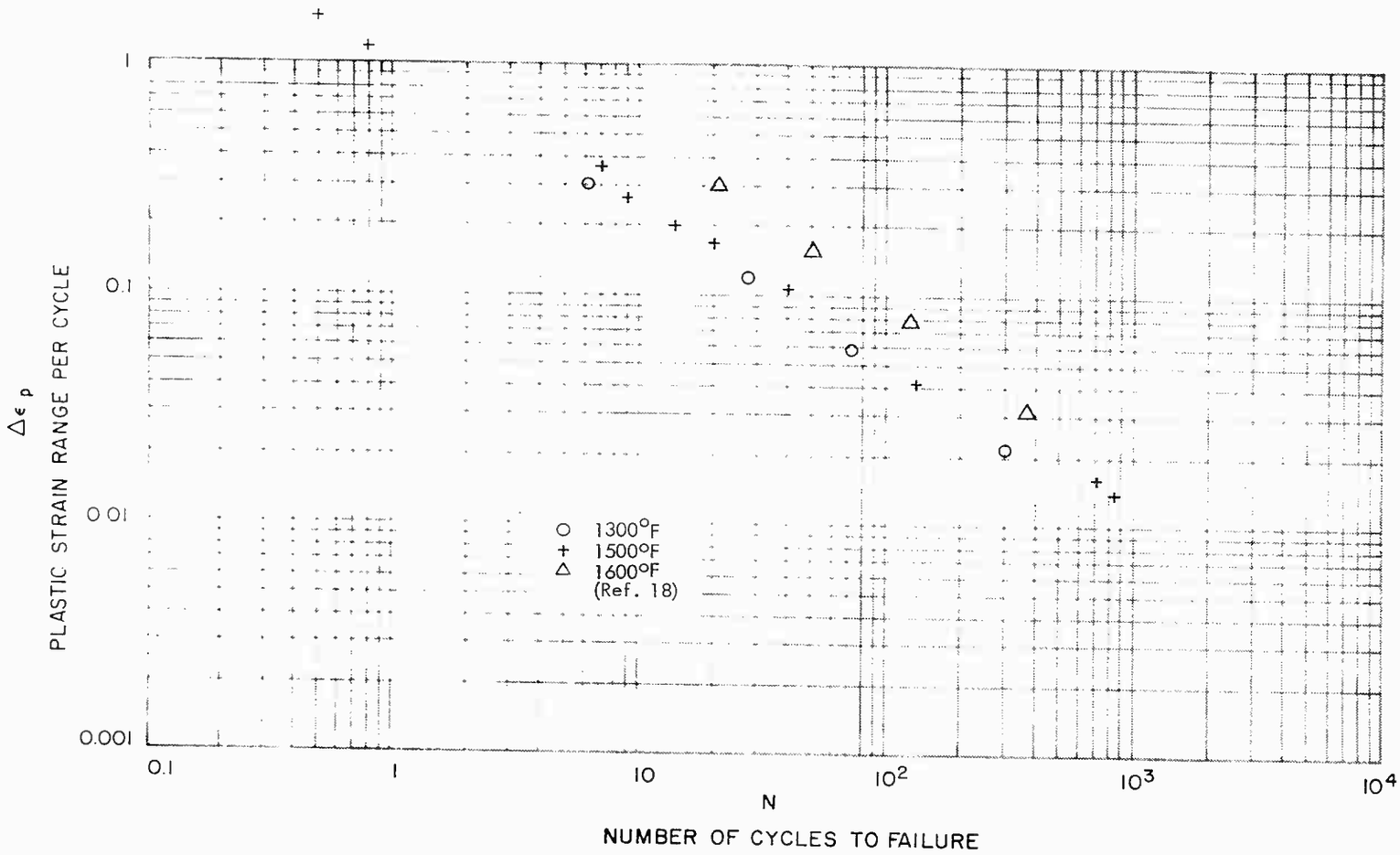

Fig. 3-14 Mechanical Cycling of Fine-Grain Inconel at Elevated Temperatures

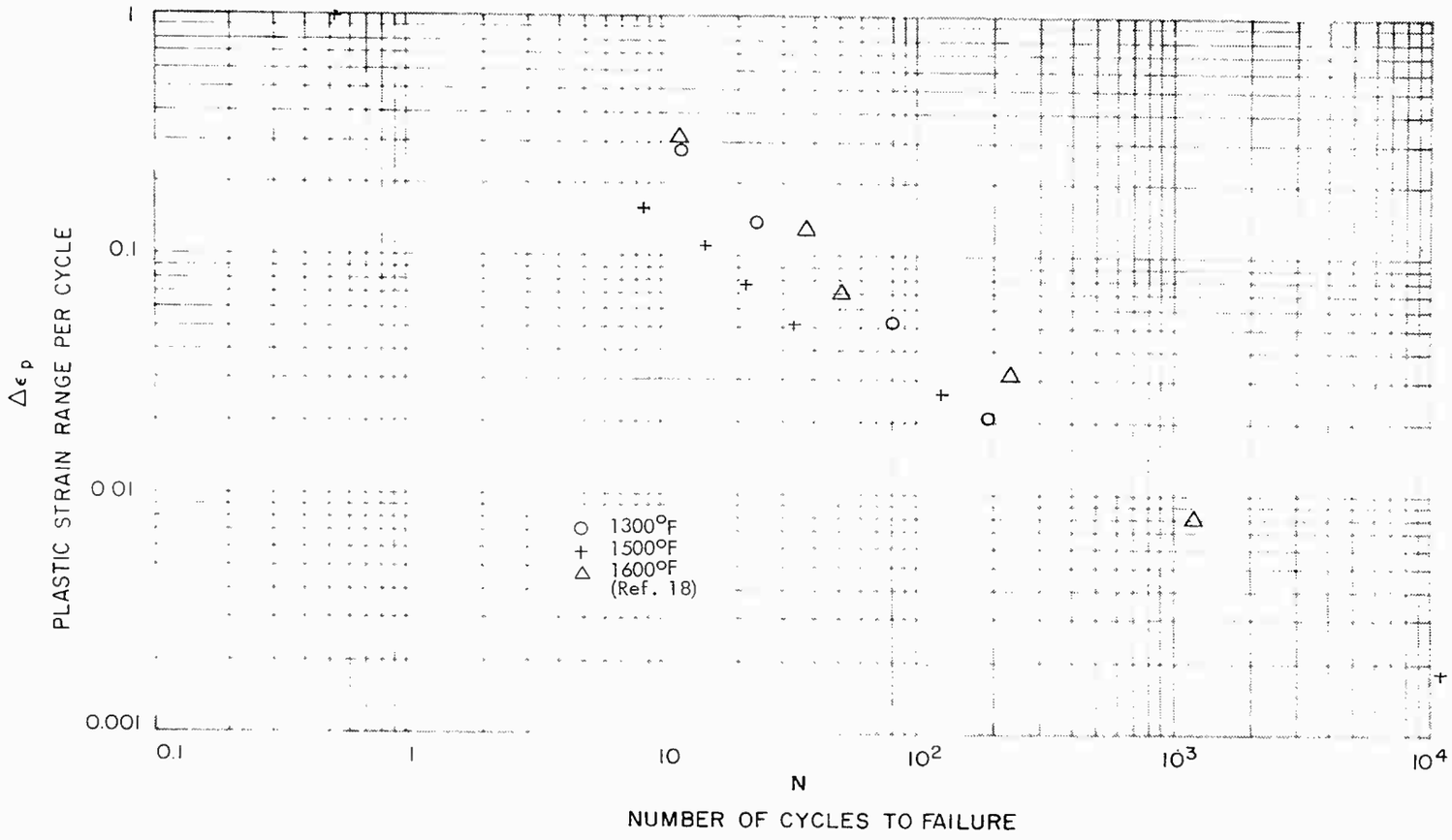

Fig. 3-15 Mechanical Cycling of Coarse-Grain Inconel at Elevated Temperatures

Section 4

THERMAL CYCLING

4.1 GENERAL

Thermal cycling as defined here differs from mechanical cycling in the following way: In thermal cycling, the specimen remains the same length during cycling, while in mechanical cycling the length changes as the strain changes. For thermal cycling, the specimen can be completely restrained between rigid structure and then heated to a maximum temperature, or it could be completely restrained in its expanded configuration after being heated to maximum temperature. Either method of restraint gives the same results, as Coffin (Ref. 19) discovered.

One of the simplest ways of describing the fundamentals of thermal cycling is through discussion of a mechanically constrained bar (Fig. 4-1). The bar is cycled between two

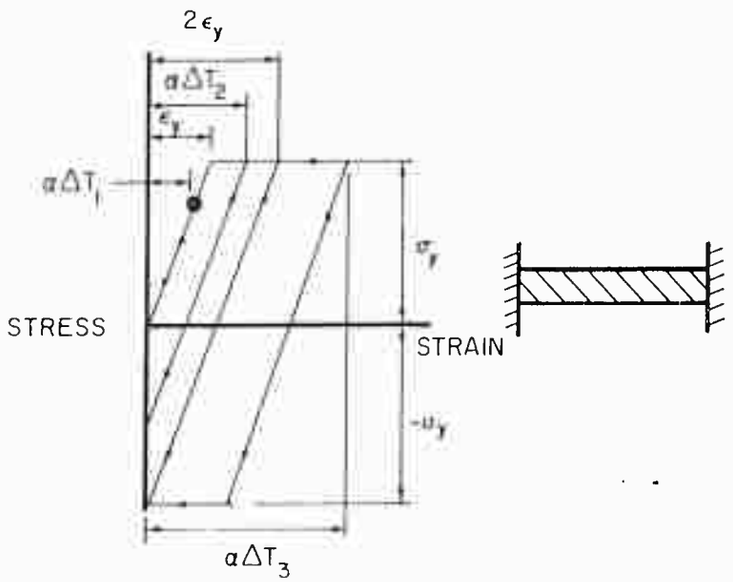

Fig. 4-1 Ideal Plastic Stress-Strain Curve

temperatures so that it attempts to expand and contract alternately. The bar, being constrained against expansion or contraction, is accordingly thermally stressed. Even though there is no external evidence of a change in the length, the bar is being subjected to a mechanical strain equal to the thermal strain that would result if the constraints were absent.

In showing graphically the mechanism of thermal cycling, an ideally plastic material is assumed. The hypothetical stress-strain curve is shown in Fig. 4-1. It consists of a straight line with some slope from the vertical between the origin and the yield stress and a horizontal constant stress line during yielding.

If one assumes that the bar is uniformly heated to a thermal strain of $(\alpha \Delta T)$, constrained, and then uniformly cooled to a $\Delta T = 0$, there are three possible cycling paths on the ideal stress-strain curve. These three cycling paths are as follows: (1) the thermal strain $(\alpha \Delta T_1)$ is less than the yield strain ϵ_y; (2) thermal strain $(\alpha \Delta T_2)$ is greater than ϵ_y but less than $2\epsilon_y$; (3) thermal strain $(\alpha \Delta T_3)$ is greater than $2\epsilon_y$. All of the thermal cycling data reported here are for thermal strains greater than twice the yield strain. The net strain for these data is zero:

$$\alpha \Delta T - \Delta \epsilon_e - \Delta \epsilon_p = 0$$

where

$\Delta \epsilon_e$ = elastic strain range
$\Delta \epsilon_p$ = plastic strain range
$\alpha \Delta T$ = thermal strain range

and end constraint deflection is neglected.

Most materials, when subjected to plastic strain, show strain hardening or softening which results in a changing stress-strain curve during cycling. Even the Baushinger

effect changes the stress-strain curve because it reduces the yield stress in one direction. Therefore, the ideal stress-strain curve shown above is not realistic, but it does show the paths of straining.

A considerable amount of experimental work has been done with thermal cycling on various materials by several investigators (Refs. 3, 4, 16, 17, 19, 21–29). All of this work covered only a small range of total strain ($\alpha\Delta T$) from 0.006 to 0.015 in./in., which resulted in cycles-to-failure from 7 to the limit reported here of 10,000 cycles. Only eight test points are below 270 cycles-to-failure (Fig. 1-3). Included in Fig. 1-3 is the scatterband for mechanical cycling at room temperature. Data from all six materials tested lie within a small scatterband, as did mechanical cycling data for elevated temperatures, but this band is almost horizontal, which suggests that thermal cycling differs from mechanical cycling and is nearly independent of the temperature change ΔT for temperatures and materials included in the data. Coffin's original work (Ref. 3) with type 347-stainless steel encouraged subsequent experimental work. The recent work has been devoted to an extension of Coffin's work in an attempt to substantiate or to refute it, and all of the effects of various parameters that have been investigated lie within this very narrow horizontal scatterband. It is probable that the conclusions reached by these investigators were influenced by the limited range of data.

Coffin and many other investigators used the parameter plastic strain range ($\Delta\epsilon_p$) for predicting cycles to failure. For the cycles investigated, only three materials were within the plastic strain range where failure occurred in less than 10,000 cycles. These results are plotted in Fig. 4-2. The cycle range is from 400 to 10,000 cycles, which hardly covers the complete low-cycle range, and the scatter is larger than it was for mechanical cycling at room temperature.

Only the following four parameters were investigated for thermal cycling, and their effects on cycles-to-failure will be discussed in detail.

1. Strain amplitude
2. Stress concentrations
3. Temperature
4. Hold time at maximum temperature

Prior thermal cycling effects on the stress-strain and creep-rupture characteristics of a material will be discussed, as well as the effect of prior creep on the thermal cycles-to-failure.

4.2 STRAIN AMPLITUDE

As in mechanical cycling, there are two strain parameters, total and plastic, to be considered for thermal cycling, and each parameter has a different effect on the cycles-to-failure. The total strain range, defined as $(\alpha \Delta T)$, has almost no effect on cycles-to-failure. Coffin (Ref. 3) measured the total strain for thermal cycling of 347-stainless steel at various temperature changes (ΔT) at a constant mean temperature of 350° C. He plotted this measured strain against ΔT and showed that the total strain is identical with a total strain calculated by $\alpha \Delta T$ for an α of 20×10^{-6} in./in./° C. (See Fig. 4-3.) If we assume $\alpha \Delta T$ equal to the total strain range $(\Delta \epsilon_{TR})$ and a value of α at the mean temperature, the total strain range was calculated for the materials that were investigated for which temperature changes were recorded. These calculated values are plotted in Fig. 1-3 using log-log coordinates so that a comparison of total strain range vs. cycles-to-failure can be made with mechanical cycling. This plot results in an almost horizontal scatterband which indicates that the cycles-to-failure are not affected by total strain for the materials investigated. The band is below that for mechanical cycling at room temperature, the two approaching each other at an N of 10,000 cycles. A semilog plot of total strain vs. cycles-to-failure does not improve the conclusions either (Fig. 4-4).

Plastic strain range appears to be a better parameter because it has an effect on cycles-to-failure. As seen in Fig. 4-2, an increase in plastic strain results in a definite decrease in cycles-to-failure. The four materials plotted are the only ones for which plastic strain was recorded and were tested only from 400 to 10,000 cycles. The difficulty in drawing specific conclusions regarding the effects of plastic strain range is due to the vagueness of the methods used to separate this strain from the total strain range. For the four materials plotted, no explanation was given as to how the plastic strain was determined. Two methods used to determine this component are (1) to read the strain directly from a cycle stress-strain curve or (2) to assume that the elastic portion is equal to twice the yield strain at an assumed temperature. The first method is best because it accounts for the strain hardening or softening due to cyclic straining and there are no assumptions made. The second method is only an assumption, but it does have some merit as previously discussed. However, Mehringer and Felgar (Ref. 21) showed that the plastic strain was too small to calculate with any accuracy for cast DCM and cast Udimet 500. In fact, they suggest using stress range as a parameter. Stress range was shown to be an unusable parameter in the discussion of mechanical cycling at room temperature, but it could possibly be the predominate parameter for thermal cycling.

4.3 STRESS CONCENTRATIONS

In Ref. 24, Coffin thermal-cycled a specimen with a 0.04-in.-diam. hole and showed that stress concentrations reduce the cycles-to-failure. These data, which are the only experimental test results in the literature, are presented in Figs. 4-5 and 4-6. They show that the notched data fall outside of the scatterband of the other material (Fig. 4-5) and lie below and to the left of the unnotched results (Fig. 4-6).

4.4 TEMPERATURE

The effect of temperature on cycles-to-failure has been studied by investigating four temperature combinations as follows:

a. Constant mean temperature varying the maximum temperature

b. Constant minimum temperature varying the maximum temperature

c. Constant temperature differential varying the maximum temperature

d. Varying maximum temperature with a varying minimum temperature

All four temperature combinations decrease the cycles-to-failure with an increase in maximum temperature.

The effect of constant mean temperature for 347-stainless steel is shown in Fig. 4-6. Four materials S-816, Inconel 550, Crucible 422 and cast DCM are plotted in Fig. 4-7 for a minimum temperature of 200° F. Figures 4-8 and 4-9 show the effect of an increasing maximum temperature for a constant temperature differential. Varying the minimum temperature with maximum temperature is recorded in Figs. 4-10 and 4-11 All of these figures are constructed with semilog coordinates which appear to give a definite slope to the curve, but when these results are replotted to log-log coordinates to total strain as shown in Fig. 1-3, these various effects seem unimportant. The calculation of the total strain was performed by assuming a coefficient of linear expansion (α) at a mean temperature multiplied by the temperature differential (ΔT). Since this assumption has been shown above to be valid as a reasonable approximation, the effects of various temperature combinations would appear to be of minor importance for thermal cycling.

4.5 HOLD TIME AT MAXIMUM TEMPERATURE

Hold time at maximum temperature for isothermal cycling was shown previously to be important, but for thermal cycling it showed no effect on cycles-to-failure for the three investigations that were made. Clauss and Freeman (Ref. 23) varied the hold time from 15 sec to 60 sec for Inconel 550 and S-816 with no effect for increased hold times (Figs. 4-12 and 4-13). Coffin (Ref. 3) studied 347-stainless steel at hold times of 6, 18, 60 and 180 sec and again no effects on cycles-to-failure were observed (Fig. 4-14). However, the total elapsed time at maximum temperature with hold time for all three materials (Fig. 4-15) before fracture occurred was obviously greater for longer hold times.

The general effect of strain cycling is to produce a small crack or several small cracks, and with continued cycling these cracks will serve as stress-raisers and cause premature failure. Thermal cycling does not result in this effect. Coffin (Ref. 3) thermal-cycled some specimens of 347-stainless steel between 200° C and 500° C for 2,000 to 10,000 repetitions in 2,000-cycle intervals. Following this cycling, true stress-strain tests were carried out to observe the structural changes in the material resulting from the previous cycling. Such a test should bring out clearly the progressive deterioration of the polycrystalline structure, the brittleness, or the presence of fatigue cracks, should any of these possible modes of failure occur progressively with strain cycling. Figure 4-16 shows that all stress-strain curves obtained from this testing were similar regardless of number of cycles, which indicates that thermal fatigue has little effect on the material properties.

Therefore, for thermal cycling some parameters have a slight effect on life, but no definite conclusions can be made about these effects, for they only produced small changes within the scatterband. Stress concentrations do reduce cycles-to-failure, and thermal cycling is independent of temperature differences or total strain ($\alpha \Delta T$). Only the plastic strain parameter has some merit, but it is difficult to calculate the plastic strain, and data are quite limited in which the plastic component has been recorded.

The effects of unconstrained thermal cycles on the material properties and the effects of thermal cycling on the stress-rupture life were also investigated.

The Lockheed-California Company (Ref. 28) has obtained some mechanical properties of René 41 and L-605 alloys after exposure to ten thermal unconstrained cycles and two soak times. The thermally cycled specimens were tested for mechanical properties at four temperatures. At these four temperatures, the mechanical properties were almost identical to the tensile properties for no-soaking cycles at the same test temperatures. Nine cycle frequencies were tested (Fig. 4-17). The results of three cycles (Nos. 1, 2, and 3) were slightly lower for René 41, but all of the cycle frequencies

resulted in almost identical effects for the L-605 alloy. The soak times were 10 and 20 hours at 1800° F and 2000° F. The 20-hour soak at 2000° F resulted in mechanical properties at room temperature which were 65 percent of the room-temperature properties for both materials. The soaking at 1800° F reduced the properties for René 41 more than they did for the L-605 alloy. These ultimate- and yield-strength properties are listed in Tables 4-1 and 4-2.

Clauss and Freeman (Ref. 29) investigated the effect on ductility and stress-rupture life for S-816 and Inconel 550 exposed to prior thermal cycling. They also investigated the effect on thermal cycles-to-failure after exposure to stress rupture. The ductility of S-816 decreased after exposure to thermal cycling, while no effect was observed for Inconel 550. After an exposure of prior thermal cycling, the stress-rupture life of S-816 was increased but the life for Inconel 550 was decreased. Prior stress-rupture exposure of 40,000 psi at 1350° F decreased the cycles of thermal cycling to failure for S-816, although a stress exposure of 56,500 psi at 1350° F to Inconel 550 increased the cycles of thermal cycling-to-failure.

In summary, the fatigue failure mechanism of thermal cycling is not comparable to mechanical cycling, and each investigator has investigated only a relatively small region of cycles-to-failure. Therefore, a fundamental experimental investigation should be initiated to determine the material behavior phenomenon due to thermal cycling. Such an investigation should be accompanied by a theoretical study to discover the factors responsible for thermal-cycling fracture phenomena.

Table 4-1

MECHANICAL PROPERTIES OF RENE 41 AND L-605 ALLOYS
AFTER EXPOSURE TO TEN THERMAL UNCONSTRAINED CYCLES

Test Temp. To Obtain Properties	Thermal Unconstrained Cycles						No Soak Cycles	
	Cycles 1, 2, 3		Cycles 1A, 2A, 3A		Cycles 1B, 2B, 3B			
	F_{tu} *	F_{ty}	F_{tu}	F_{ty}	F_{tu}	F_{ty}	F_{tu}	F_{ty}
Rene 41								
R. T.	181 164 165	125 115 107	167 176 174	122 120 118	182 183 179	130 136 132	188	138
1700° F					57 56 56	53 49 49	58	55
1800° F			34 38 32	27 26 26			36	28
2000° F	7.9 7.8 8.2	4.7 5.0 4.8					7.6	4.6
L-605								
R. T.	123 118 134	66 66 88	121 112 133	67 67 86	116 138 132	69 88 81	145	71
1700° F					36 35 35	29 30 29	35	25
1800° F			26 26 26	16 16 17			26	18
2000° F	13.9 11.6 11.0	7.6 8.6 9.0					10.8	7.7

*All stresses are in kips per square inch

Table 4-2

ROOM-TEMPERATURE PROPERTIES RESULTING FROM PRIOR THERMAL SOAKING

Material	No Soak		Soak for 10 hr at 1800°		Soak for 10 hr at 2000°		Soak for 20 hr at 1800°		Soak for 20 hr at 2000°	
	F_{tu}*	F_{ty}	F_{tu}	F_{ty}	F_{tu}	F_{ty}	F_{tu}	F_{ty}	F_{tu}	F_{ty}
Rene´41	173	140	129	75	126	76	117	70	112	74
L-605	143	73	135	73	117	66	134	76	93	61

*All stresses are in kips per square inch.

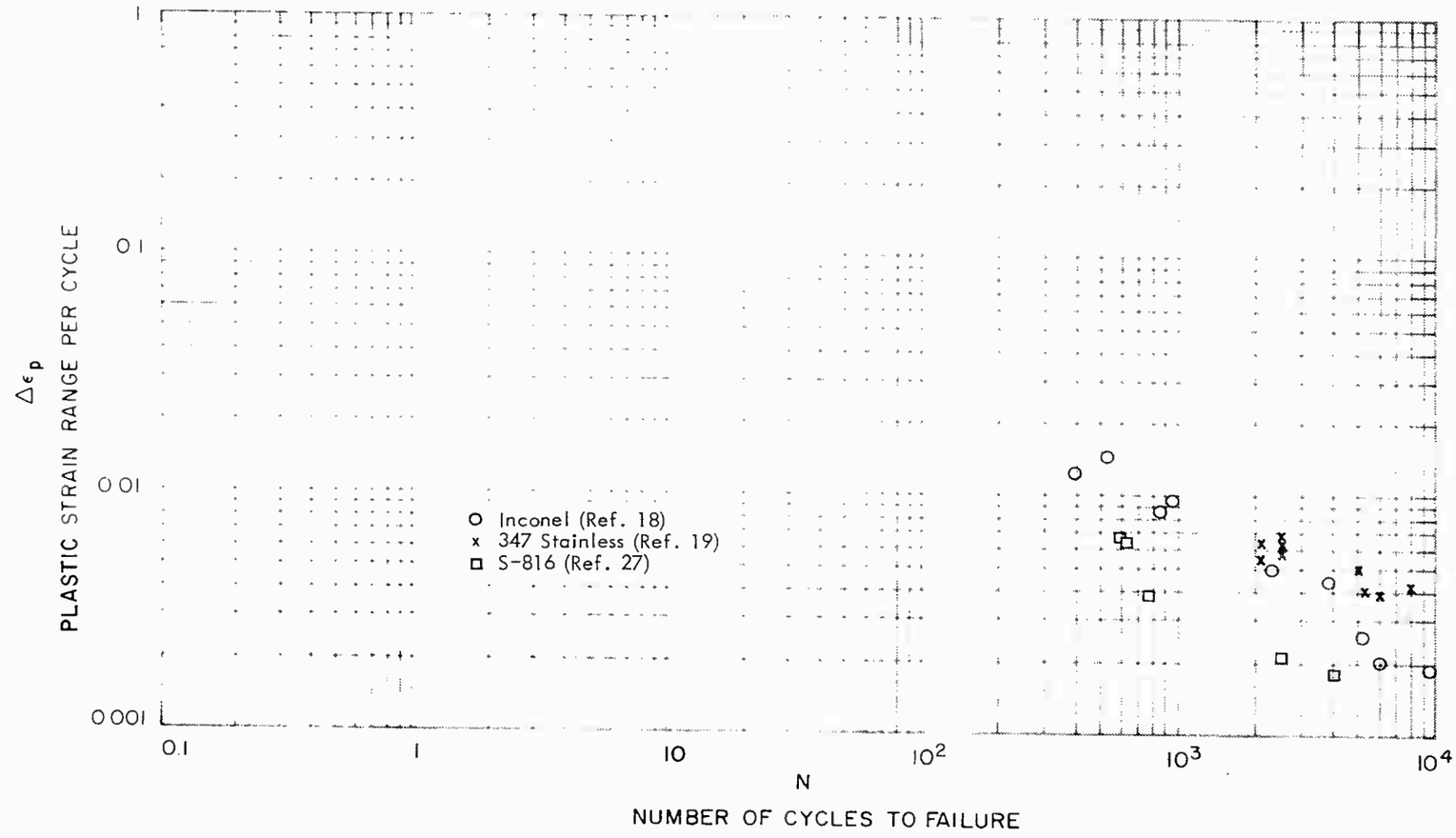

Fig. 4-2 Thermal Cycling of Various Materials — Plastic Strain vs. Cycles-to-Failure

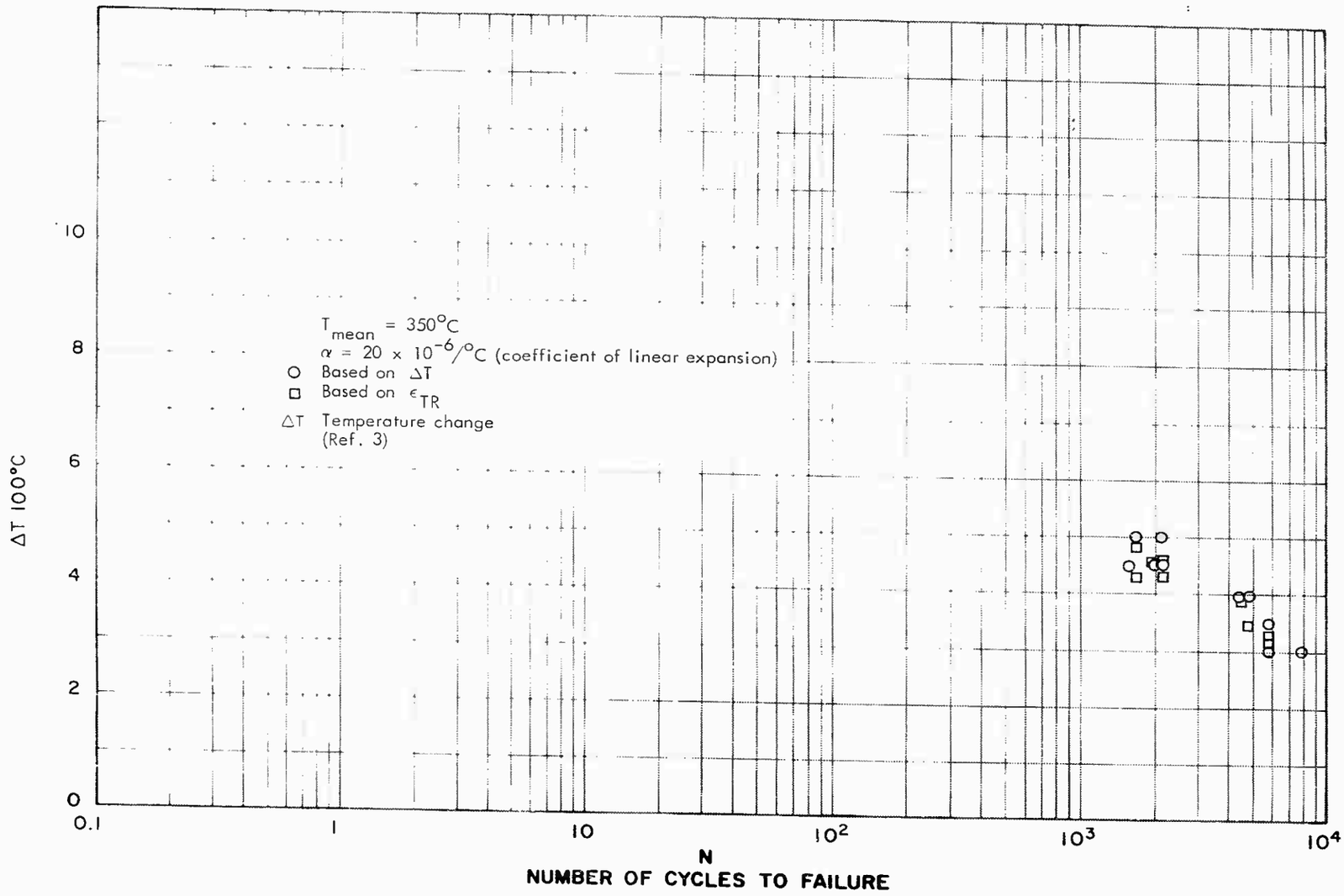

Fig. 4-3 Thermal Cycling of 347 Steel – Comparing Total Strain With Temperature Change

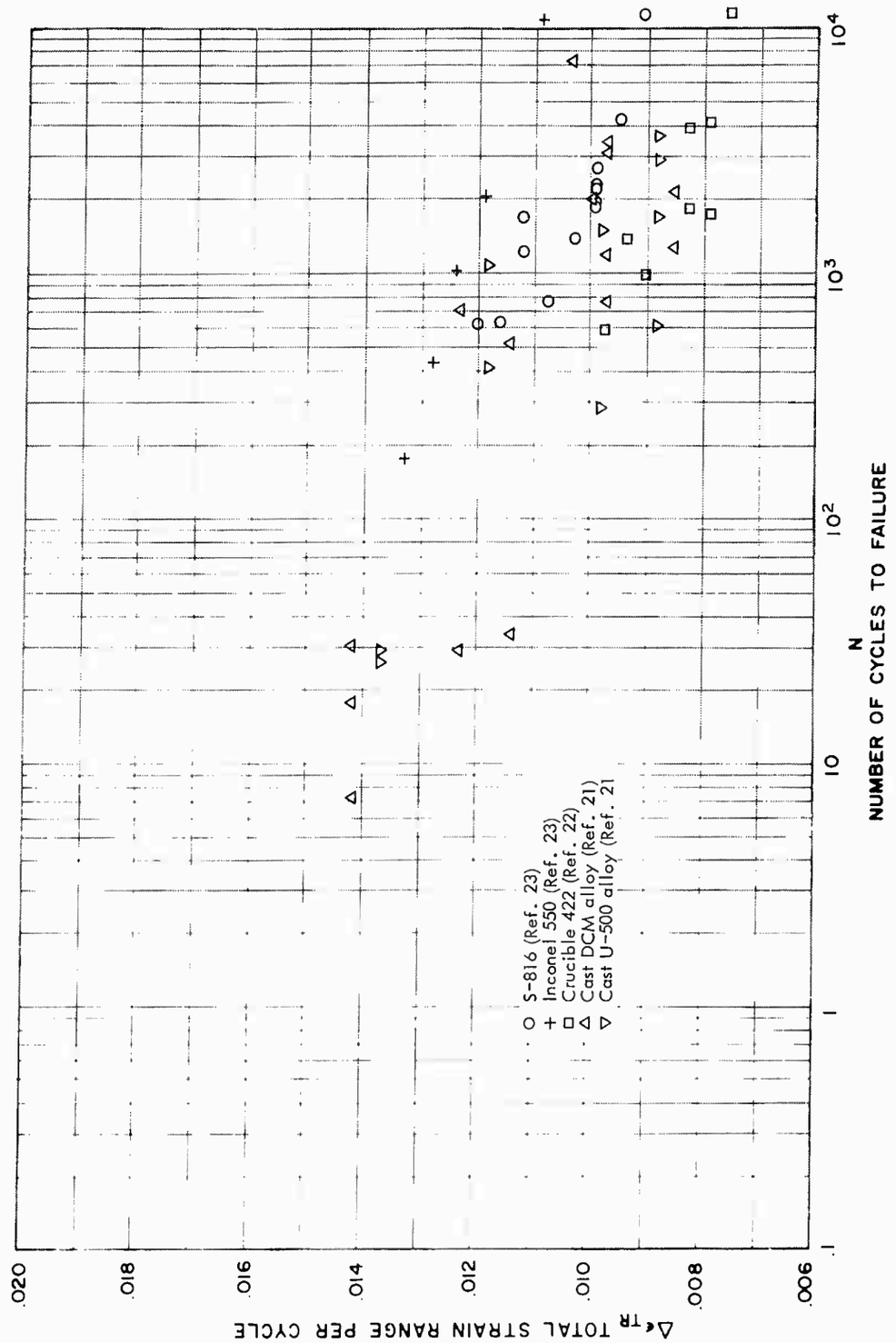

Fig. 4-4 Thermal Cycling of Various Materials – Semilog Total Strain vs. Cycles-to-Failure

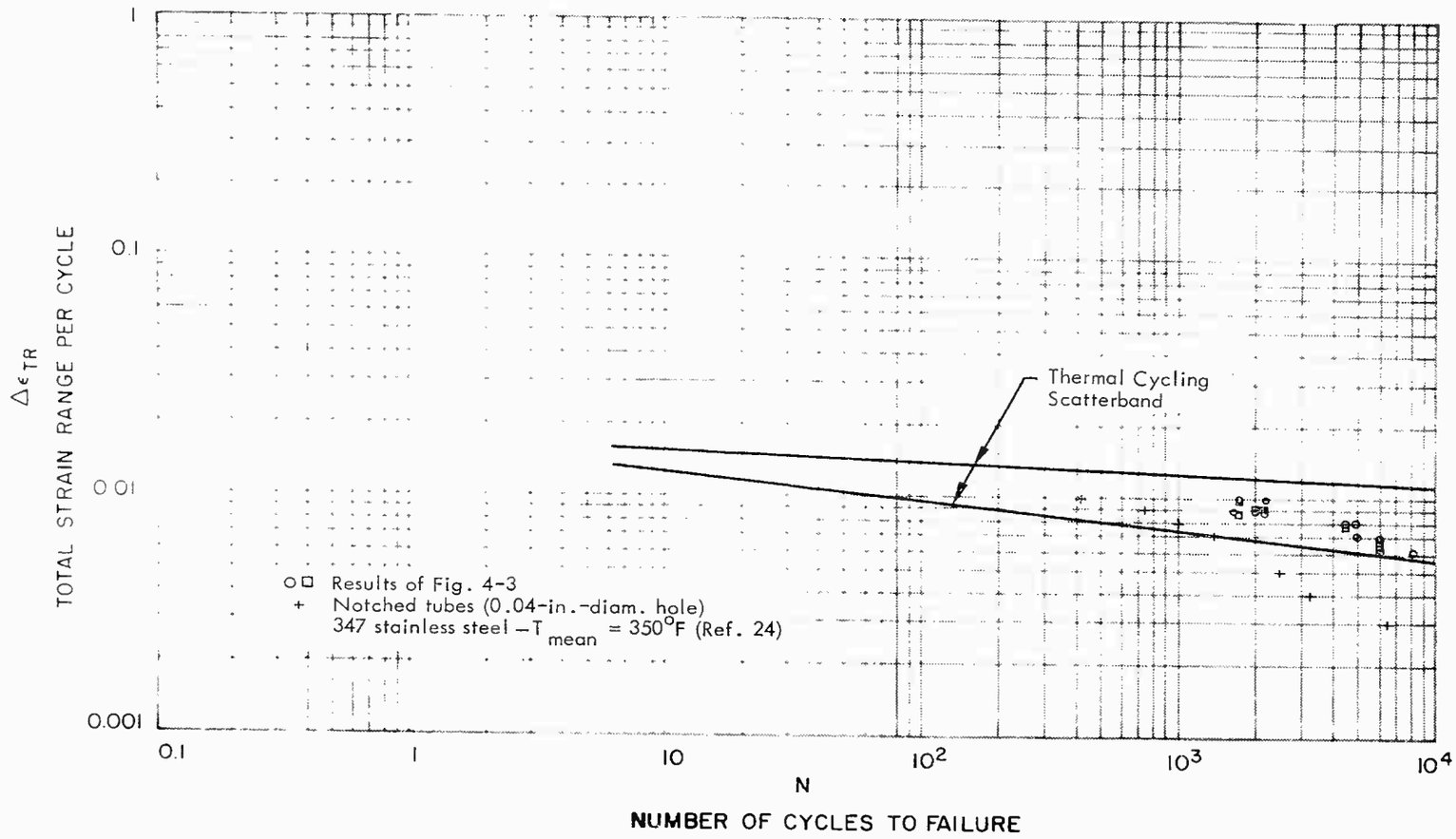

Fig. 4-5 Thermal Cycling of Type-347 Steel With a Stress Concentration Compared With Thermal Cycling of Smooth Speciments

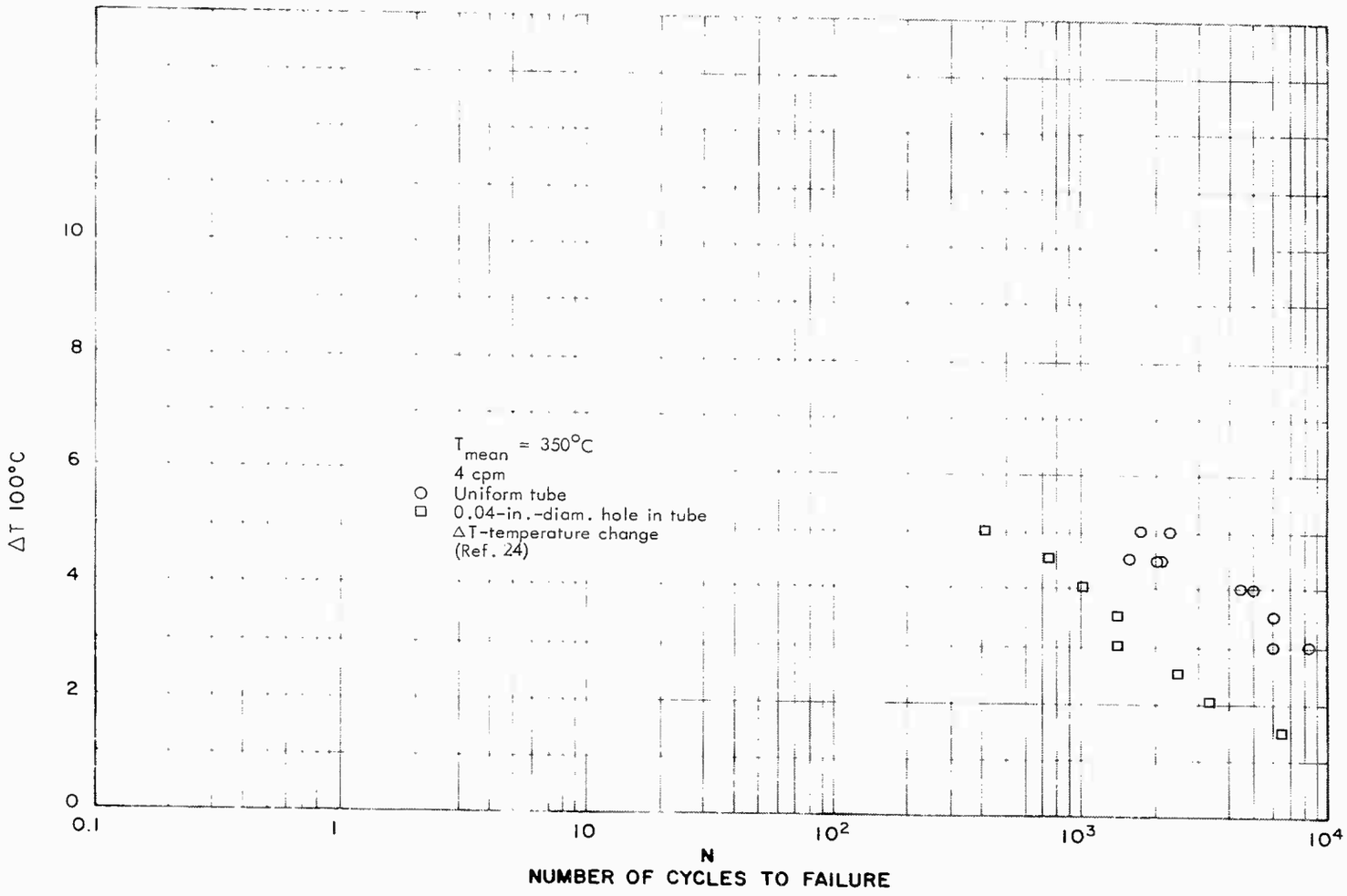

Fig. 4-6 Thermal Cycling of Type-347 Steel Comparing Notched and Unnotched Results

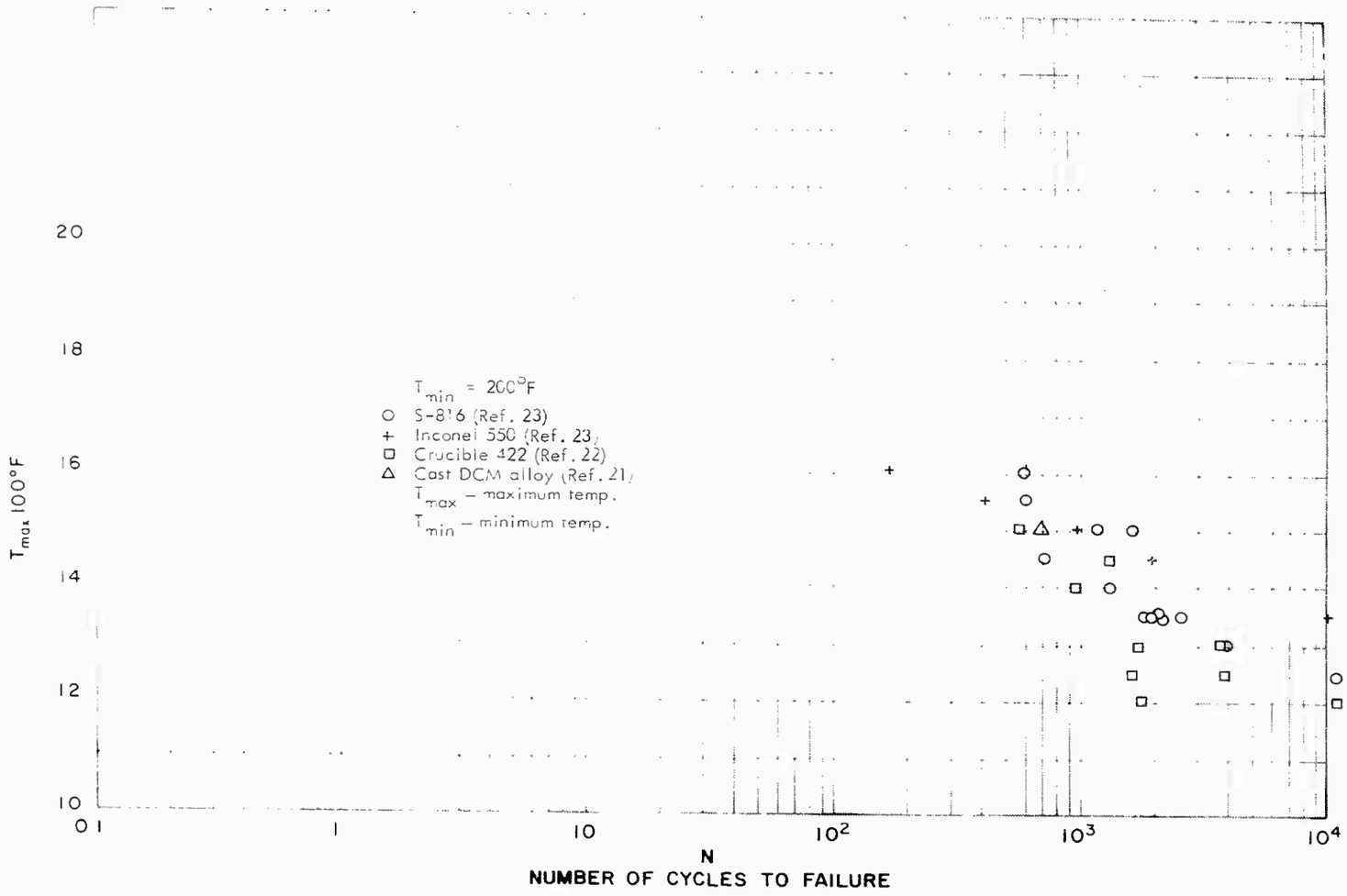

Fig. 4-7 Thermal Cycling at a Constant Minimum Temperature Varying the Maximum Temperature

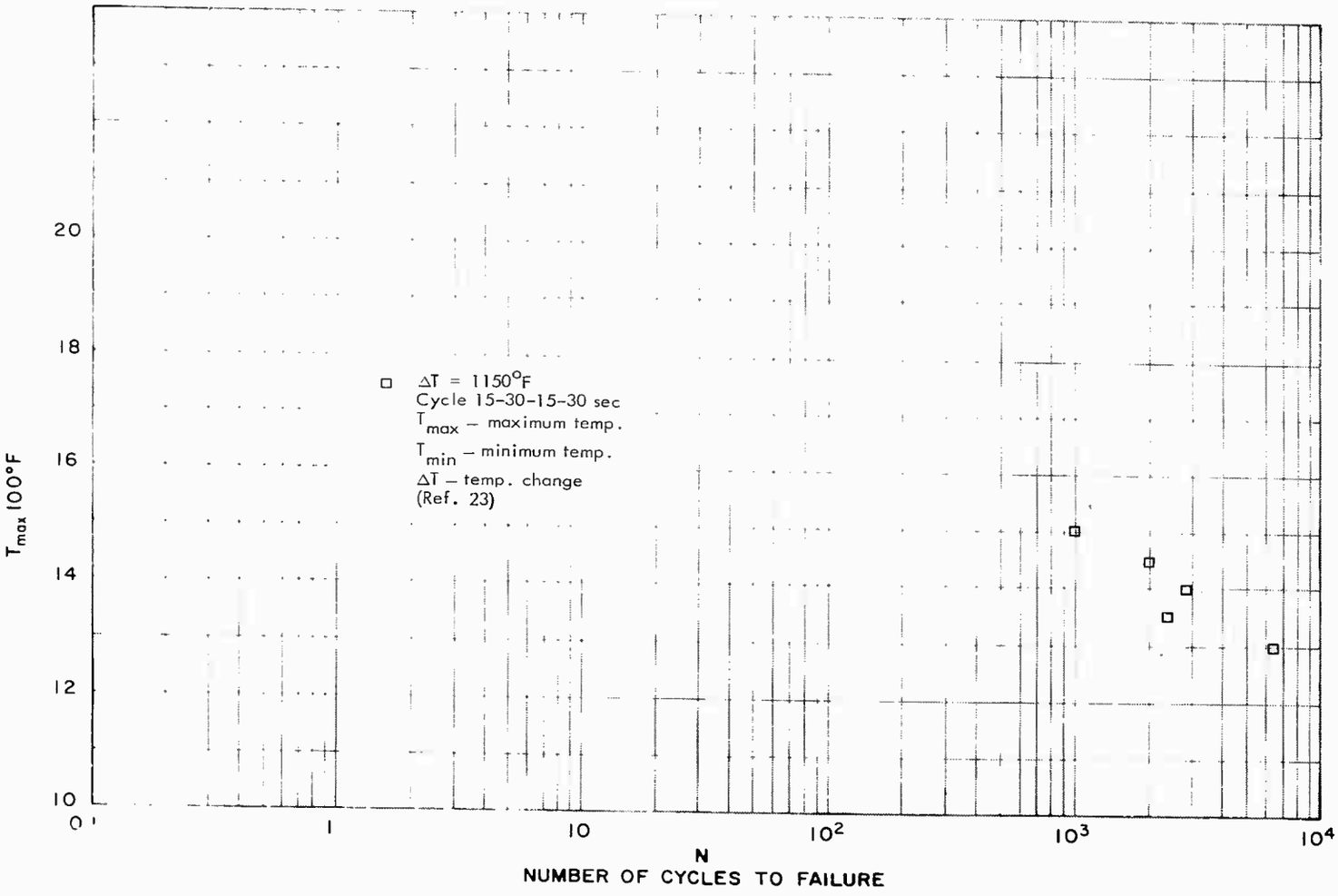

Fig. 4-8 Thermal Cycling of S-816 Steel at a Constant Minimum Temperature and at a Constant Temperature Change

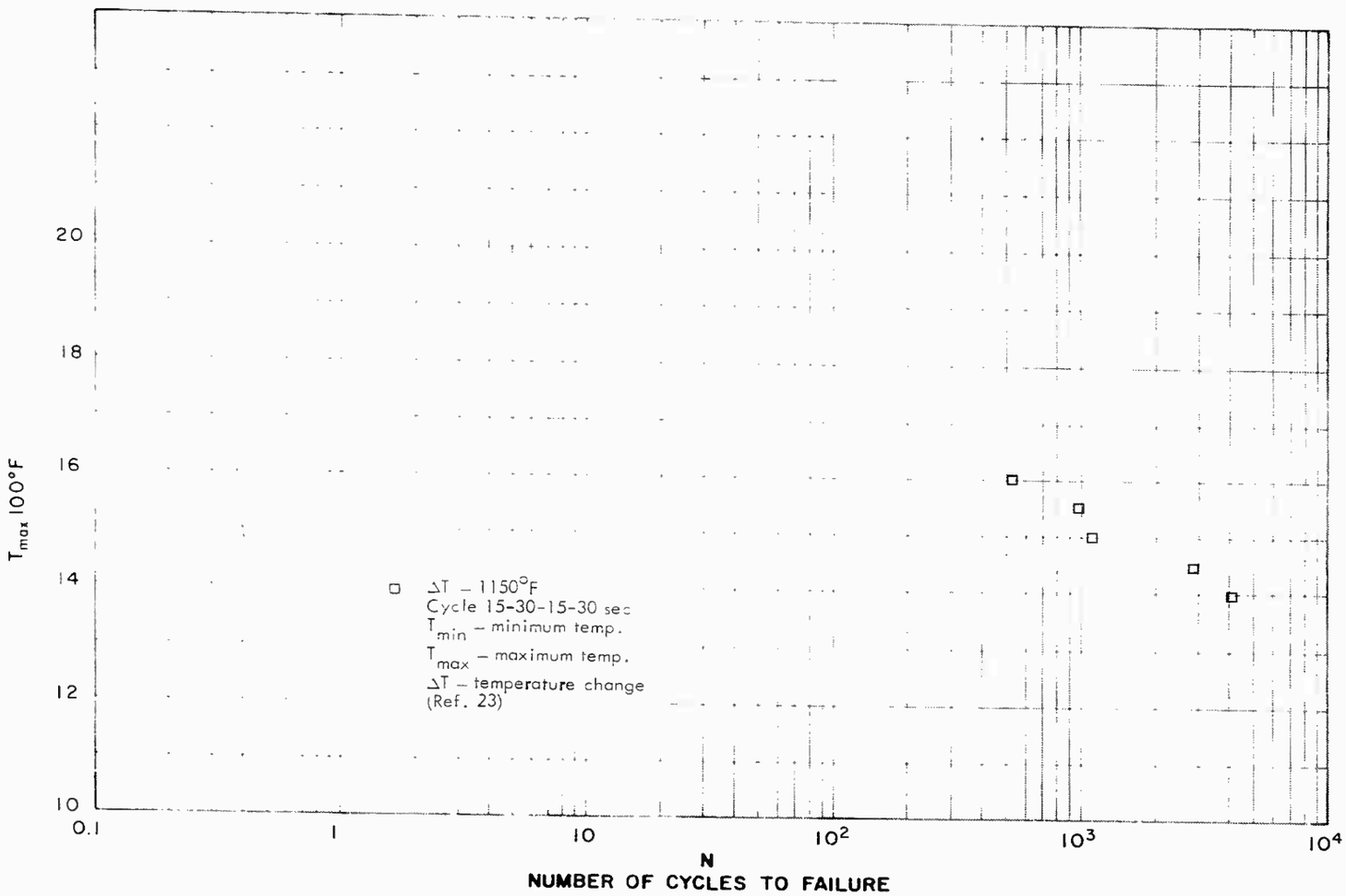

Fig. 4-9 Thermal Cycling of Inconel 550 at a Constant Minimum Temperature and at a Constant Temperature Change

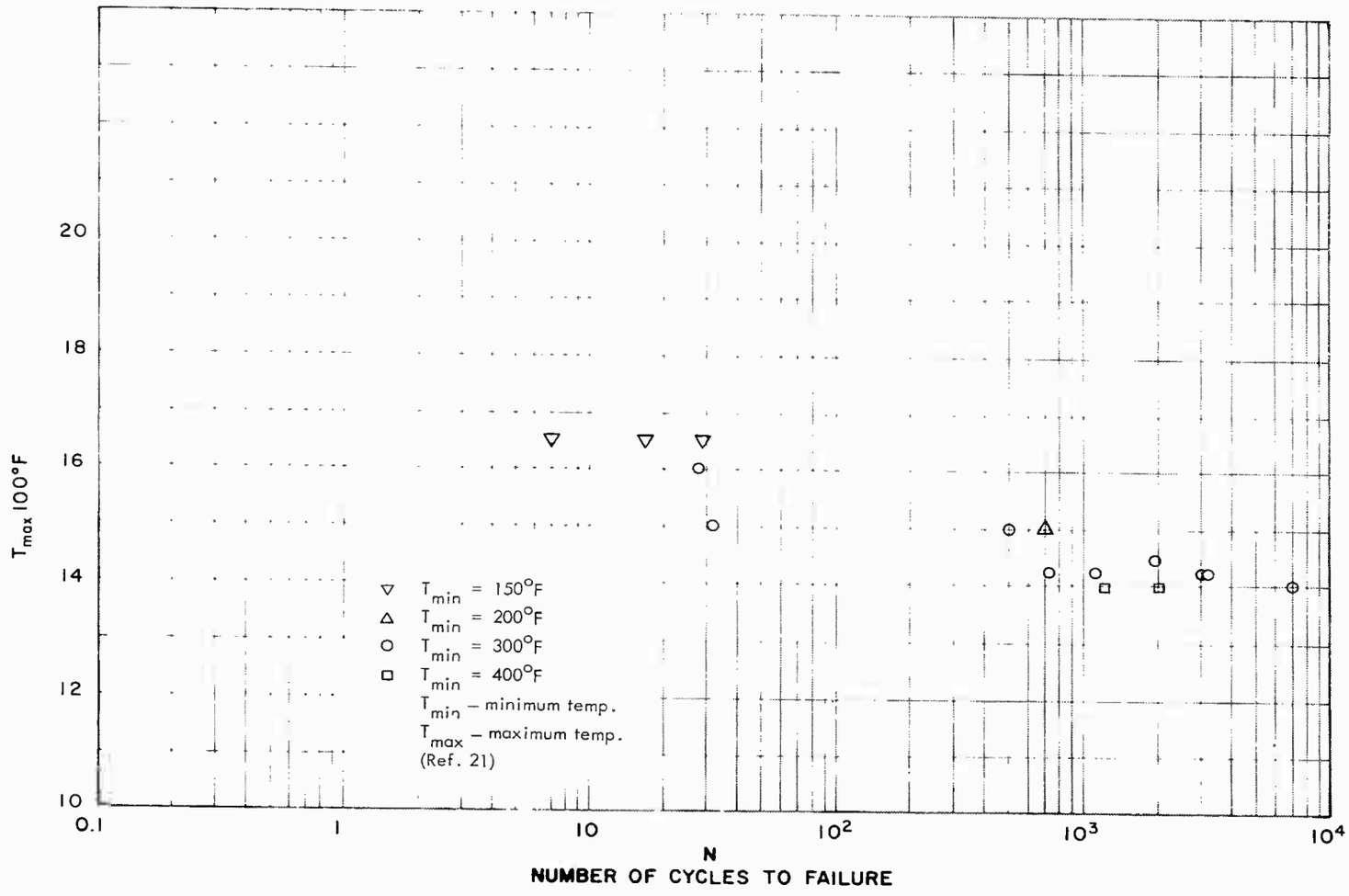

Fig. 4-10 Thermal Cycling of Cast DCM Steel at Various Minimum Temperatures

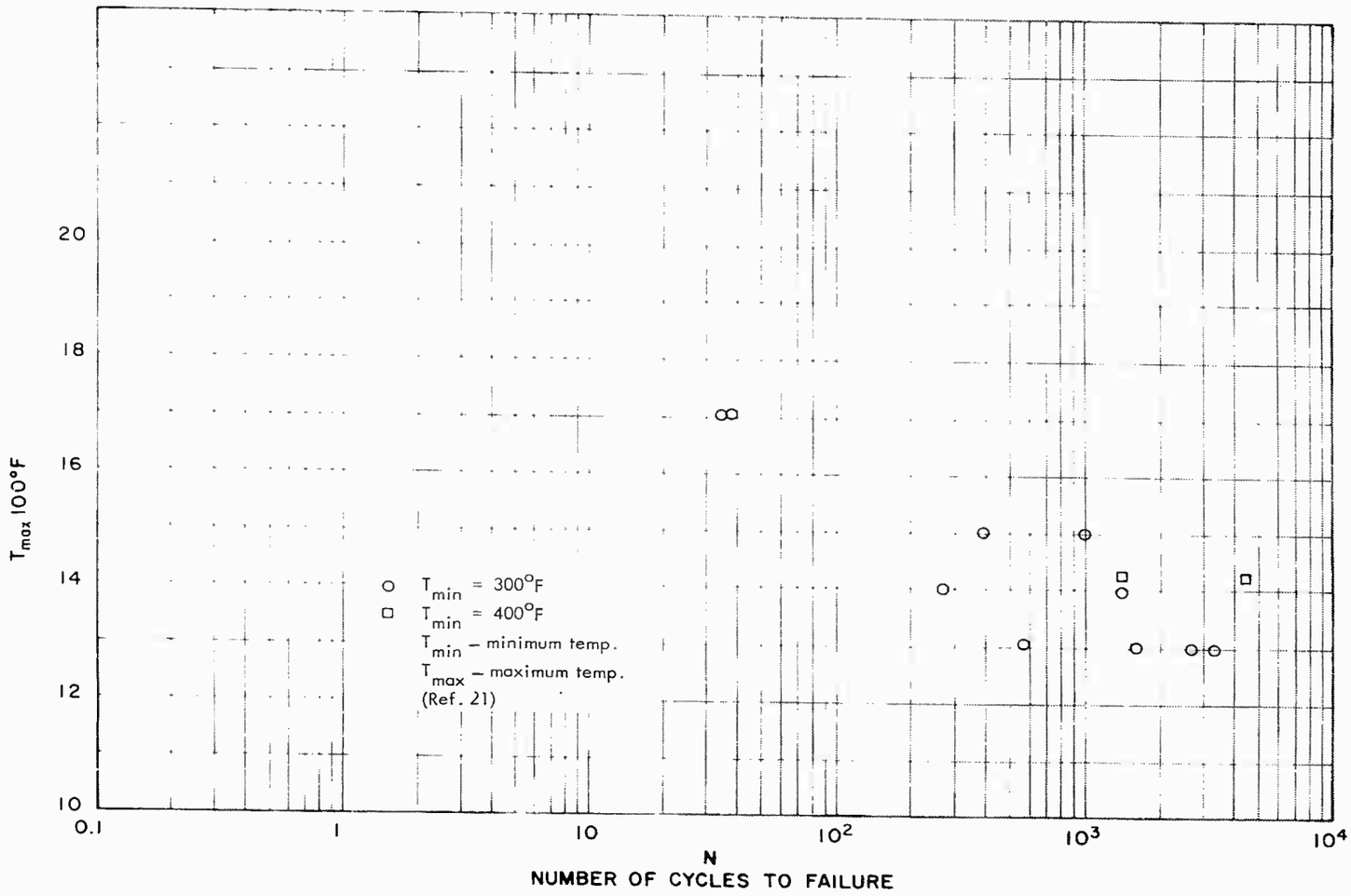

Fig. 4-11 Thermal Cycling of Cast Udimet 500 at Various Minimum Temperatures

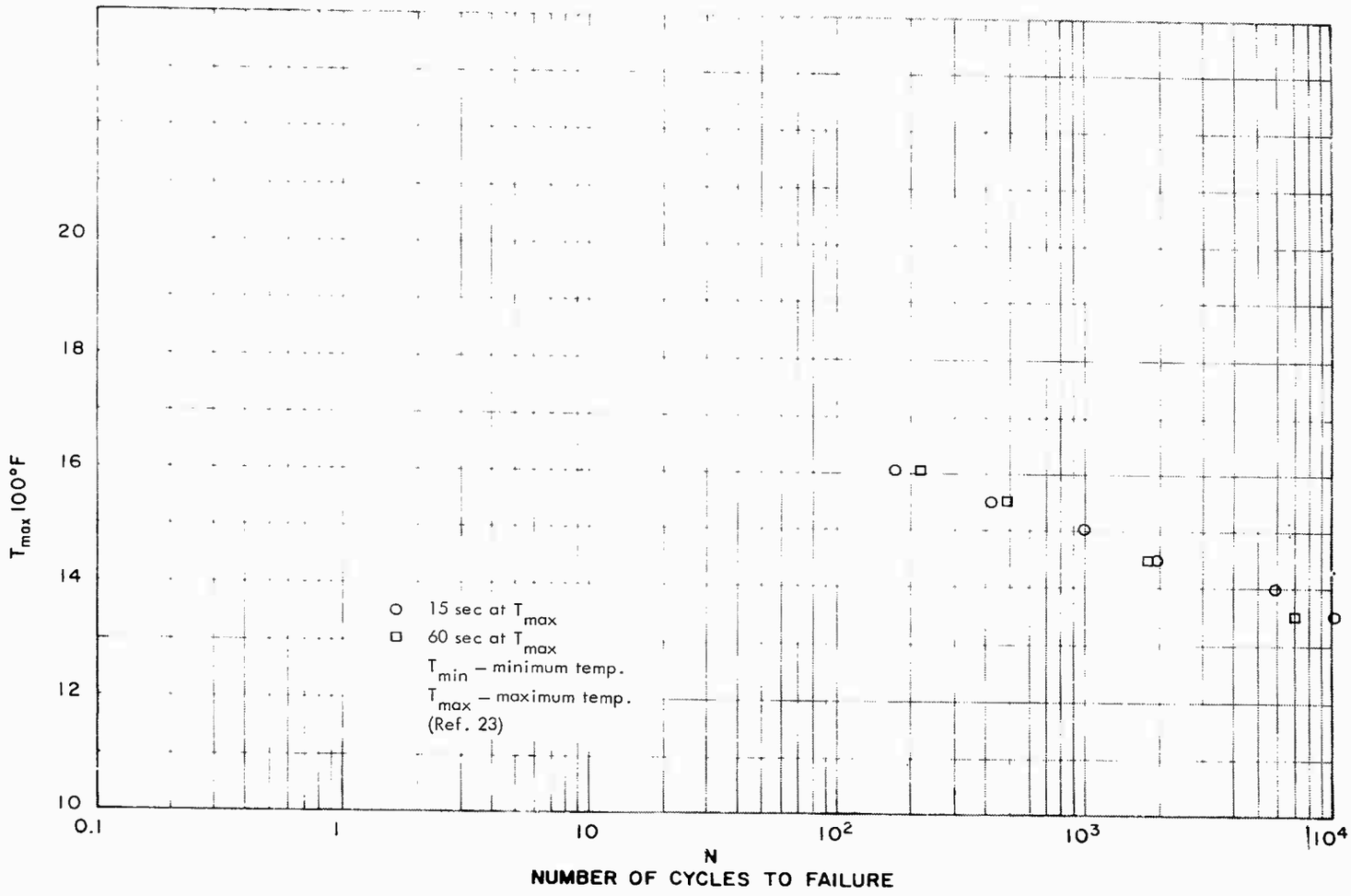

Fig. 4-12 Thermal Cycling of Inconel 550 at Two Constant Hold Times at Maximum Temperatures

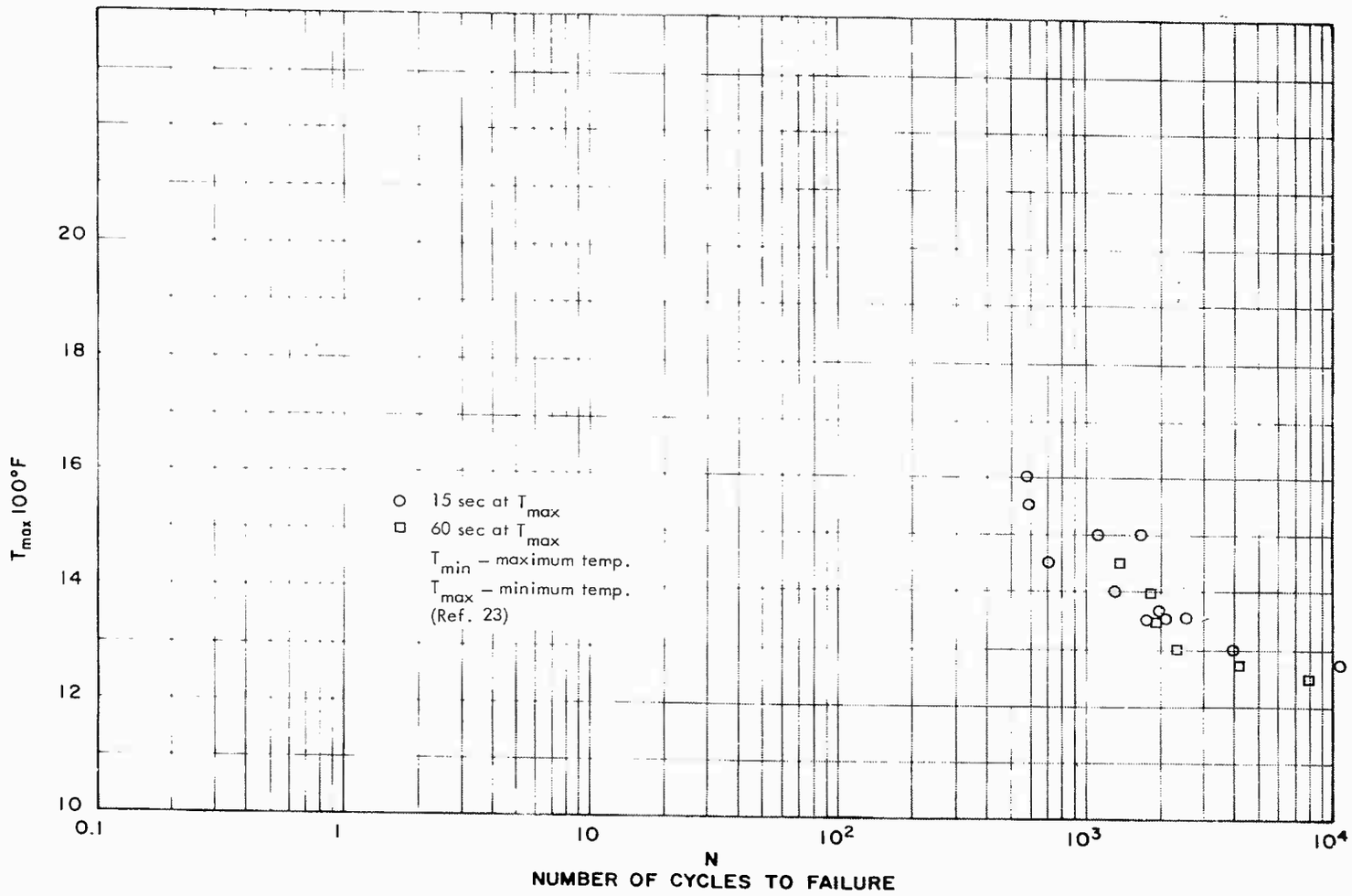

Fig. 4-13 Thermal Cycling of S-816 Steel at Two Constant Hold Times at Maximum Temperatures

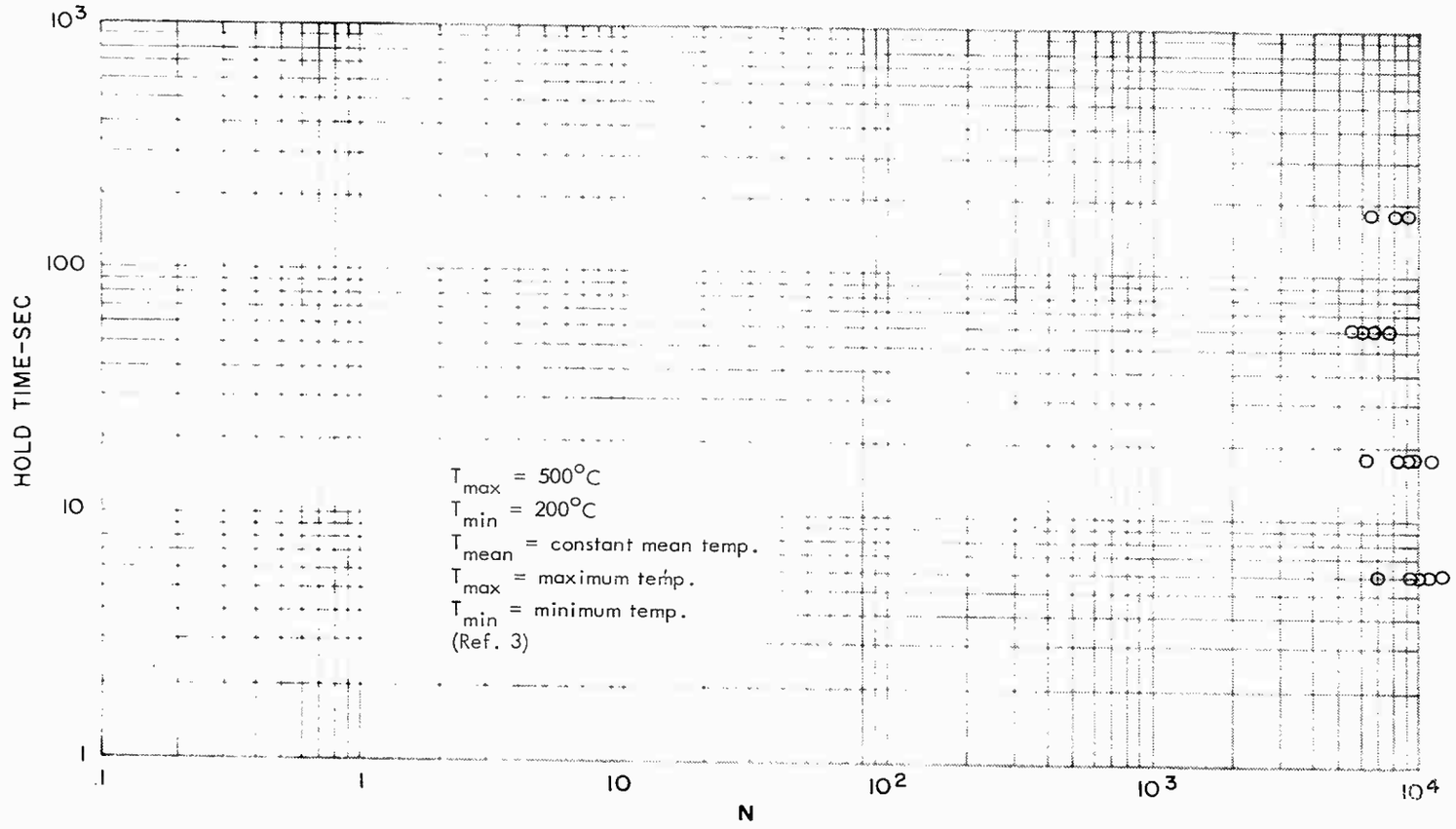

Fig. 4-14 Thermal Cycling of Type-347 Steel at Various Hold Times at Maximum Temperature

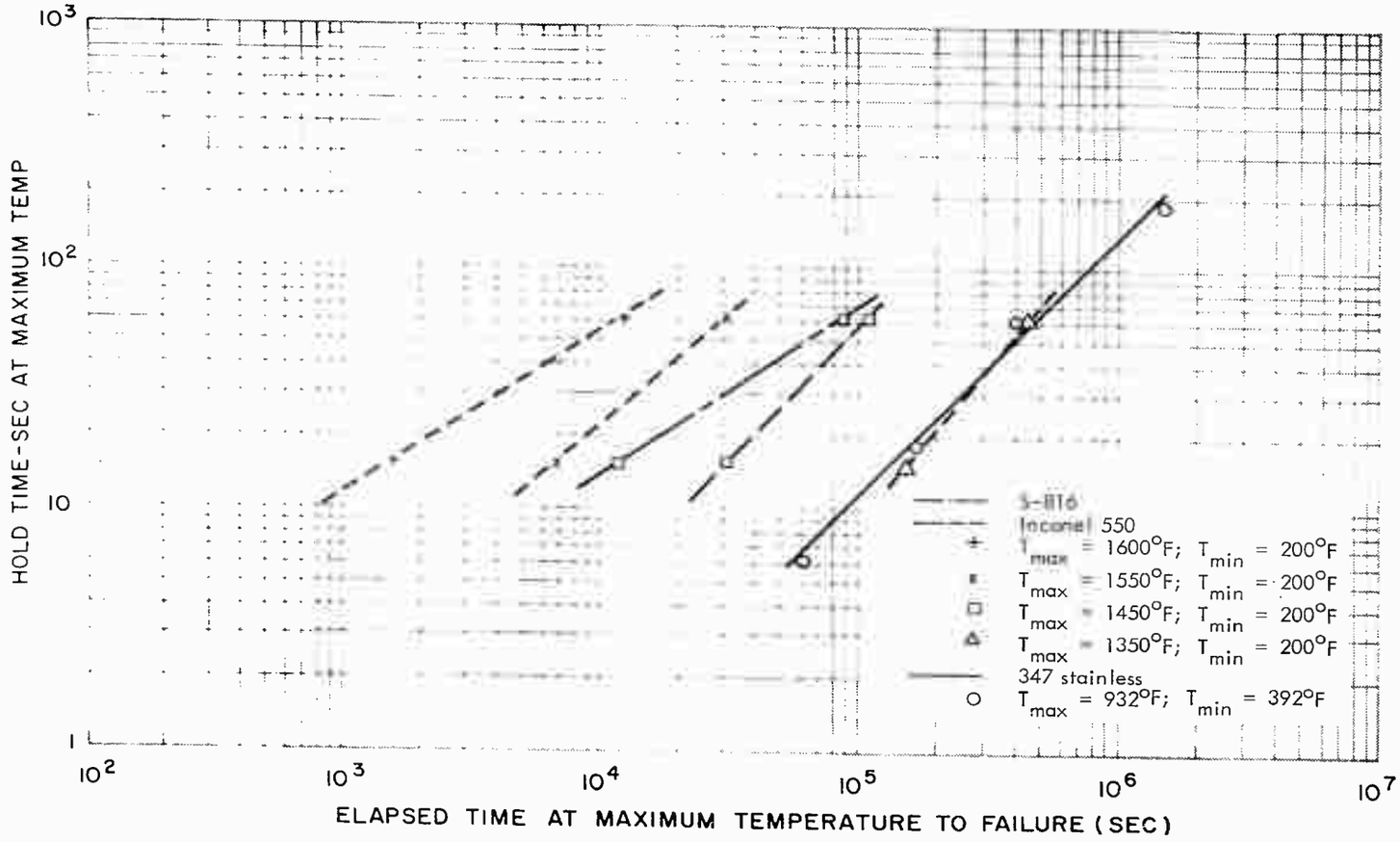

Fig. 4-15 Elapsed Time at Maximum Temperature for Thermal Cycling

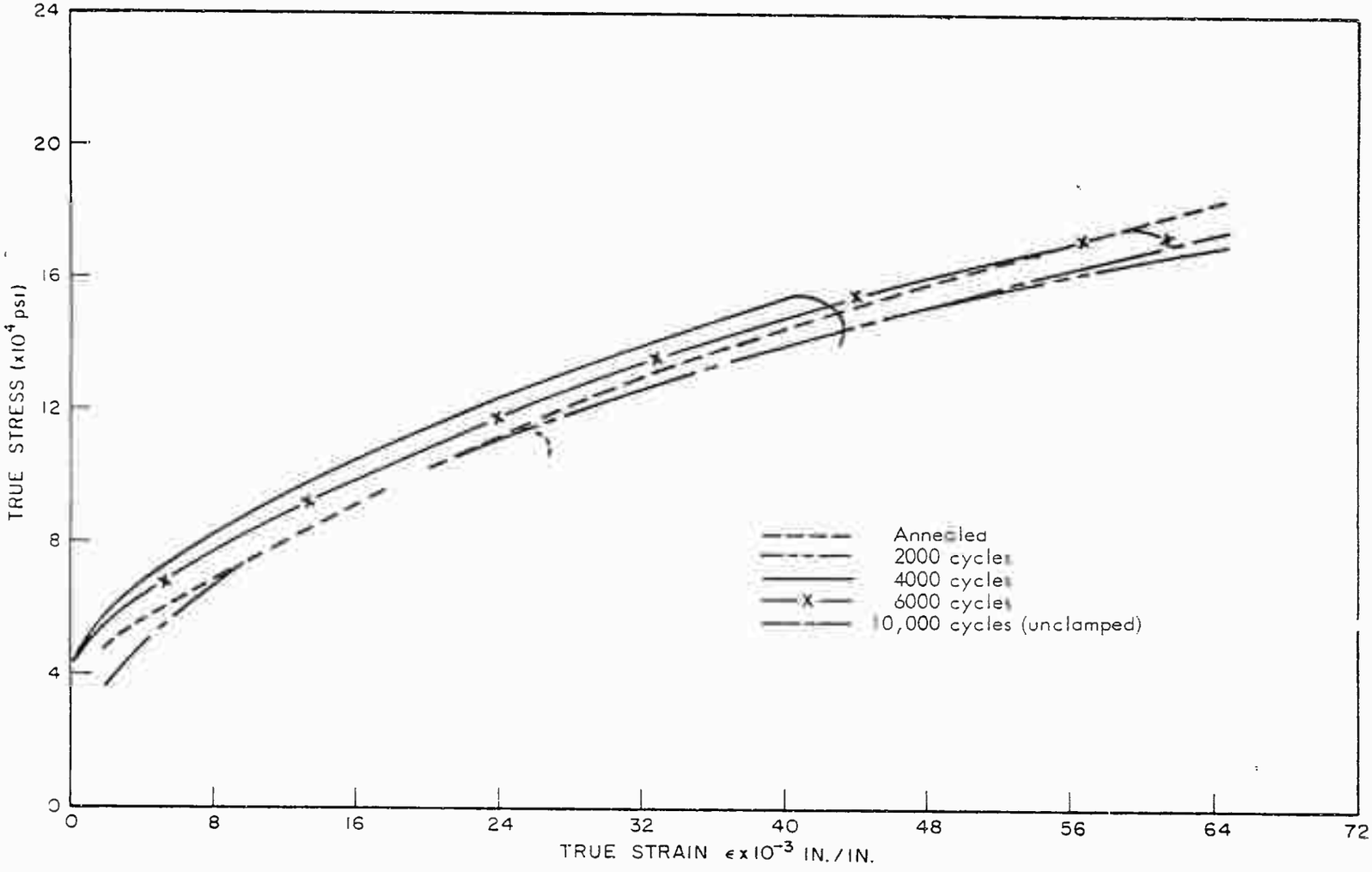

Fig. 4-16 True Stress-Strain Curves Following Thermal Cycling of Type-347 Stainless Steel

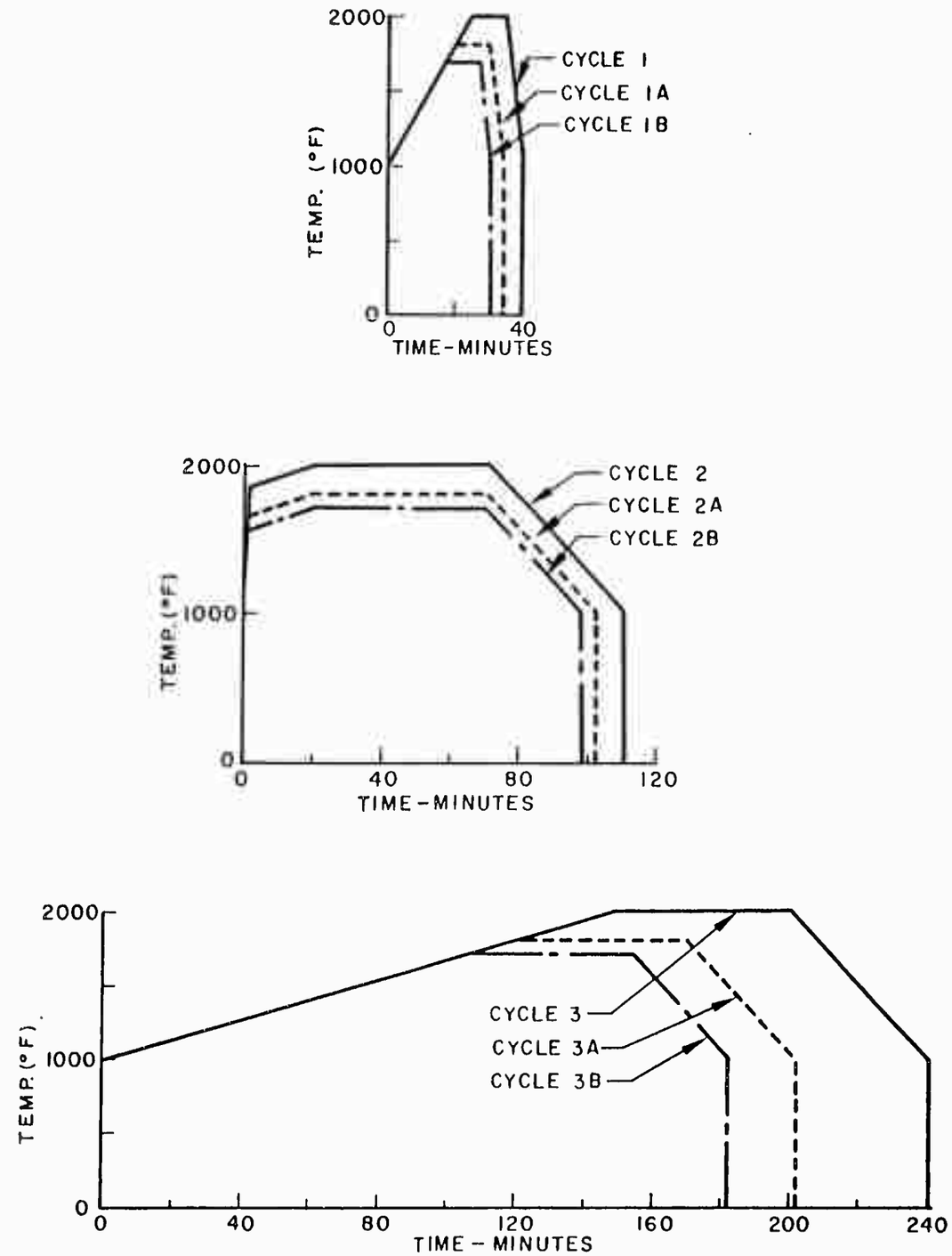

Fig. 4-17 Thermal Unconstrained Cycles

Section 5

BIAXIAL STRESS CYCLING

Strain cycling at a biaxial stress ratio of one-half or less can be obtained by reversed bending of a wide flat sheet which yields the maximum biaxiality of one-half whenever the width-to-thickness ratio (W/t) is greater than 8 and Poisson's ratio is one-half. For values of W/t below eight, the stress biaxiality varies approximately linearly with W/t. Sachs, Gerberich and Weiss (Ref. 9) have studied reversed bending cycling on three materials (A-302 steel, 5454-0 aluminum and 2024-T4 aluminum) and the effects of strain ratios, width-to-thickness ratios, and elevated temperatures. Low studied two aluminum alloys and three steels at a constant W/t ratio which is discussed in Section 2. Their testing did not include results at low cycles and high strains because of excessive curvature and buckling. Failure did occur at the center of the surface where biaxiality is greatest and ductility is usually least.

In general, the effects of the stress ratios, width-to-thickness ratios, and elevated temperatures were identical to uniaxial mechanical cycling at room temperature. Figures 5-1 through 5-8 show that most of the test results lie within the band for mechanical cycling at room temperature. The stress ratio of 0.875 resulted in three points outside of the scatter for A-302 steel and 5454-0 aluminum in Figs. 5-1 and 5-2 which is similar to uniaxial cycling. The test results on 2024-T4 aluminum at a stress ratio of (-1) shown in Figs. 5-3 and 5-6 fell below the scatterband at the highest strain ranges. Several points were above the scatter for A-302 steel for various W/t ratios in Figs. 5-4 and 5-7; however, some of Gucer's results (Ref. 30) for the same material for a W/t ratio of 5.0 were outside of the scatter, indicating that the results may be correct, but unexplained.

Although a few points did not lie within the scatterband, it is encouraging to note that the biaxial stress condition produced the same results as uniaxial testing.

Although the condition of biaxiality is a special case applicable to cylindrical pressure vessels, it does afford the opportunity to predict fatigue life from uniaxial experimental results.

In Refs. 31, 32, and 33, results are reported on the effects on cycles-to-failure of cycle frequency, welding, and notches for A-302 and A-201 steels. As expected, the notched and welded specimens gave results below the scatterband, and the frequency resulted in very little effect on cycles-to-failure. These data are quite limited, and all of the experimental results are greater than 2,000 cycles-to-failure (Fig. 5-9).

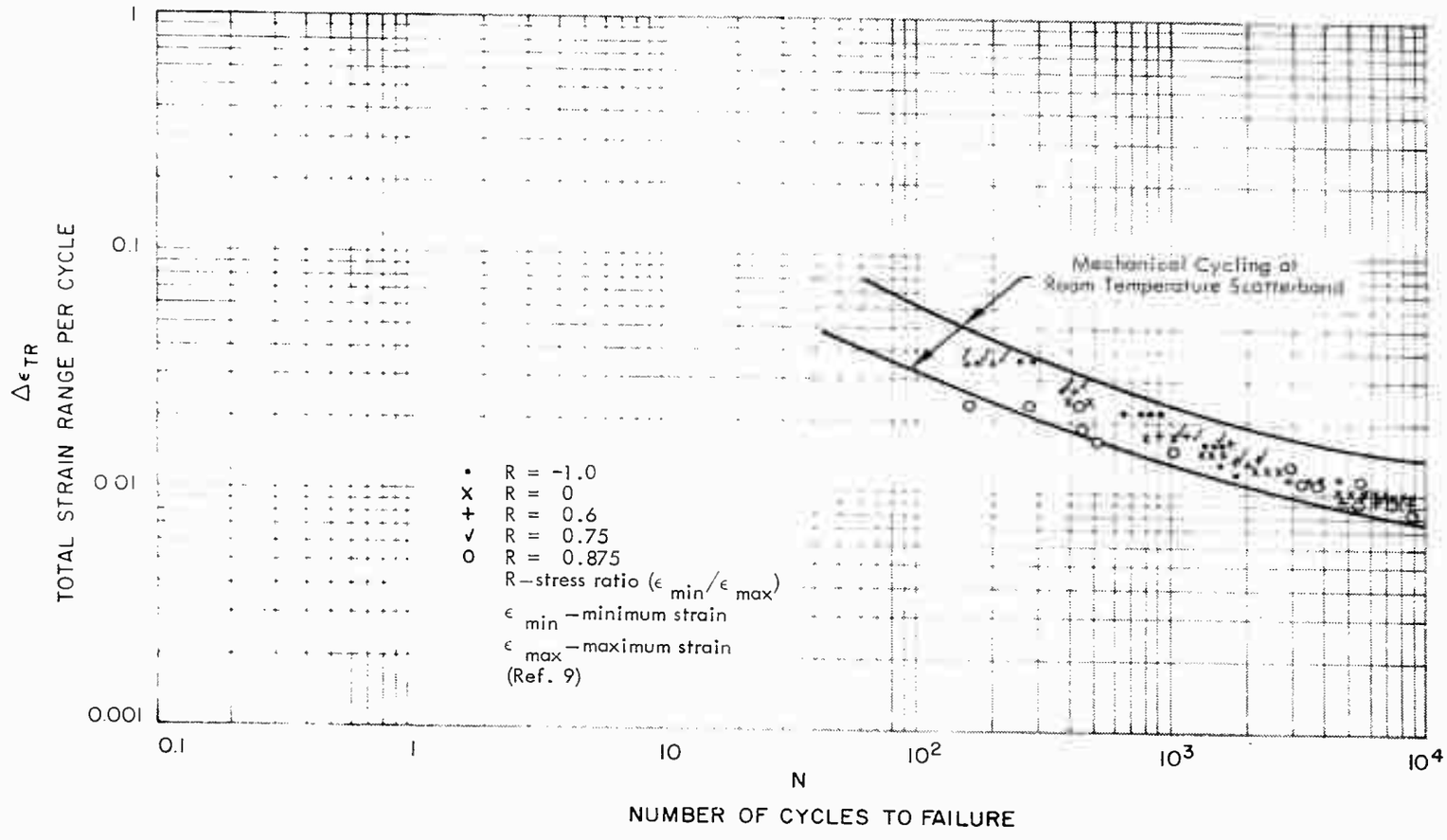

Fig. 5-1 Bending Cycles for A-302 Steel at Various Stress Ratios

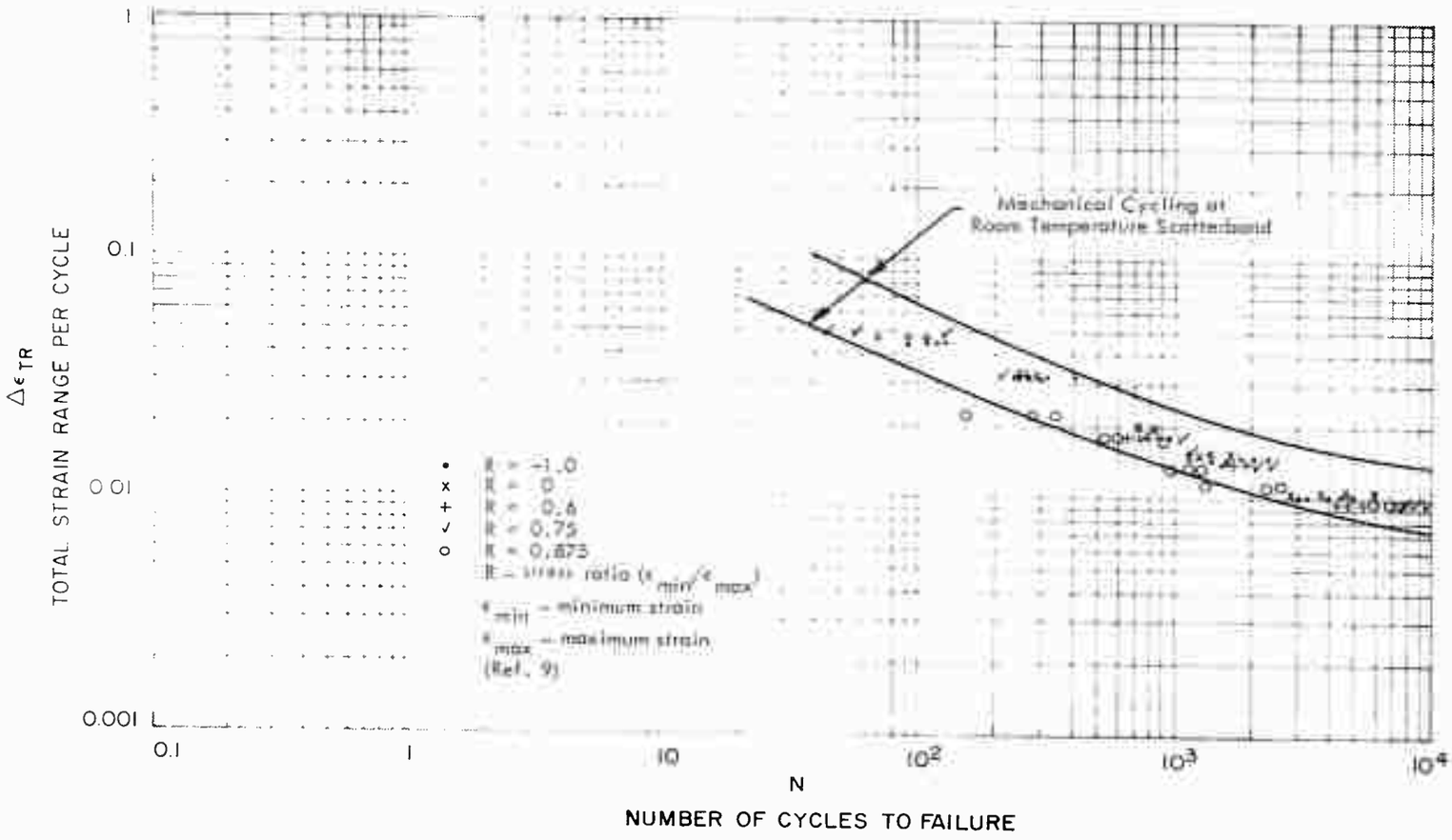

Fig. 5-2 Bending Cycles for 5454-0 Aluminum at Various Stress Ratios

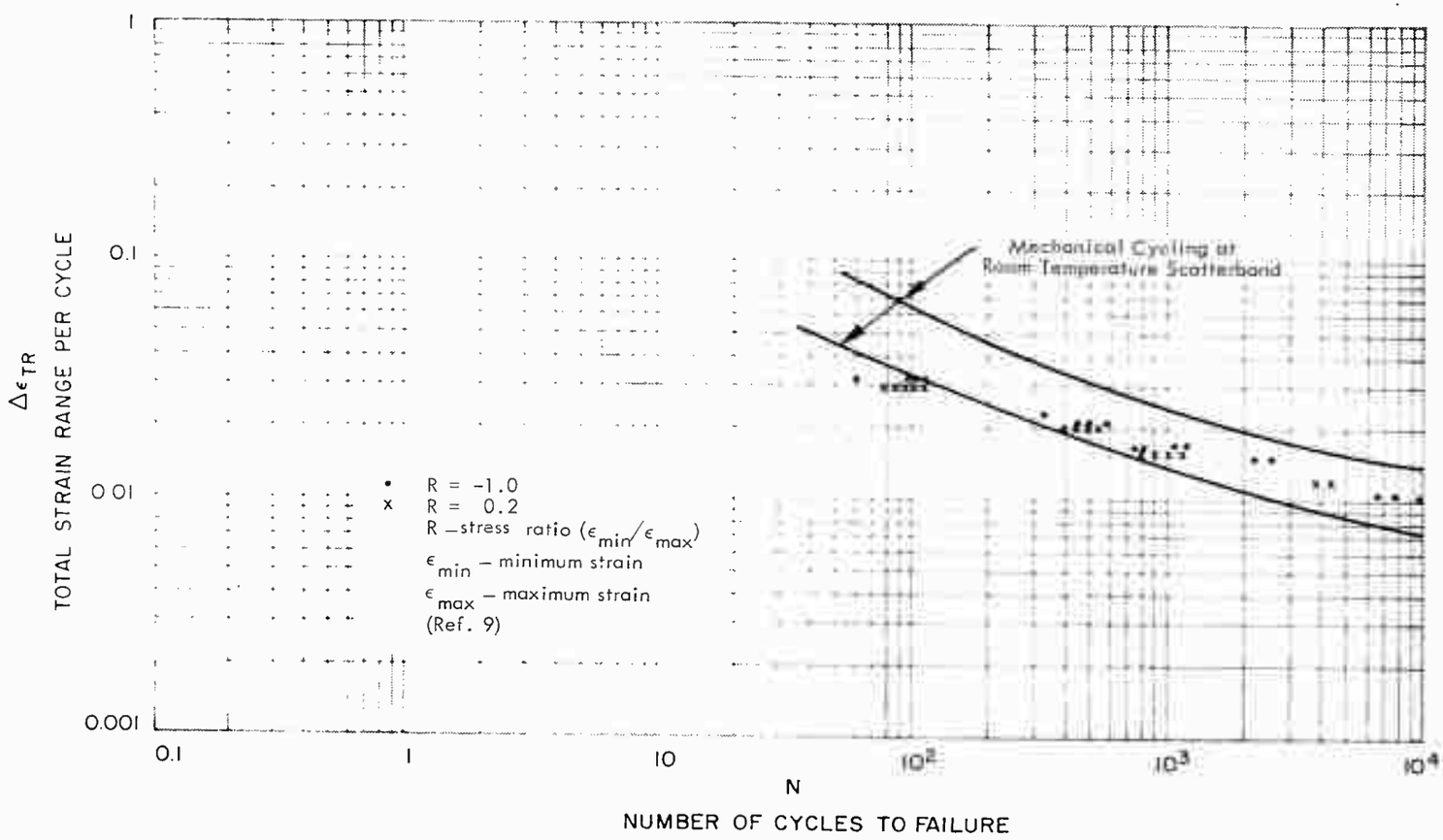

Fig. 5-3 Bending Cycles for 2024-T4 Aluminum at Various Stress Ratios

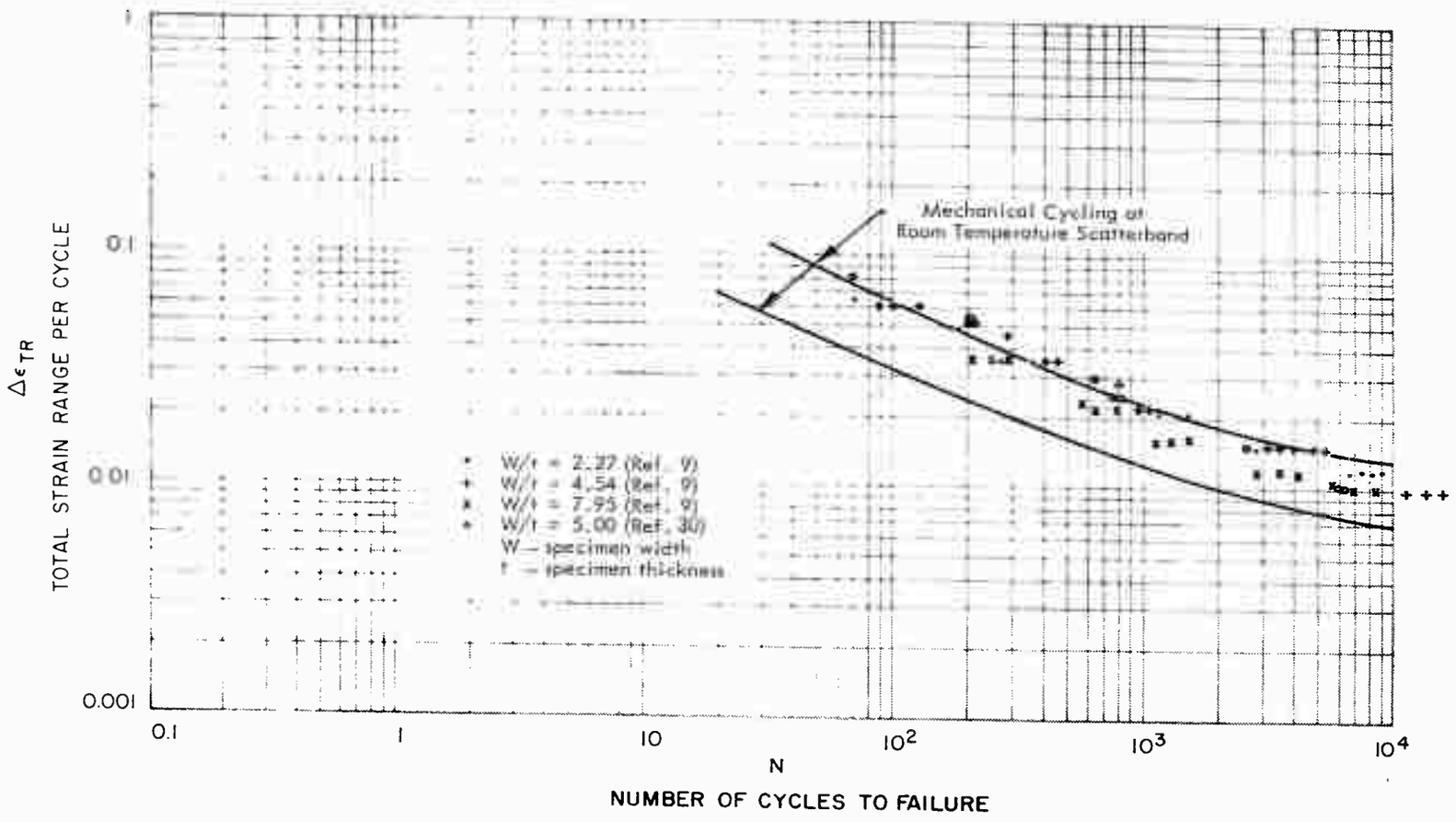

Fig. 5-4 Bending Cycles for A-302 Steel at Various Specimen Width-to-Thickness Ratios

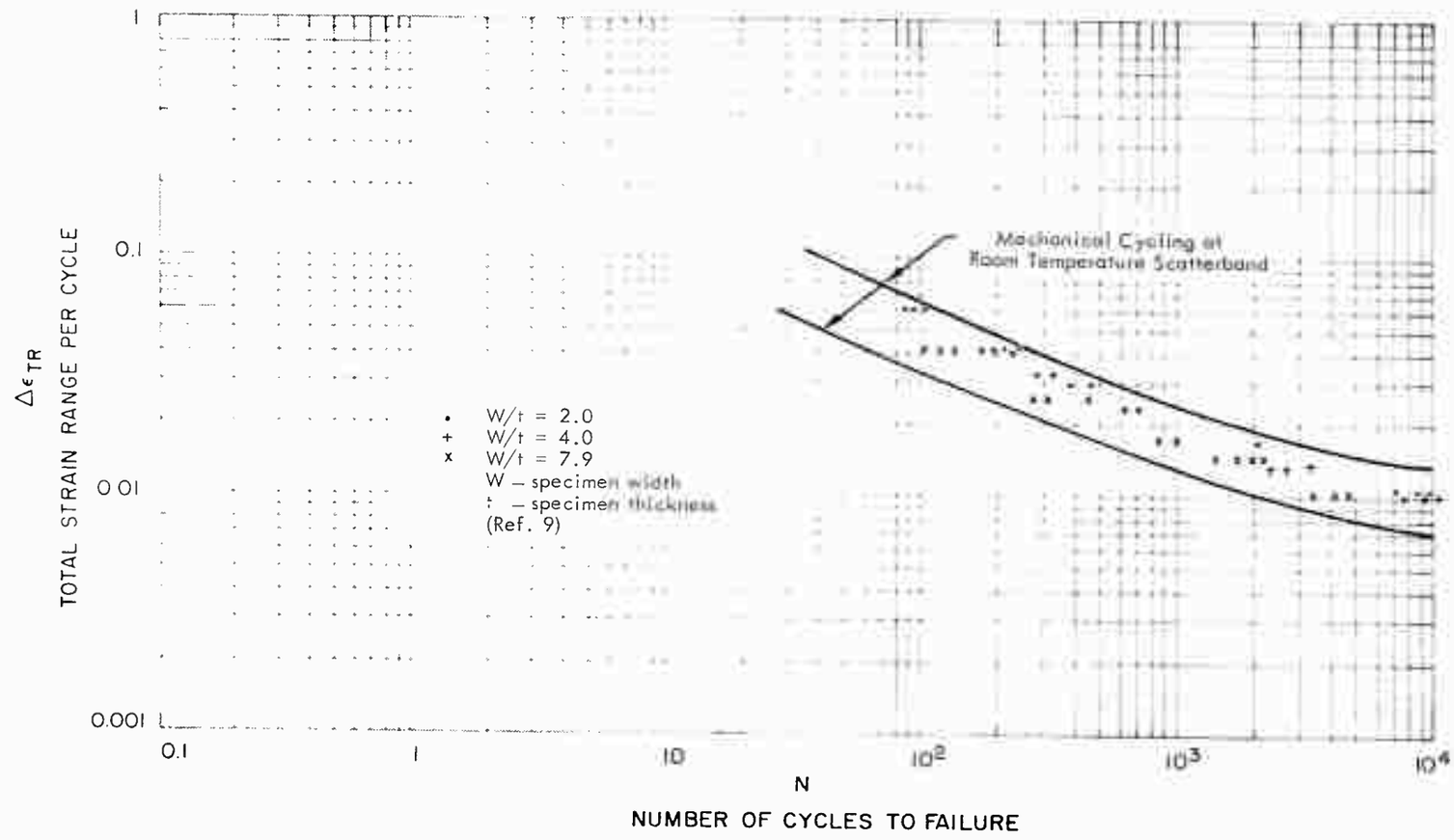

Fig. 5-5 Bending Cycles for 5454-0 Aluminum at Various Specimen Width-to-Thickness Ratios

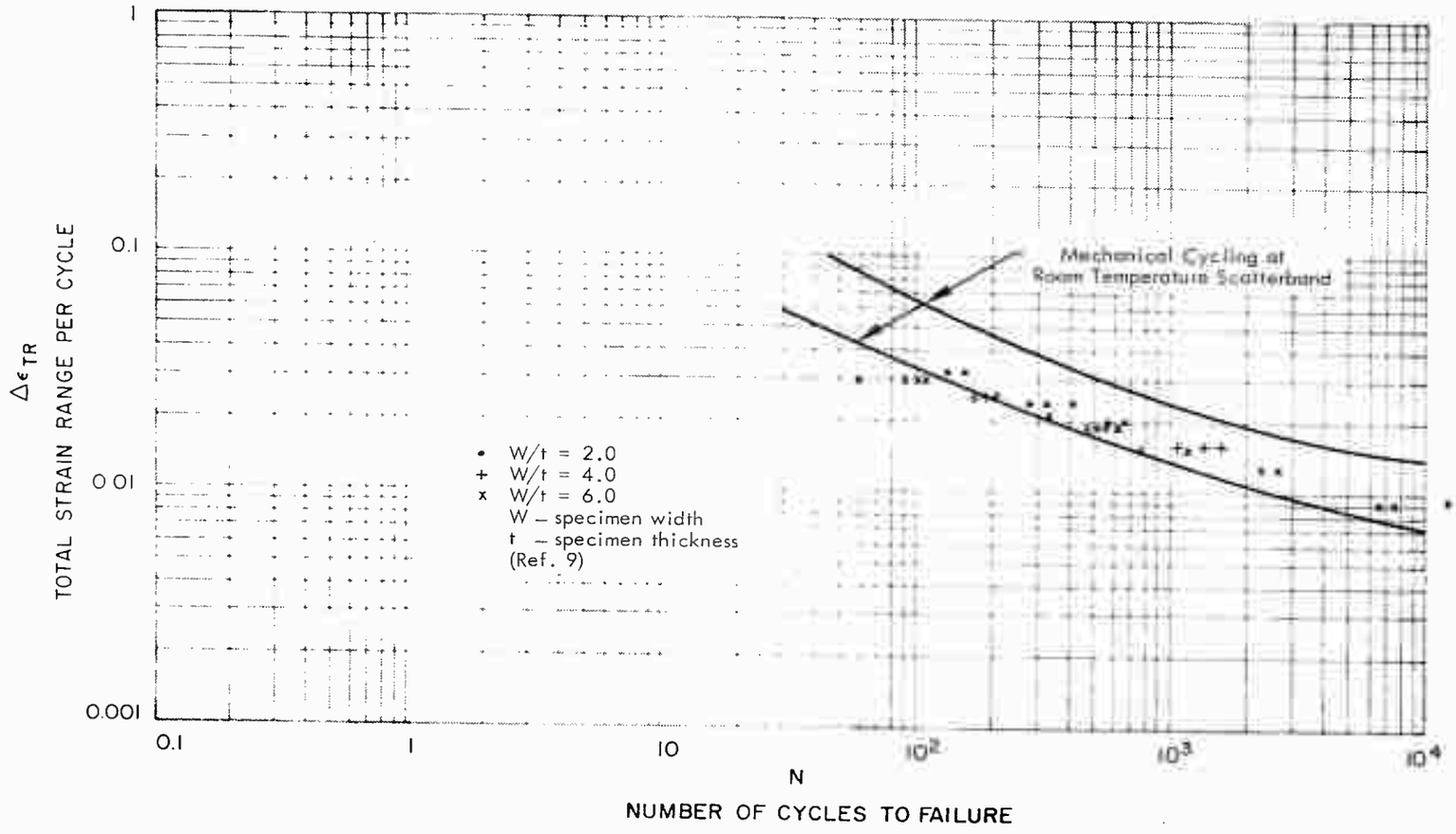

Fig. 5-6 Bending Cycles for 2024-T4 Aluminum at Various Specimen Width-to-Thickness Ratios

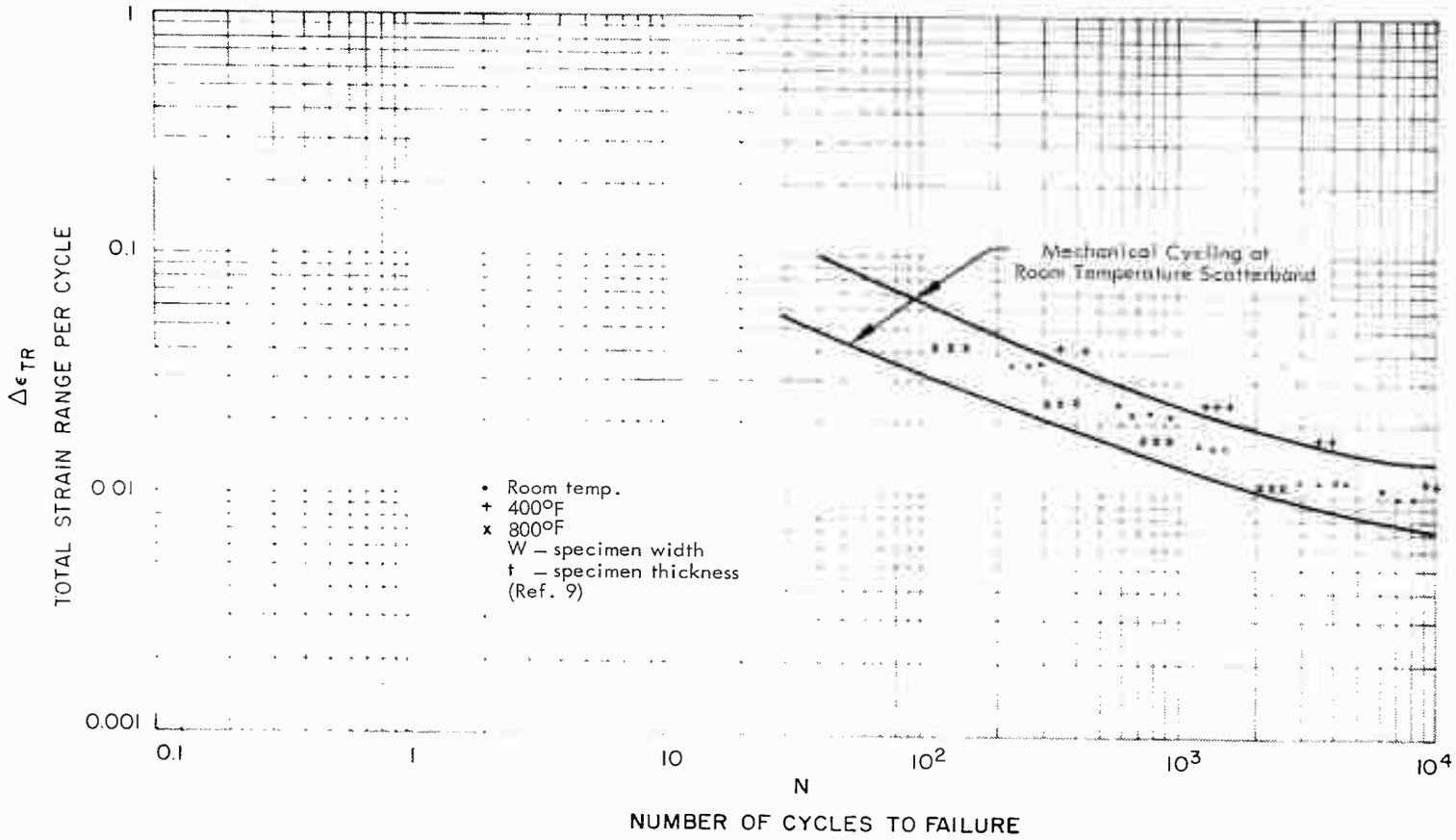

Fig. 5-7 Bending Cycles for A-302 Steel at Various Elevated Temperatures

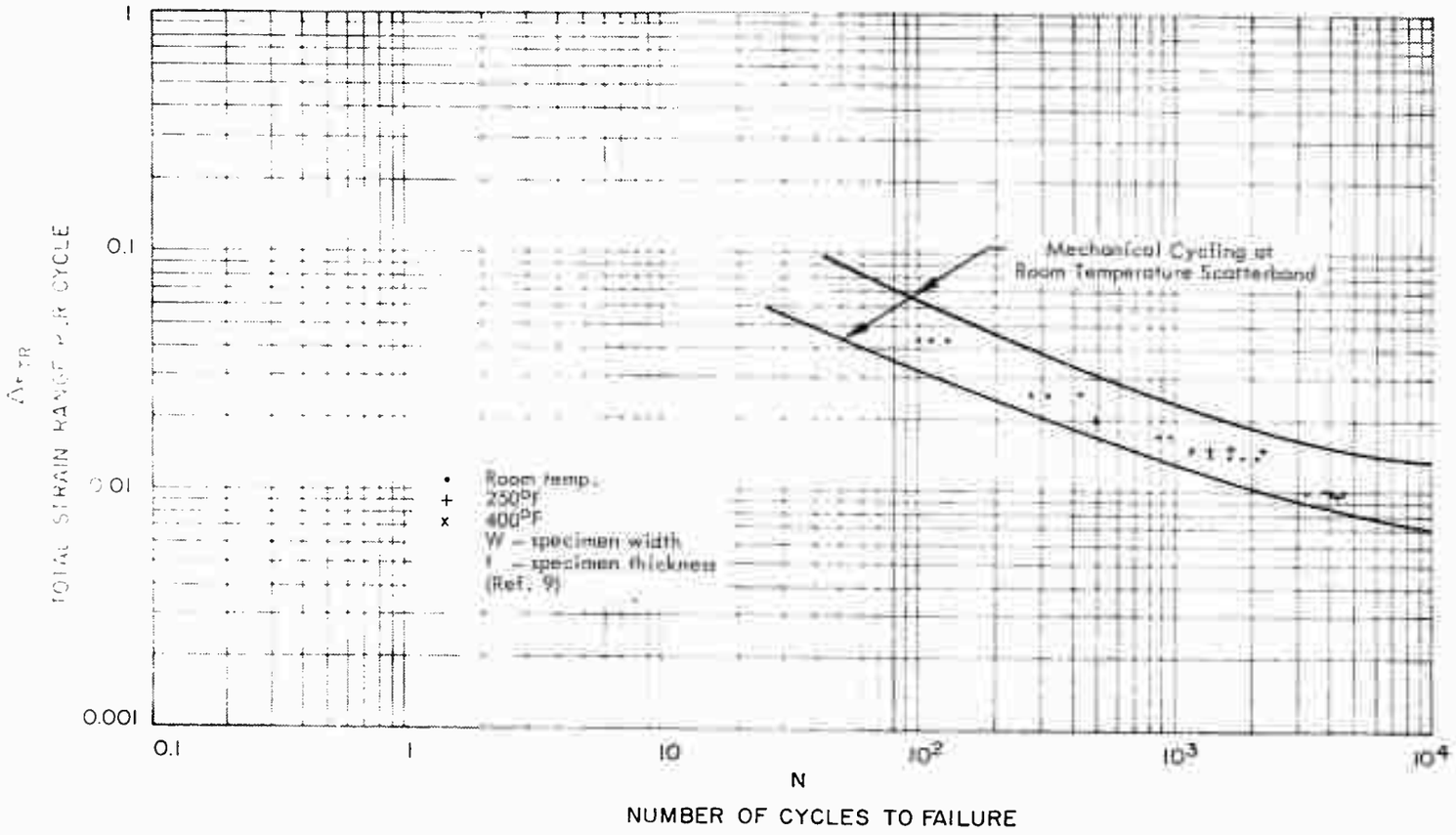

Fig. 5-8 Bending Cycles for 5454-0 Aluminum at Various Elevated Temperatures

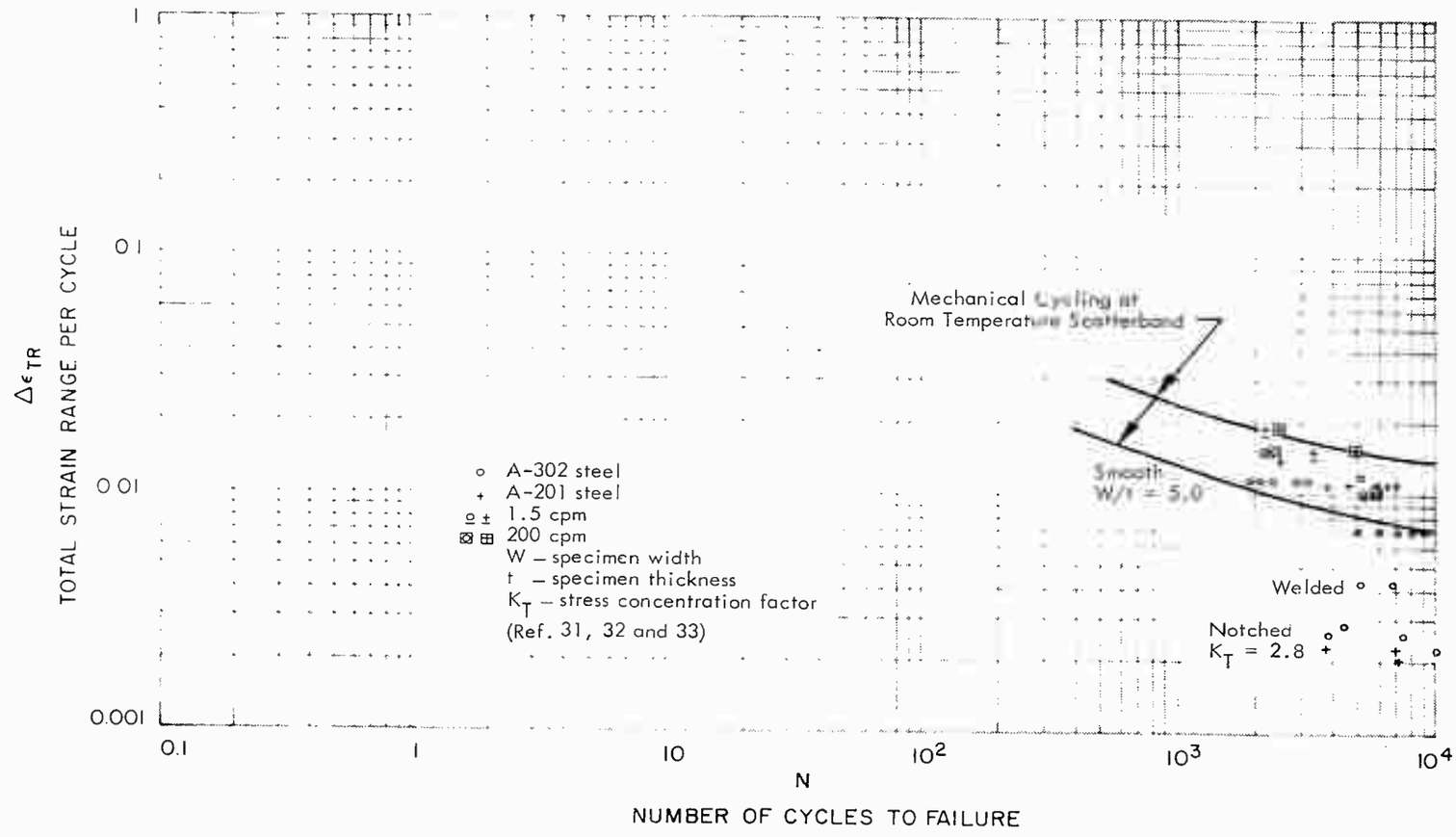

Fig. 5-9 Bending Cycles for A-302 and A-201 Steel

Section 6

METHODS OF PREDICTING LOW CYCLE FATIGUE

There appears to be no single expression which will accurately predict the cycles-to-failure for all materials for all three cycling conditions (mechanical loading at room temperature, mechanical loading at elevated temperature, and thermal variation with mechanical fixity). A single expression can be derived for mechanical cycling at room temperature and elevated temperature which is conservative for all cycles between 1/4 and 10,000. This expression is extremely conservative for cycles greater than 200 (Fig. 1-1) and is written as follows:

$$N = \left[\frac{0.289}{\Delta\epsilon_{TR}} - \frac{1}{2}\left(\frac{1+R}{1-R}\right)\right]^2 \qquad (6.1)$$

Additional experimental results are necessary for thermal cycling before a more accurate expression for predicting cycles-to-failure can be determined.

Several investigators (Refs. 3, 4, 7 and 9) have arrived at expressions for predicting the cycles-to-failure. Manson arrived at the relationship

$$N = K/\epsilon^n \qquad (6.2)$$

where K and n are material constants determined from tests and ϵ is plastic strain.

From plotting the data of Sachs et al. (Ref. 2) for 24-ST aluminum which pertained to mechanical cycling at room temperature, Manson found the exponent n equal to three. Concurrently, Coffin (Ref. 19) arrived at a similar expression from his investigations on thermal cycling of 347-stainless steel as follows:

$$N^k \Delta\epsilon_p = C \qquad (6.3)$$

where C and k are material constants determined from tests and $\Delta\epsilon_p$ is the plastic strain range per cycle.

Coffin's data yielded an exponent k equal to +1/2 which would be an exponent n equal to 2 for Manson's relationship. Coffin found that by plotting the total plastic strain ($N\Delta\epsilon_p$) against cycles-to-failure (N) on log-log coordinates with the fracture ductility (ϵ_f) used for $\Delta\epsilon_p$ at N equal to 1/4, the plot resulted in a straight line. The plot for annealed as well as cold-worked 347-stainless steel gave similar linear relationships. The constant C varied with each material and is determined from Eq. (6.3) assuming $\Delta\epsilon_p = 2\epsilon_f$ at N = 1/4, which neglects the elastic strain portion of the fracture ductility.

If one uses these assumptions and sets k = 1/2, C becomes equal to ϵ_f and the expression becomes

$$N = \left[\frac{\epsilon_f}{\Delta\epsilon_p}\right]^2 \tag{6.4}$$

D'Amato and Sachs (Refs. 7 and 9) concurrently established that any expression relating the variables of strain cycling must include the strain ratio R .

D'Amato assumed Coffin's relationship valid, and in his work used the form:

$$N^{C_1}\epsilon_R = C_2$$

where C_1 and C_2 are material constants determined from tests and ϵ_R is the total strain range.

Since $\epsilon_R = \epsilon_{max}(1 - R)$, D'Amato's relation becomes

$$N^{C_1} = \frac{C_2}{\epsilon_{max}(1 - R)} \tag{6.5}$$

D'Amato found that C_1 was the same for all configurations tested and that C_2 varied substantially with configuration.

Sachs assumed the same form for the relationship among the parameters of this problem, as did Coffin, but introduced the mean strain ϵ_m to yield:

$$N = \left[\frac{\epsilon_f - \epsilon_m}{2 \epsilon_{TR}} \right]^a \tag{6.6a}$$

Dividing each term within the brackets by ϵ_{max} and using Coffin's assumptions that $a = 2$ and $\epsilon_f \sim \epsilon_{TR} \sim \epsilon_{max}$ (or $2 \epsilon_{TR} = \Delta\epsilon_{TR}$) at $N = 1/4$ yields:

$$N = \left[\frac{\frac{\epsilon_f}{\epsilon_{max}} - \frac{1 + R}{2}}{1 - R} \right]^2 \tag{6.6b}$$

or substituting $\epsilon_{max} = \frac{\Delta\epsilon_{TR}}{1 - R}$ yields:

$$N = \left[\frac{\epsilon_f}{\Delta\epsilon_{TR}} - \frac{1}{2}\left(\frac{1 - R}{1 - R}\right) \right]^2 \tag{6.6c}$$

A plot of Sachs' expression with experimental results is shown in Fig. 1-5 and there is good correlation between the calculations and experimental results for cycles less than 200.

Manson (Ref. 34) arrived at a relationship based upon stress range $(\Delta\sigma)$ for predicting cycles-to-failure as

$$\Delta\sigma = G N^k$$

From tests, he found $G = 2\,\sigma_f$ and $k = 0.12$, which yielded

$$\Delta\sigma = 2\,\sigma_f\,N^{-0.12} \tag{6.7}$$

Manson then used Coffin's expression with a plastic strain range of

$$\epsilon_p = M\,N^Z$$

A good approximation is given by $Z = -1/2$, while the plastic strain range per cycle at $N = 1/4$ is 1.5 times the true logarithmic ductility D.

$$D = \ln\left(\frac{1}{1 - R_a}\right)$$

where $R_a = \dfrac{A_o - A}{A_o}$

Substituting these values into the preceding expression gives $M = 0.75\,D$ to account for all strain ratios. As a result

$$\epsilon_p = 0.75\,D\,N^{-1/2} \tag{6.8}$$

Combining the stress range with the plastic strain range will yield a relationship between the stress and strain for converting experimental stress data to the strain data, or vice versa. That is,

$$\Delta\sigma = G\left(\frac{\epsilon_p}{M}\right)^{k/z}$$

or

$$\Delta\sigma = 2\,\sigma_f\left(\frac{\Delta\epsilon_p}{3\,D}\right)^{0.24} \tag{6.9}$$

The stress-plastic strain relation appears to be valid, but certain restrictions regarding its use are indicated. The plastic strain range was applicable only to thermal cycling where, for that loading condition, it had to be estimated; total strain range was the better parameter for mechanical cycling. The expression would be similar if total strain were the parameter. However, the exponent is only an approximation, and to obtain better correlation it would have to be determined for each material, which is an impractical step.

Equations (6.2), (6.3) and (6.4) are all equivalent with similarly defined terms. If we change ϵ of Eq. (6.2) to plastic strain range $\Delta\epsilon_p$ and K to $C^{1/k}$, as well as n to 1/k (constants determined from tests), these expressions can be rewritten as

$$N = \left[\frac{C}{\Delta\epsilon_p} \right]^{1/k}$$

When $1/k = 2$ and $C = \epsilon_f$, then

$$N = \left[\frac{\epsilon_f}{\Delta\epsilon_p} \right]^2$$

D'Amato's expression (6.5) can be written as

$$N = \left[\frac{C_2}{\epsilon_R} \right]^{1/C_1}$$

where $\epsilon_R = \epsilon_{max}(1 - R)$ and $R = \epsilon_{min}/\epsilon_{max}$.

Then $\epsilon_R = \epsilon_{max} - \epsilon_{min}$, which is the definition of the total strain range $\Delta\epsilon_{TR}$ so

$$N = \left[\frac{C_2}{\Delta\epsilon_{TR}} \right]^{1/C_1}$$

If we make the assumptions that at $N = 1/4$, $\Delta\epsilon_p = \Delta\epsilon_{TR} = 2\,\epsilon_f$, and $1/C_1 = 2$, then $C_2 = \epsilon_f$ and Eq. (6.10) becomes identical to Eq. (6.4)

$$N = \left[\frac{\epsilon_f}{\Delta\epsilon_{TR}}\right]^2 \tag{6.10}$$

Sachs, by assuming that Coffin's expression (6.3) is valid, derives his expression (6.6a) with the introduction of the mean strain ϵ_m.

The mean strain ϵ_m can be easily introduced by assuming a cycling between ϵ_{max} and ϵ_{min} where ϵ_{max} is almost equal to the fracture ductility ϵ_f as shown in Fig. 6-1.

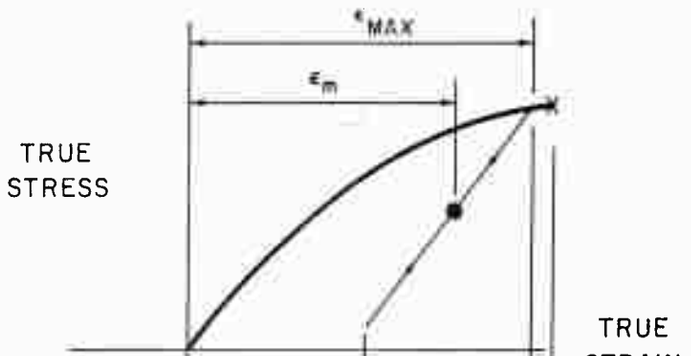

Fig. 6-1 Cycling About a Mean Strain

In solving for the constant C in Coffin's expression (6.3), set $k = 1/2$, $N = 1/4$ cycle, set $\Delta\epsilon_p = \Delta\epsilon_{TR} = 2\,(\epsilon_{max} - \epsilon_m)$ per cycle as indicated by Fig. 6-1 above, then

$$C = \left(\frac{1}{4}\right)^{1/2}\left[2\,(\epsilon_f - \epsilon_m)\right] = \epsilon_f - \epsilon_m$$

Substituting the values for C , $\Delta\epsilon_p$ and k into Coffin's Eq. (6.3) will give an equation for predicting cycles-to-failure for cycling about a mean strain as follows:

$$N = \left[\frac{\epsilon_f - \epsilon_m}{\Delta\epsilon_{TR}} \right]^2 \qquad (6.11)$$

Rewriting expression (6.11) by changing the exponent 2 to an a and by changing $\Delta\epsilon_{TR}$ to $2\,\epsilon_{TR}$ results in Sachs' expression (6.6a). If the mean strain is equal to zero, then the expression above reduces to expression (6.4) as

$$N = \left[\frac{\epsilon_f}{\Delta\epsilon_{TR}} \right]^2$$

It has been shown that the expressions of Manson, Coffin, D'Amato and Sachs, (6.2), (6.3), (6.5), and (6.6a), respectively, reduce to the same equations when $\epsilon_m = 0$, $\Delta\epsilon_p = \Delta\epsilon_{TR}$ and $R = -1$. Expression (6.6b) can easily be derived from $\epsilon_m = (\epsilon_{max} + \epsilon_{min})/2$, $\Delta\epsilon_{TR} = \epsilon_{max} - \epsilon_{min}$, and $R = \epsilon_{min}/\epsilon_{max}$ when substituted into expression (6.6a). It is also obvious from Fig. 1-5 that the strain ratio, R, or mean strain must be included in an expression for predicting cycles-to-failure. Although all of the data plotted for mechanical cycling in Figs. 1-1 and 1-2 are for a mean strain of zero, a general expression is written for the lower boundary of the scatterband with a slope of -1/2 up to 500 cycles and a slope of -1/5 beyond 500 cycles, where the strain ratio is ineffective.

$$N_{<500} = \left[\frac{0.289}{\Delta\epsilon_{TR}} - \frac{1}{2}\left(\frac{1+R}{1-R}\right) \right]^2 \qquad (6.12a)$$

and

$$N_{<500} = \left[\frac{0.0447}{\Delta\epsilon_{TR}} \right]^5 \qquad (6.12b)$$

The strain ratio (R) was included in expression (6.12a) because Sachs (Fig. 1-5) had shown it to be necessary for 24ST, although there is not sufficient data available for all materials to justify the inclusion of such a term in the predicting equation. The general expression (6.12a) is somewhat conservative over the range of endurance and extremely conservative for cycles greater than 500, so expression (6.12b) is valid for cycles greater than 500 cycles. Expressions (6.12a) and (6.12b) are submitted for all materials with the total strain range and strain ratios as the predominate parameters. They are inadequate for predicting failure due to thermal cycling. It would be unconservative for thermal cycling if one used the plastic strain range per cycle in place of the total strain range parameter. These expressions are plotted as the dashed lines in Figs. 1-1 and 1-2, for $R = -1$.

Section 7

THERMAL SHOCK CRITERIA

7.1 INTRODUCTION

The term thermal shock customarily pertains to the brittle fracture of a material exposed to a single near-instantaneous change of temperature. When a material is subjected to high thermal gradients, excessive stress may result; should these stresses reach the critical or ultimate value in a single cycle of temperature application, thermal fracture of the material occurs.

In addition to certain material considerations to be discussed below for the three thermal-shock criteria – brittle materials, short time exposure, or ductile materials – the structural configuration is very important in limiting critical stresses. Localized stress concentrations caused by sharp corners, surface irregularities, holes, notches, or flaws in the microstructure may also initiate rapid thermal cracking. Structural constraints which limit or prevent free thermal expansion similarly cause structural damage by thermal shock. Such constraints include edge fixity, structural combinations of materials having dissimilar expansion coefficients, and size or thickness effects.

7.2 BRITTLE MATERIALS

To assess quantitatively a material's capability to resist thermal shock conditions, performance indexes or shock-resistance factors have been suggested for brittle materials in Refs. 35 through 43.

Embodied in these parameters are combinations of five different material properties as follows:

- Breaking strength σ_b
- Modulus of elasticity, E

- Poisson's ratio, μ
- Coefficient of linear expansion, α
- Thermal conductivity, k

Manson (Ref. 37) and others have suggested two separate thermal-shock parameters to define shock resistance as follows:

$$P_1 = (k\,\sigma_b)/(E\,\alpha)$$

$$P_2 = \sigma_b/(E\,\alpha)$$

These are derived from time-temperature-stress relations pertaining to a homogeneous flat plate. The underlying assumption that stress in these parameters be based upon an elastic analysis is justified because brittle failure is not encumbered with the complexities of plastic flow. Even certain semiductile materials, under the impact loadings accompanying thermal shock, behave in a brittle manner. Nondimensional stress (ratio of actual stress to the stress which would exist with complete restraint to thermal expansion) is

$$\sigma' = \frac{\sigma\,(1-\mu)}{E\,\alpha\,T_o} \tag{7.1}$$

where T_o = initial uniform temperature of plate above ambient temperature of zero.

The maximum nondimensional stress is

$$\sigma'_{max} = \frac{\sigma_b\,(1-\mu)}{E\,\alpha\,T_o} = \frac{P_2\,(1-\mu)}{T_o} \tag{7.2}$$

From a heat flow analysis to determine maximum stress as a function of heat transfer, a reasonable fit is given by

$$\frac{1}{\sigma'_{max}} = 1.5 + \frac{3.25}{\beta} - 0.5\, e^{-16/\beta} \qquad (7.3)$$

where β = nondimensional heat transfer parameter, ah/k.

a = plate half-thickness

h = heat transfer coefficient

k = thermal conductivity

If we base the breaking stress analysis on Eq. (7.3), we obtain differing results depending upon whether the heat-transfer parameter is small or large.

7.2.1 Small β

For thin plates and relatively low heat transfer coefficients,

$$\frac{1}{\sigma'_{max}} \approx \frac{3.25}{\beta} \qquad (7.4)$$

which gives

$$\frac{E\,\alpha\,T_o}{\sigma_b\,(1-\mu)} = \frac{3.25\,k}{ah} \qquad (7.5a)$$

or

$$T_{o\,max} = \frac{k\,\sigma_b}{E\,\alpha} \cdot \frac{3.25\,(1-\mu)}{ah} \qquad (7.5b)$$

Eq. (7.5b) indicates that the maximum shock temperature is dependent upon the material properties $k\,\sigma_b/E\,\alpha$ followed by a heating parameter (which also contains Poisson's ratio due to the similarity of μ for all materials). Note that the material property parameter is identically P_1.

7.2.2 Large β

Again considering Eq. (7.3), for large values of β

$$\sigma'_{max} \approx 1 \tag{7.6}$$

or

$$\frac{\sigma_b(1 - \mu)}{E\ \alpha\ T_o} = 1 \tag{7.7a}$$

Rearranging terms yields

$$T_{o_{max}} = \frac{\sigma_b}{E\ \alpha}(1 - \mu) \tag{7.7b}$$

The thermal shock index is now identically P_2, since the conductivity term drops out as an applicable physical property. If the plate thicknesses are great, heat transfer high, or conductivity low, the surface temperature changes to that of the surrounding fluid before any temperature difference can be felt within the plate. The stress under such circumstances is independent of conductivity. At higher β (high values of ah), the effect of good conductivity diminishes until there is no beneficial effect whatsoever of high thermal conductivity. Since reversal of the index of merit, T_o, may occur with rate of quenching, test conditions for material comparisons should closely simulate actual expected environmental conditions.

Another item to consider is the determination of a correct breaking strength, σ_b. Weibull has developed a statistical theory of strength (Ref. 38) which indicates a plausible approach to this problem. This analysis is known as the "maximum risk of rupture." Weibull felt that this analysis better described the failure mechanism than the "maximum stress theory of fracture." Basically, Weibull's theory concerns probability of failure.

Applying this concept to experimentally determined values of breaking stress can account for effects of stress distribution. The paper advocates use of a bending test rather than a standard (uniform-stress) tensile test, since the bending test simulates more closely the stress distribution which exists under thermal shock conditions. Moreover, thermal shock often results in biaxial (often 1:1) stress ratios, and for even closer simulation, the biaxial condition should be duplicated in testing.

7.3 SHORT EXPOSURE TIMES

The preceding analyses pertained to a quenching-type of thermal exposure, that is, long-duration shock and tensile stress formation at the surface of the material. With rapid surface heating, or short time exposure, however, failure may occur within the material. In those cases where the duration of the shock is not sufficient for maximum stresses to be attained, two parameters become significant – conductivity of the material and actual duration of the shock. To examine the variation of nondimensional stress σ' with time, the product $(\beta \times \theta)$ is selected at the independent variable. The dimensionless time θ is defined as

$$\theta = \frac{kt}{\rho c a^2}$$

where k = thermal conductivity
t = time
ρ = material density
c = specific heat
a = plate half-thickness

The artifice of using the product $(\beta\theta)$ eliminates the effect of conductivity from the independent parameter since $\beta \propto \frac{1}{k}$ and $\theta \propto k$. When stress curves are plotted as a function of time for different conductivities, it can be seen that materials with low rather than high conductivities may be preferable; at short exposure times, the heat pulse induces less severe tensile stresses within the specimen.

7.4 DUCTILE MATERIALS

A study of the thermal shock characteristics of several different nozzle blade ductile materials has recently been made (Ref. 44). Repeated cycling of wedge-shaped specimens (1750° F to 45° F) was conducted until thermal shock failure occurred. (Perhaps, more appropriately, this multicycle capability should be called thermal fatigue.) The significant information obtained was that the total elongation increased with increasing resistance; in fact, the data (reciprocal of measured strain at failure vs. cycles-to-failure) plotted well as a straight line on a log-log graph. The test materials all had similar thermal properties (α, k, c), yet showed widely differing resistance to thermal shock.

There is no apparent or direct way of utilizing the aforementioned relationship as a criterion for shock resistance of semiductile materials. The breaking strain had no relation to any measured mechanical or thermal property. A third property perhaps strongly influencing the results appeared to be the metallurgy of the test specimen. Consequently, this type of cyclic test to determine thermal-shock-resistance capabilities would be required for each configuration, duplicating as closely as possible the shock environment.

The authors noted an interesting sidelight which may be of significance: Perhaps the material property related to high plastic deformation is the impact resistance. Certainly the high speed of loading for determining notch-impact strength simulates, as a first approximation, the temperature shock loading. Comparisons between resistance to thermal shock cracking and Charpy impact strength showed good agreement.

Section 8
CONCLUSIONS AND RECOMMENDATIONS

All available published data on uniaxial and biaxial mechanical cycling at a strain ratio of minus one at room and elevated temperatures resulted in a relatively small scatterband for all materials when plotting the total strain vs. cycles-to-failure using log-log coordinates. The lower boundary of this scatterband is approximately a straight line with a negative slope of one-half. Deviations from the narrow scatterband result when cycling is at strain ratios other than minus one, at low frequencies, and at extreme temperatures. Thermal cycling did not lie within the narrow scatterband. Perhaps an even narrower band of scatter would be obtained if, in all cases, the total strain could have been normalized by dividing by the respective quarter-cycle fracture strains. However, these fracture strains were unavailable for so many of the data that, in general, normalization was not attempted.

Equivalent methods of predicting cycles-to-failure as functions of fracture ductility, mean strain and total strain or plastic strain range per cycle have been derived by several investigators. In general, the methods have been found to give reliable predictions only to mechanical cycling.

The following additional experimental investigations are recommended for all three cycling conditions:

1. Mechanical cycling at room temperature
   (a) cycle other materials
   (b) cycle at various strain ratios
   (c) include stress concentrations
   (d) obtain quarter-cycle fracture strain

2. Mechanical cycling at elevated temperatures
   (a) cycle other materials
   (b) cycle at various strain ratios
   (c) include stress concentrations
   (d) cycle at higher strains
   (e) cycle at higher temperature
   (f) vary the cycle frequency
   (g) obtain quarter-cycle fracture strain
3. Thermal cycling
   (a) basic research to determine mechanism of failure
4. Combination of thermal cycling and mechanical cycling
5. Effects of high strain cycling on creep rupture properties
6. Cumulative damage for other materials

Recommendations for future analytical work include a program for evaluating the existing plastic strength analyses to determine which analysis can predict the stresses or strains best when a structure is subjected to high cyclic stresses and aerodynamic heating.

Section 9

REFERENCES

9.1 CITED REFERENCES

1. American Society for Testing Materials, "References on Fatigue," (annual series) sponsored by ASTM Committee E-9 on Fatigue), ASTM STP Nos. 9-B through 9-L, 1950–1960, Philadelphia

2. G. Sachs, et al., "Low-Cycle Fatigue of 24 ST in Direct Stress," Trans. A.I.M.E., Vol. 175, 1948, p.469

3. L. F. Coffin, Jr., "A Study of the Effects of Cyclic Thermal Stresses on a Ductile Metal," Trans. A.S.M.E., Aug 1954, pp. 931–951

4. S. S. Manson, Behavior of Materials Under Conditions of Thermal Stress, NACA Report 1170, 1954

5. H. Lin and A. A. Kirsch, An Exploratory Study on High-Stress Low-Cycle Fatigue of 2024 Aluminum in Axial Loading, WADC TN 56-317, Aug 1956

6. T. H. Pian and R. D'Amato, Low-Cycle Fatigue of Notched and Unnotched Specimens of 2024 Aluminum Alloy Under Axial Loading, WADC TN 58-27, Feb 1958

7. R. D'Amato and R. DeBoer, A Study of the Relationship Between Notched and Unnotched Specimens of 2024 Aluminum Alloy in the Low-Cycle Fatigue Regime, WADC TN 59-2, May 1959

8. R. D'Amato, A Study of the Strain Hardening and Cumulative Damage Behavior of 2024 Aluminum Alloy in the Low-Cycle Fatigue Range, WADD TR 60-175, Apr 1960

9. Syracuse University Research Institute, Low-Cycle Fatigue of Pressure Vessel Materials, by G. Sachs, W. W. Gerberich, and V. Weiss, Met. Res. Lab. Report No. MET 575-601IT5, 1960

10. L. F. Coffin, Jr. and J. F. Tavernelli, "The Cyclic Straining and Fatigue of Metals," Trans. Met. Soc. of A.I.M.E., Vol. 215, Oct 1959, pp. 794–806

11. A. C. Low, "Short-Endurance Fatigue," (paper No. 15 of Session 2 presented at International Conference on Fatigue of Metals, Institute of Mechanical Engineers, London and New York, 1956)

12. S. R. Valluri, "A Unified Engineering Theory of High Stress Level Fatigue," (presented at National IAS-ARS Joint Meeting, Los Angeles, 13–16 Jun 1961)

13. A. Johansson, "Fatigue of Steels at Constant Strain Amplitude and Elevated Temperature," (Colloquium on Fatigue, IUTAM, Stockholm, May 1955)

14. E. E. Baldwin, C. J. Sokol, and L. F. Coffin, Jr., "Cyclic Strain Fatigue Studies on AISI Type 347 Stainless Steel," ASTM Preprint No. 64, Annual Meeting, 1957

15. Douglas Aircraft Co., Investigation of Thermal Effects on Structural Fatigue, WADD TR 60-410, Part I, Aug 1960

16. P. W. Swindeman and D. A. Douglas, "Failure of Structural Metals Subjected to Strain-Cycling Conditions," Trans. ASME, Series D, Vol. 81, Jun 1959, pp. 203–212

17. Harry Majors, Jr., "Thermal and Mechanical Fatigue of Nickel and Titanium," Trans. A.S.M., Vol. 51, 1958, pp. 421

18. C. R. Kennedy and D. A. Douglas, Plastic Strain Absorption as a Criterion for High Temperature Design, Oak Ridge National Lab., Report ORNL-2360 (58/05818) 2 May 1958

19. L. F. Coffin, Jr., "Thermal Stress and Thermal Stress Fatigue," (proceedings for short course, Materials Engineering Design for High Temperatures, conducted by the Pennsylvania State University, 30 June to 4 July 1958, pp. 187–233)

20. C. R. Kennedy, private communications, Oak Ridge National Lab., Oak Ridge, Tennessee

21. F. J. Mehringer and R. P. Felgar, "Low-Cycle Fatigue of Two Nickel-Base Alloys by Thermal-Stress Cycling," (paper No. 59-A-58 presented at 1959 Annual Meeting of ASME, Atlantic City, 29 Nov–4 Dec 1959)

22. F. J. Clauss, Thermal Fatigue of Ductile Materials: III–Behavior of Crucible 422 Steel, NASA TN D-69, Oct 1959

23. F. J. Clauss and J. W. Freeman, Thermal Fatigue of Ductile Materials: I–Effect of Variations in the Temperature Cycle on the Thermal-Fatigue Life of S-816 and Inconel 550, NACA TN 4160, Sep 1958

24. L. F. Coffin, Jr., "The Problem of Thermal Stress Fatigue in Austenitic Steels at Elevated Temperatures," Symposium on the Effect of Cyclic Heating and Stressing on Metals at Elevated Temperatures, ASTM STP No. 165, 17 Jun 1954, pp. 31–51

25. ----, "Design Aspects of High-Temperature Fatigue with Particular Reference to Thermal Stresses," Trans. ASME, Apr 1956, pp. 527–533

26. ----, "Thermal Stress and Thermal Stress Fatigue," Proc. Soc. for Experimental Stress Analysis, Vol. 15, No. 2, pp. 117–131, 1958

27. F. J. Clauss, "Thermal Fatigue of Ductile Materials," Proc. Fourth Sagamore Conference, 1958, p. 174

28. Lockheed Aircraft Corp., Calif. Division, Mechanical Properties of Thermally Cycled René 41 and L-605 Alloys, Report No. 15074, Burbank, Calif.

29. F. J. Clauss and J. W. Freeman, Thermal Fatigue of Ductile Materials: II–Effect of Cyclic Thermal Stressing on the Stress-Rupture Life and Ductility S-816 and Inconel 550, NACA TN 4165, Sep 1958

30. D. E. Gucer, "Cumulative Fatigue of High Plastic Strains," Trans. ASM, Vol. 54, 1961, pp. 176–185

31. C. E. Bowman and T. J. Dolan, "Biaxial Fatigue Properties of Pressure Vessel Steels," Welding Journal, Welding Research Supplement, Vol. 18, No. 11, Nov. 1953, pp. 529-s–538-s

32. J. H. Gross, D. E. Gucer, and R. D. Stout, "The Plastic Fatigue Strength of Pressure Vessel Steels," Welding Journal, Welding Research Supplement, Vol. 19, No. 1, Jan. 1954, pp. 31-s–39-s

33. J. H. Gross and R. D. Stout, "Plastic Fatigue Properties of High-Strength Pressure-Vessel Steels," Welding Journal, Welding Research Supplement, Apr 1955, pp 161-s–166-s

34. S. S. Manson, "Thermal Stresses in Design: Part 19–Cyclic Life of Ductile Materials," Machine Design, 7 Jul 1960, pp. 139–144

35. -----, "Thermal Stresses in Design, Part 1: Appraisal of Brittle Materials," Machine Design, 12 Jun 1958, pp. 114–120

36. -----, "Thermal Stresses in Design, Part 2: Quantitative Techniques for Brittle Materials," Machine Design, 26 Jun 1958, pp. 99–103

37. -----. Behavior of Materials Under Conditions of Thermal Stress, NACA Report 1170, 1954

38. S. S. Manson and R. W. Smith, "Theory of Thermal Shock Resistance of Brittle Materials Based on Weibull's Statistical Theory of Strength," J. Am. Ceram. Soc., Jan 1955, pp. 18–27

39. W. G. Lidman and A. R. Bobrowsky, Correlation of Physical Properties of Ceramic Materials with Resistance to Fracture by Thermal Shock, NACA TN 1918, Jul 1949

40. W. D. Kingery, "Factors Affecting Thermal Stress Resistance of Ceramic Materials," J. Am. Ceram. Soc., Jan 1955, pp. 3–15

41. W. R. Buessem, "Thermal Shock Testing," J. Am. Ceram. Soc., Jan 1955, pp. 15–18

42. W. R. Buessem and E. A. Bush, "Thermal Fracture of Ceramic Materials Under Quasi-Static Thermal Stresses (Ring Test)," J. Am. Ceram. Soc., Jan 1955, pp. 27–32

43. R. L. Coble and W. D. Kingery, "Effect of Porosity on Thermal Stress Fracture," J. Am. Ceram. Soc., Jan 1955, pp. 33–37

44. M. J. Whitman, R. W. Hall, and C. Yaker, Resistance of Six Cast High-Temperature Alloys to Cracking Caused by Thermal Shock, NACA TN 2037, Feb 1950

9.2 UNCITED REFERENCES

Pre-1950

Oberg, T. T. and Johnson, J. B., "Fatigue Properties of Metals Used in Aircraft Construction at 3450 to 10,600 Cycles," ASTM Proceedings, Vol. 37, Part II, 1937, pp. 195–203

Orowan, E., "Theory of the Fatigue of Metals," Proc. Roy. Soc., (London), Vol. 171, Series A, 1939, pp. 79–10

1950

Smith, F. C., Brueggeman, W. C., and Narwell, R. H., Comparison of Fatigue Strength of Bare and Alclad 24ST3 Aluminum Alloy Sheet Specimens Tested at 12 and 1000 Cycles Per Minute, NACA TN 2231, Dec 1950

1951

Weismann, M. H. and Kaplan, M. H., "The Fatigue Strength of Steel Through The Range From 1/2 to 30,000 Cycles of Stress," ASTM Proceedings, Vol. 50, 1951, pp. 649–664

Norton, F. H., Refractories, 3rd ed., New York, McGraw-Hill, 1951

1952

Shuetts, E. A., "Plastic-Flow and Work-Hardening Phenomena in Magnesium Alloys During Fixed Deflection Fatigue Tests," ASTM Proceedings, Vol. 52, 1952, pp. 804–817

Burke, J. E. and Turkalo, A. M., "Deformation of Zinc Crystals by Thermal Ratcheting," Trans. A.I.M.E., Vol. 194, 1952, pp. 651–656

Theilsch, H., "Thermal Fatigue and Thermal Shock," (Bulletin No. 10 of the Welding Research Council of the Engineering Foundation, 29 West 39 St., N.Y., Apr 1952)

1953

Hardrath, H. F., Landers, C. B., and Utley, Jr., E. C., Axial-Load Fatigue Tests on Notched and Unnotched Specimens of 61S-T6, 347, and 403, NACA TN 3017, Oct 1953

1954

Sachs, G., Survey of Low-Alloy Aircraft Steels Heat-Treated to High Strength Levels: Part 2 – Fatigue, WADC TR 53-254, Jan 1954

Weibull, W., A New Method for the Statistical Treatment of Fatigue Data, SAAB TM 30, 14 May 1954

1955

Coffin, L. F., Jr., "Thermal Stress Fatigue in Austenitic Stainless," Metal Progress, Vol. 68, Sep 1955, pp. 180–182

Heywood, R. B., "Effect of High Loads on Fatigue," Aircraft Engineer (England), Vol. 27, No. 332, Dec 1955, p. 405

1956

Majors, Harry, Jr., Thermal Shock and Fatigue – Literature Survey, Office of Ord. Res., U. S. Army, Tech. Rep. 1, Contr. DA-01-009 ORD-454, Proj. M1230, Jun 1956

Lin, H. and Kirsch, A. A., An Exploratory Study of High-Stress Low-Cycle Fatigue of 2024 Aluminum in Axial Loading, WADC TM 560317, Aug 1956

McEvily, A. J., Jr., Illg, W., and Hardrath, H. F., Static Strength of Aluminum Alloy Specimens Containing Fatigue Cracks, NACA TN 3816, Oct 1956

Illg, W., Fatigue Tests on Notched and Unnotched Sheet Specimens of 2024-T3 and 7075-T6 Aluminum Alloys and of SAE 4130 Steel with Special Consideration of the Life Range From 2 to 10,000 Cycles, NACA TN 3866, Dec 1956

1957

Coffin, L. F., Jr., "Thermal Stress Fatigue," Product Engineering, Jun 1957, pp. 175-179

Broom, T. and Ham, R. K., "The Hardening and Softening of Metals by Cyclic Stressing," Proc. Roy. Soc., Series A, No. 1229, Oct 1957

Goldin, R., "Thermal Creep Design Criteria," Aero. Engr. Review, Vol. 16, Part 2, Dec 1957, p. 36-41

Sach, C. and Schuen, G., "Relation Between Direct-Stress and Bending Fatigue of High Strength Steels," ASTM Bull., Vol. 57, 1957, p. 667

1958

Manson, S. S., "Thermal Stresses in Design: Part 1 - Appraisal of Brittle Materials," Machine Design, 12 Jun 1958

-----, "Thermal Stresses in Design: Part 2 - Quantitative Techniques for Brittle Materials," Machine Design, 26 Jun 1958

-----, "Thermal Stresses in Design: Part 3 - Basic Concepts of Fatigue in Ductile Materials," Machine Design, 7 Aug 1958

-----, "Thermal Stresses in Design: Part 4 - Causes of Fatigue in Ductile Materials," Machine Design, 21 Aug 1958

-----, "Thermal Stresses in Design: Part 5 - Interpretation of Fatigue Data for Ductile Materials," Machine Design, 21 Aug 1958

Brooks, W. A., Jr., Temperature and Thermal-Stress Distributions in Some Structural Elements Heated at a Constant Rate, NACA TN 4306, Aug 1958

McEvily, A. J., Jr., and Illg, W., The Rate of Fatigue-Crack Propagation in Two Aluminum Alloys, NACA TN 4394, Sep 1958

Ross, A. S. and Morrow, Jr., Cyclic Stress Behavior of A-286 Alloy for Conditions of Controlled Strain, TAM Report M563, Univ. of Ill., Sep 1958

NATO Advisory Group for Aeronautical Research and Development, A Design Philosophy for Repeated Thermal Loading, Report 213, 1958

Aeronautical Research Council, Regularities in Creep and Hot-Fatigue Data; Part I, by A. Graham and K. F. A. Walles, Report C.P.N 379, London, 1958

-----, Regularities in Creep and Hot-Fatigue Data; Part II, by A. Graham and K. F. A. Walles, TRCP No. 380, London, 1958

Sachs, G. and Taber, A. T., Relations Governing Low-Cycle Fatigue – A Summary of the Pertinent Literature, AEC Contr. at (30-1)-2141, Syracuse Univ., 1958

1959

Manson, S. S., "Thermal Stresses in Design: Part 6 – Elastic Stress Analysis," Machine Design, 22 Jan 1959

—----, "Thermal Stresses in Design: Part 7 – Exact and Approximate Solutions," Machine Design, 5 Feb 1959

—----, "Thermal Stresses in Design: Part 8 – Elastic Stresses by Energy Methods," Machine Design, 19 Feb 1959

—----, "Thermal Stresses in Design: Part 9 – Elastic Stress Solutions," Machine Design, 5 Mar 1959

—----, "Thermal Stresses in Design: Part 10 – Elastic Stresses by Minimizing Residuals," Machine Design, 19 Mar 1959

Baron, H. G., Summary of ARDE Work on Thermal Stress Fatigue, ARDC Memo (MX) 18160, ASTIA AD No. 237337, Apr 1960

Kroll, W. D., Aerodynamic Heating and Fatigue, NASA Memo 684-59W, Jun 1959

Manson, S. S., "Thermal Stresses in Design: Part 11 – Stresses Under Plastic Flow and Creep." Machine Design, 9 Jul 1959

-----, "Thermal Stresses in Design: Part 12 – Plastic Stresses and Strains by Successive Approximations," Machine Design, 23 Jul 1959

Buckley, W. H. and Strasser, G., Study of Design Criteria for Structures Subject to Aerodynamic Heating, WADC TR 59-482, Jul 1959

Manson, S. S., "Thermal Stresses in Design: Part 13 – Incremental Solutions for Plastic Stresses and Strains," Machine Design, 6 Aug 1959

Knolls Atomic Power Laboratory, Bibliography on Thermal Stresses and Low-Cycle Fatigue, by D. R. Miller, KAPL 2048, 20 Aug 1959

WADC Symposium, Proceedings on Fatigue of Aircraft Structures, WADC TR 59-507 Aug 1959

Avery, H. S., "The Mechanism of Thermal Fatigue," Metal Progress, Vol. 76, No. 2, Aug 1959, pp. 67–70

Manson, S. S., "Thermal Stresses in Design: Part 14 – Strain Gage Applications," Machine Design, 29 Oct 1959

-----, "Thermal Stresses in Design: Part 15 – Strain Gage Applications," Machine Design, 13 Nov 1959

-----, "Thermal Stresses in Design: Part 16 – Measurements of Photoelasticity," Machine Design, 26 Nov 1959

Coffin, L. F. and Tavernelli, J. F., "A Compilation and Interpretation of Cyclic Strain Fatigue Tests on Metals," Trans. ASME, Vol. I, 1959, pp. 439–450

Grover H. J., "Fatigue of Materials at High Temperatures," Metal Fatigue, New York, McGraw-Hill, 1959

Padlog, J. and Rattinger, I., "Low-Cycle Fatigue Strength of Pressurized Components," (paper presented at ASTM Meeting, San Francisco, 1959)

Manson, S. S., "Thermal Stresses in Design: Part 17 – Determining a Safe Working Stress," Machine Design, Jun 1960, p. 109

-----, "Thermal Stresses in Design: Part 18 – Working Stress for Ductile Materials," Machine Design, 23 Jun 1960, p. 153

-----, "Thermal Stresses in Design: Part 19 – Cyclic Life of Ductile Materials," Machine Design, 7 Jul 1960, p. 139

-----, "Thermal Stresses in Design: Part 20 – Thermal Cycling With Steady Stress," Machine Design, 21 Jul 1960, p. 161

-----, "Thermal Stresses in Design: Part 21 – Effect of Mean Stress and Strain on Cyclic Life," Machine Design, 4 Aug 1960, p. 129

-----, "Thermal Stresses in Design: Part 22 – Cumulative Fatigue Damage," Machine Design, 10 Aug 1961, p. 129

Parkes, E. W., "Effects of Repeated Thermal Loading," Aircraft Engineering, Aug 1960

Padlog, J., Hugg, R. D., and Holloway, G. F., Inelastic Behavior of Structures Subjected to Cyclic, Thermal, and Mechanical Stressing Conditions, WADD TR 60-271, Dec 1960